Universidad Carlos III de Madrid

CREATION OF CONTACT SENSORS FOR ANTHROPOMORPHIC ROBOT HAND

Bachelor's Thesis

Author: Joaquín Blanco Sánchez

Bachelor: Biomedical Engineering

Tutor: David Álvarez Sánchez

Date: July 8th, 2015

Título: Creation of contact sensors for anthropomorphic robot hand

Autor: Joaquín Blanco Sánchez

Tutor: David Álvarez Sánchez

EL TRIBUNAL

Presidente: Juan José Vaquero López

Vocal: Santiago Martínez de la Casa Díaz

Secretario: Mónica Abella García

Realizado el acto de defensa y lectura del Trabajo de Fin de Grado el día 8 de Julio de 2015 en Leganés, en la Escuela Politécnica Superior de la Universidad Carlos III de Madrid, acuerda otorgarle la CALIFICACIÓN de

VOCAL

SECRETARIO PRESIDENTE

AGRADECIMIENTOS

En primer lugar, me gustaría dar las gracias a los profesores que nos han acompañado durante estos duros cuatro años de carrera. Su sabiduría y experiencia nos ha convertido en lo que somos hoy, Ingenieros Biomédicos.

Me gustaría agradecer especialmente a mi tutor, David, la oportunidad de trabajar en este proyecto al igual que todo su apoyo y paciencia, especialmente para tratar con un alumno de fuera de su departamento. También a los compañeros del Robotics Lab por toda su ayuda y colaboración.

A los compañeros del laboratorio de bioingeniería por estar siempre dispuestos a echarnos una mano con todo y a abrirnos la puerta cien veces al día. Mención especial para Angélica, el alma y pilar fundamental del laboratorio.

A mis profesores del cole, Marta y Miguel, quienes han seguido mi trayectoria y siempre consiguen arrancarme una sonrisa.

A mis amigos, viejos y nuevos, españoles y de otras nacionalidades. Mi vida no sería lo mismo sin vosotros. Alba, de quien fui separado al nacer. Irene, a quien no se le escapa una. Noe, bendita sea tu paciencia por aguantarme. Lorena, cuyas historias nunca tienen desperdicio. Dani, con quien la frase *sofá y vino* ha cobrado un nuevo significado. Iván, más un hermano que un amigo.

Finalmente, a mi familia, por su apoyo y cariño en cada paso del camino. Mi madre, mi padre y mi hermana, sin los que jamás habría llegado hasta aquí. Mi madre, quien ha pasado el mismo número de noches en vela por la carrera que yo. Mi padre, quien nunca dudó de mi capacidad. Mi hermana, quien con su *mendruguín* consigue quitarme todas las preocupaciones.

INDEX

INDEX OF FIGURES

INDEX OF TABLES

ABSTRACT

The work included in this project is framed in one of the lines of research carried out within Robotics Lab at University Carlos III of Madrid in collaboration with the Systems Engineering and Automation Department.

The general goal of this project is the proper calibration and integration of tactile sensor in the robotic hand Gifu Hand III. This is quite important because Gifu Hand III does not incorporate any extrinsic sensor to measure the force applied on its surface and therefore it is not possible to recognize objects being manipulated without direct visual contact.

First of all, the behavior of the sensors to be integrated was observed. Then a calibration strategy was designed and a mathematical model defining the behavior of the sensors was described. Once all this was done, it was time to integrate the sensors in the robotic hand. For this purpose new phalanges were designed and the sensors were integrated onto their surfaces. They were later covered with a rubber fabricated in the lab in order to improve grasping performance. Finally this structure was assembled in the hand.

Key words:

Robotic hand, tactile sensors, calibration, mathematical model, integration, rubber.

RESUMEN

El trabajo incluido en este proyecto se enmarca dentro de una de las líneas de investigación llevadas a cabo en el Laboratorio de Robótica (Robotics Lab) de la Universidad Carlos III de Madrid en colaboración con el departamento de Ingeniería de Sistemas y Automática.

El objetivo general de este proyecto es la correcta calibración e integración de sensores táctiles en la mano robótica Gifu Hand III. Esto es muy importante dado que la mano robótica Gifu Hand III no incorpora ningún sensor extrínseco para medir la fuerza aplicada sobre la superficie de la mano y por lo tanto no es posible reconocer los objetos a manipular sin contacto visual directo.

Primero de todo, se hizo una observación inicial del comportamiento de los sensores que iban a ser integrados. A continuación se diseñó una estrategia de calibración y se definió un modelo matemático que describe el comportamiento de los sensores. Una vez realizado todo esto, había que integrar los sensores en la mano robótica. Para este propósito nuevas falanges fueron diseñadas y los sensores integrados en su superficie. Posteriormente fueron cubiertos con una goma fabricada en el laboratorio con el fin de mejorar el rendimiento del agarre. Finalmente esta estructura fue montada en la mano.

Palabras clave:

Mano robótica, sensores táctiles, calibración, modelo matemático, integración, goma.

1. INTRODUCTION

The Bachelor's Degree in Biomedical Engineering teaches its students how important it is to work in teams composed of people with very different backgrounds. Luckily I am one of those students. Since the very first day of class people from a huge variety of fields have trained us, from biologists to engineers passing through doctors and physicists. This has given me the opportunity to participate in projects and practices from different departments as well as the opportunity to expand my knowledge. All this made me looked for a project for my Bachelor's Thesis not only outside of the Biomedical and Aerospace Engineering Department but also outside of my comfort zone. And I found it.

This project for the *Creation of contact sensors for anthropomorphic robot hand* is carried out within Robotics Lab at University Carlos III of Madrid in collaboration with the Systems Engineering and Automation Department.

Anthropomorphic robot body parts are not science fiction anymore. They are a reality. It was 1980 when *Star Wars: Episode V – The Empire Strikes Back* [1] was released and a completely functional robot hand was shown in the big screen for the first time. By then it was science fiction but again, today it is a reality.

Anthropomorphic robot hands with completely mechanical functionality have been developed and are already being used for prostheses. This mechanical functionality tries to mimic human grasping, which is achieved thanks to what is known as *set of three oppositions*: pad, for forces between the pads of the fingers and the thumb; palm, for forces between fingers and the palm; and side, for forces between the thumb and the side of the index finger. [2] These oppositions are used either separately or simultaneously to carry out different tasks where the geometry of the handgrip and the power applied change depending on the specific task as shown in Figure 1.

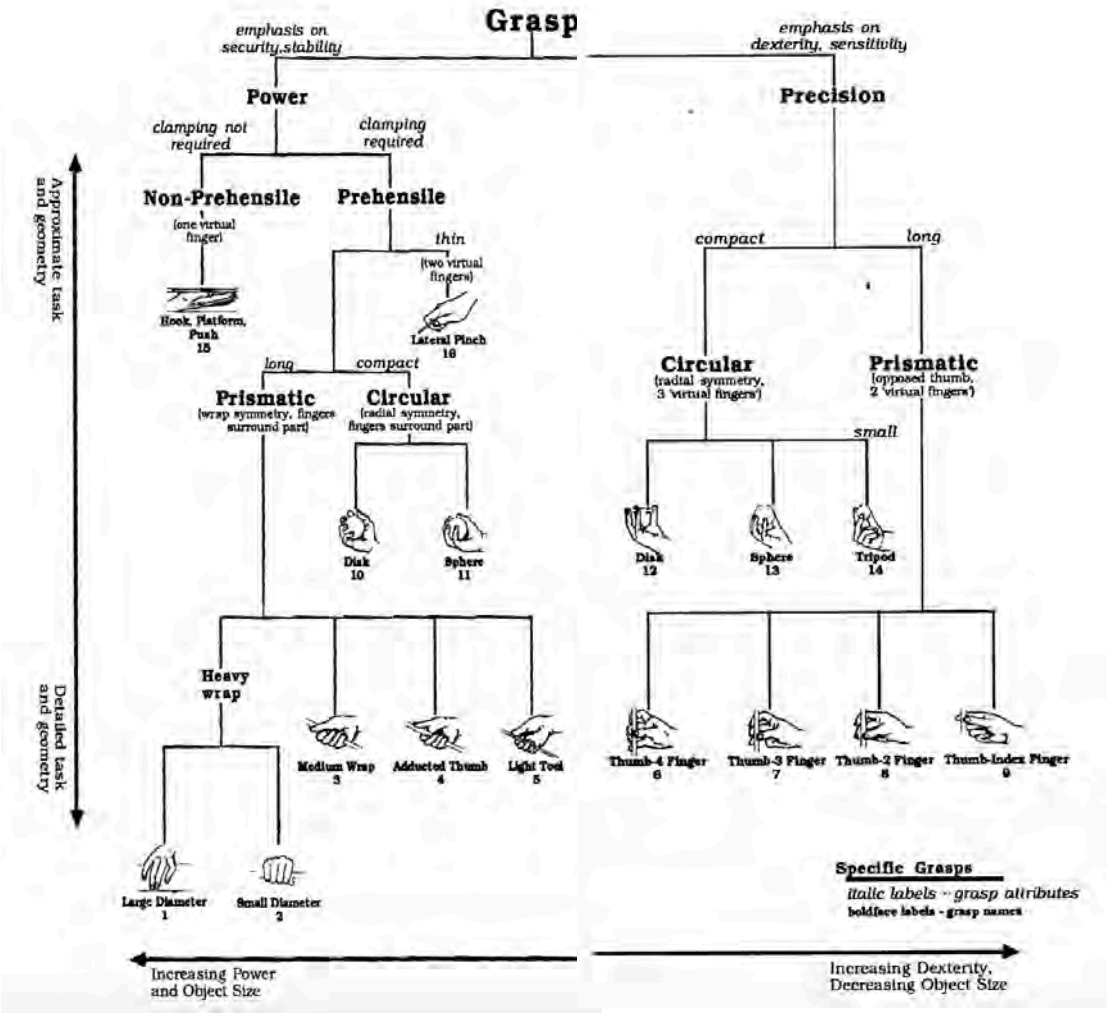

Figure 1. Power and geometry grasping diagram [2]

Human hand has evolved as a tool not only used for manipulation but also for sensation and communication. So the next logical step in the development of robotic hands is to provide them with sensibility to recognize different shapes, weights and surfaces, and that is where this project comes to life.

The creation and proper integration of contact sensors is important in order to provide robotic hands with the sense of touch. With a real hand, touching different objects results in different patterns of nerve activity. These patterns are nothing but electrical impulses sent to the brain that is in charged of interpreting them to recognize shapes, weights, materials, ...

Robotic hands can be used for manipulation tasks and until now it is known what they are *touching* and how they are *touching* it because it can be seen. Ideally contact or tactile sensors would provide with the necessary information to know what the robot hand is touching. It would not be needed to see it because it would be felt thanks to the information provided by the contact sensors. Moreover contact sensors are considered the future of neural prostheses since they could be connected to the brain to restore not only the mechanical function but also the sensory function.

1.1 Goals of the project

In this project we are going to incorporate a specific kind of contact sensors, Force Sensing Resistors (FSRs), to the anthropomorphic robot hand Gifu Hand III. The student did not choose these sensors; they were given to him. Robotics Lab acquired these sensors thanks to a collaboration with Kawasaki and Mouri Laboratory, developer of the Gifu Hand III.

The project starts with a research on calibration systems for FSRs (Section 3). Knowing the behavior of the sensors is vital for their proper integration in the hand. Although the manufacturer supplies a calibration curve, the behavior of the sensors does not seem to completely adjust to it. A calibration must be performed in order to get sure that the behavior of the sensors in the force range of our hand applications is not only the desired one but also the correct one. The calibration is a complex task that will provide with the information necessary to describe a mathematical model.

Once the mathematical model has been obtained, the sensors have to be integrated in the hand (Section 4). The integration is performed in three steps: designing of new phalanges for the fingers so that their curvature mimics that of an actual one, positioning of the sensors in the phalanges, and coverage of the sensor with a biological rubber to imitate skin properties (friction, grasping force, ...).

The final step of this project is the assembly of the new designed fingertip structures in the Gifu Hand III.

2. ROBOT HANDS AND TACTILE SENSORS

2.1 Anthropomorphic robot hands

The human hand has evolved to be a complex and adaptable manipulator. Human hands are able to reconfigure itself into different shapes by a combination of a high number of degrees of freedom and an extremely precise control given by sensors and actuators (nerves, tendons, ligaments, skin receptors, ...). These sensors are connected to the nervous system, which is controlled by the most powerful organ known: the brain.

Anthropomorphic multi-fingered hands interact with human beings through humanoid robots and that is why they are also referred as humanoid hand robots. The humanoid hand robots are used to perform works instead of humans. These works go from simple manufacturing tasks to more dangerous ones. Moreover anthropomorphic multi-fingered hands could be used for neural and mechanical prostheses.

Many anthropomorphic multi-fingered robot hands have already been developed. Actuators located outside the hand with the help of tendon cables have replaced previously mentioned natural sensors. Tendon cables are elastic producing inaccurate joint-angle control and they are also relatively long obstructing the motion of the hand. These problems have been solved with the development of hands with built-in actuators.

The German Aerospace Research Center (DLR) developed in 1997 one of the first articulated hands with built-in actuators, the DLR-Hand. Later in 2001 they presented a redesigned version with a better performance in grasping and manipulation. The DLR-Hand II consists of 4 identical fingers with 4 joints and 3 degrees of freedom each and an additional degree of freedom in the palm. This robotic hand presents a multidimensional sensor in the fingertips for force detection and analysis. This sensor presents three sensitive elastic beams and a cantilever beam that measure the forces in the X and Y axis by using torsion shear strain gauges. [3]

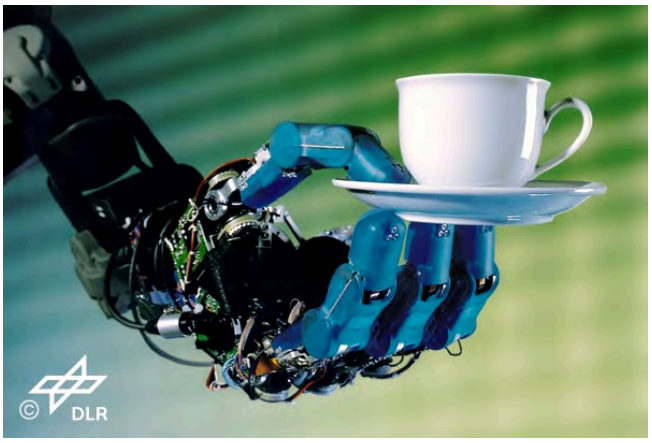

Figure 2. DLR-Hand II [3]

Shadow Robot Company has developed and commercialized the Shadow Dexterous Hand with the priority of approximating the kinematics of the human hand. It presents 5 fingers and a total of 24 joints with 20 actuated degrees of freedom. This robotic hand presents ultra sensitive touch sensors on the fingertips as well as the DLR-Hand II but in this case the sensors are Pressure Sensor Tactiles (PSTs) with a single region with high sensitivity. They could be substituted for other tactile sensors such as Force Sensing Resistors (FSRs). [4]

Figure 3. Shadow Dexterous Hand [4]

Gifu Hand III

Kawasaki and Mouri Laboratoy, at Gifu University, developed the Gifu Hand I in 1997 and then redesigned it in 1999 and 2002 looking for improvement. These two improved versions are called Gifu Hand II and Gifu Hand III respectively. All three are 5-fingered hands driven by built-in actuators. [5]

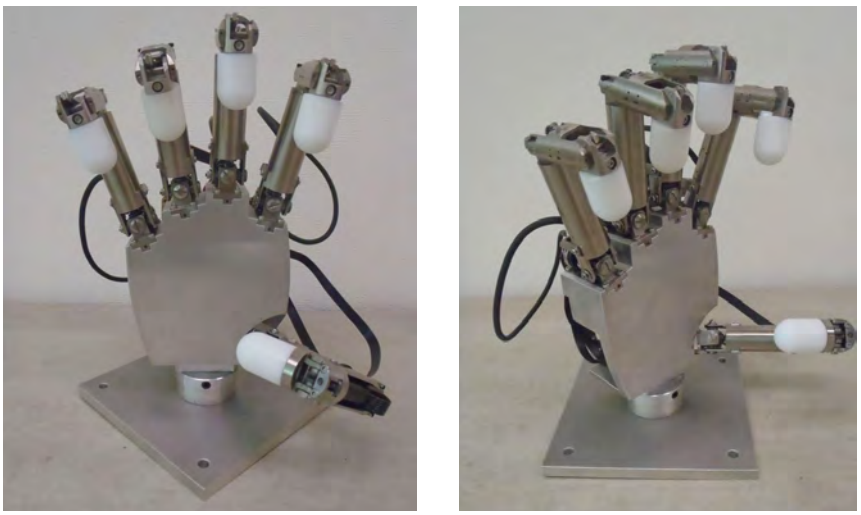

Figure 4. Gifu Hand III [5]

"The Gifu hand III has 5 fingers, the thumb has 4 joints with 4 degrees of freedom (DOF) and the finger has 4 joints with 3 DOF, and two joints axes of the thumb and the finger near the palm are orthogonal." [6]

The size and weight of the Gifu Hand III is close to that of the human hand and of course it has 5 fingers like the actual one. The hand has been designed in such a way that the number of joints and degrees of freedom is very similar to those of the human hand, 16 DOF. Manipulation of objects with the human hand is mostly done thanks to the opposability of the thumb to the other fingers. The robot hand has been designed to fulfill this opposability. Due to the built-in PC motor actuators the robot hand presents no problems associated to tendon cables.

In contrast to the previously mentioned robotic hands, Gifu Hand III presents no tactile sensors on the fingertips and there is where the aim of this project arises: integration of tactile sensors to the robotic hand Gifu Hand III.

2.2 Tactile sensors for robotic applications

Humans are able to interact and explore the surrounding environment through five traditional senses: sight, hearing, taste, smell, and touch. Sensing capabilities of future robotic systems can be improved by studying how these senses collect information from the surroundings.

Human sense of touch has been traditionally divided in three systems: cutaneous system, kinesthetic system, and haptic system. The cutaneous system requires physical contact and contributes to the alertness of stimulation thanks to skin receptors and the somatosensory area located on the central nervous system (CNS). The kinesthetic system informs about the dynamic and static body position thanks to receptors located within muscles, tendons and joints. The haptic system uses information coming from both cutaneous and kinesthetic systems to inform about distal objects and events.

These three systems are the starting point for tactile sensors in robotic applications. In their paper *Tactile sensing for mechatronics – a state of the art survey*, Lee and Nicholls defined tactile sensors as *"a device or system that can measure a given property of an object or contact event through physical contact between the sensor and the object."* [7] According to this definition, tactile sensing could be described as the process of detecting and measuring a stimulus of a contact event in a local area.

In robotics, touch sensing is defined as tactile sensing at a single contact point. Cutaneous and kinesthetic systems are analogously called in robotics the extrinsic or external and intrinsic or internal touch systems. Both extrinsic and intrinsic sensing is achieved through tactile sensors, but extrinsic touch sensors are located at the contact surface while intrinsic touch sensors are located within the mechanical structure. The term tactile sensing is used to refer to external touch sensing in robotics.

Now the question is, why is the sense of touch so important for humans and why should it be included in robotics applications? Touching allows human beings to determine shape, size or even texture while helping in the development of movement and body awareness, sometimes referred as proprioception. Proprioception is defined as the internal sense that tells humans where their body parts are without direct eye contact. In robotics, touch sensing is pretty important in manipulation tasks. A fairly big variety of tactile sensors for robotics applications have been developed. They work based on different methods of transduction in which one form of energy is converted into another form of energy. The main transduction methods are: resistive, piezoresistive, based on tunnel effect, capacitive, optical, ultrasonic, magnetic and piezoelectric.

Resistive sensors

A resistive sensor is a transducer that converts a mechanical change into an electrical signal that can be monitored (Figure 5). This change could either be a material (density, ρ) or a geometry change (area A, or length, L). This type of sensor is used in high areas applications like covering a whole robot system. [8]

Advantages: sensitive, low cost.

Disadvantages: high power consumption, single contact point, lack of contact force measurement.

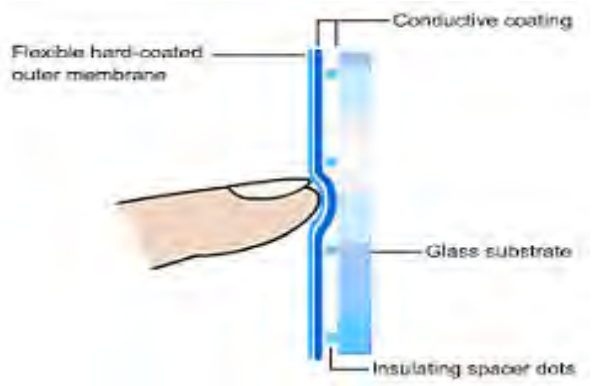

Figure 5. Example of resistive sensor [9]

Piezoresistive sensors

A piezoresistive sensor is a transducer that converts an applied mechanical load into a change of electrical resistance. Force Sensing Resistors (FSRs) are used in many experimental tactile systems like the one shown in Figure 6, including anthropomorphic robot hands. [10]

Advantages: low cost, good sensitivity, low noise, simple electronics.

Disadvantages: non-linear response, temperature sensitive, hysteresis.

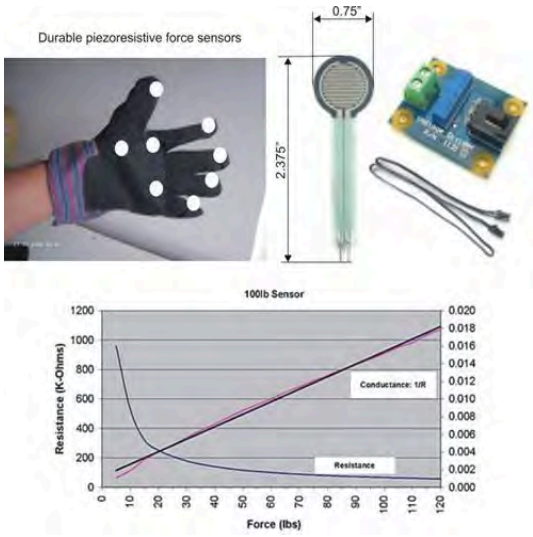

Figure 6. Example of piezoresistive sensor [11]

Tunnel effect sensors

They are based on Quantum Tunnel Composites (QTC) that have the unique capability of transforming from a perfect insulator to a conductor when deformed, as it can be seen in Figure 7. Tunnel effect sensors are being used in tactile arrays for dynamic pressure distribution measurement. [12]

Advantages: sensitive, physically flexible.

Disadvantages: non-linear response.

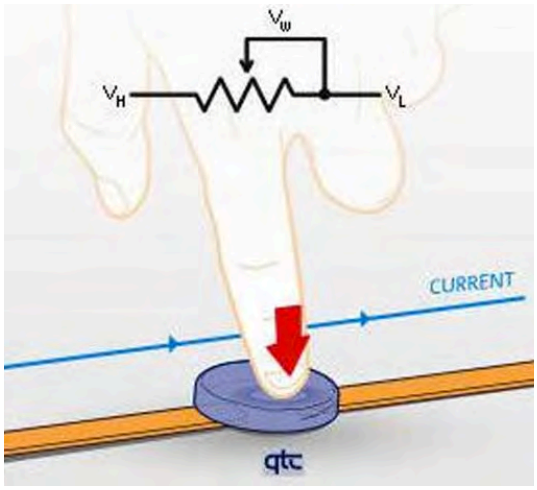

Figure 7.Example of tunnel effect sensor [13]

Capacitive sensors

A capacitive sensor is a transducer that converts an applied pressure into a change of capacitance (Figure 8). Capacitive sensors are extremely used in the technological market for human interface devices, like trackpads and touchscreens where the capacitive sensors are used as input devices. Capacitive sensors are also used in robotics as embedded artificial skin for humanoid robots. [14]

Advantages: sensitive, low cost.

Disadvantages: cross-talk, hysteresis, complex electronics.

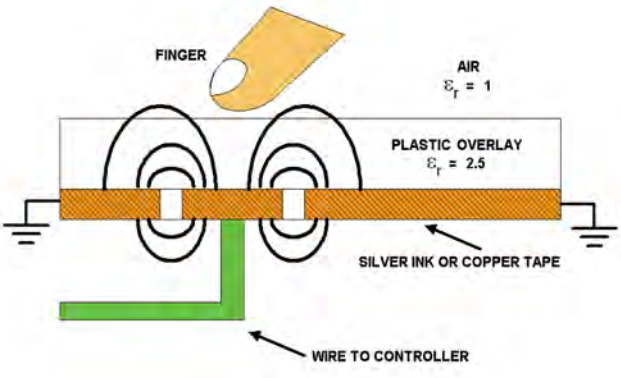

Figure 8. Example of capacitive sensor used in human interface [15]

Optical sensors

An optical sensor is a transducer that converts light or a change in light into an electrical signal. One sensor can measure the light or change in light of several light beams. Optical sensors are quite popular in photography for flash synchronization but they also have other applications such as lamps that turn on automatically in response to darkness. Nagoya University in Japan has recently used optical sensors to give human touch to robots. [16]

Advantages: sensitive, fast, immune to magnetic interference, physically flexible.

Disadvantages: power consumption, complex computations.

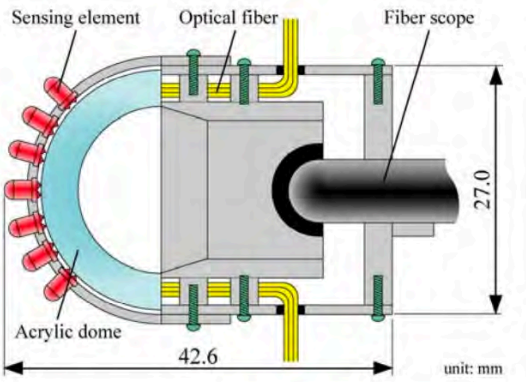

Figure 9. Optical sensor used in robotic hand by Nagoya University [16]

Ultrasonic sensors

An ultrasonic sensor like the one shown in Figure 10 is a transducer that converts ultrasound waves to electrical signals and vice versa. They are useful for sensing applications because they can detect noise occurring during motion and contact. In 2013 a LEGO robot hand was built and ultrasonic sensors were used to activate the hand. [17]

Advantages: fast dynamic response.

Disadvantages: complex electronics, temperature sensitive.

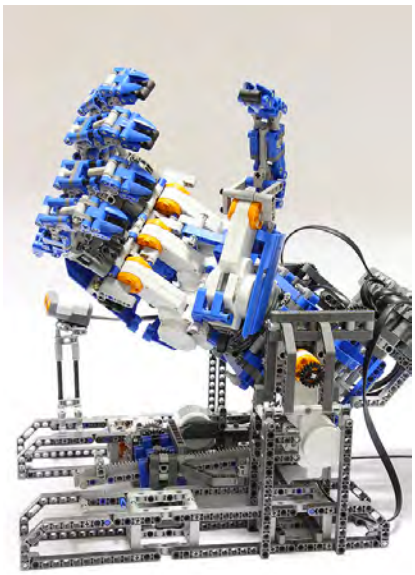

Figure 10. LEGO robot hand with ultrasonic sensors [17]

Magnetic sensors

A magnetic sensor is a transducer that measures the flux density change caused by an applied force on a small magnet. Magnetic sensors are extensively used for speed and position measurement in automotive and industrial applications. Although they have been barely used for robotics applications, Istituto Italiano di Tecnologia is performing some research about their use for flexible tactile sensing. [18]

Advantages: high sensitivity, no mechanical hysteresis, robustness.

Disadvantages: suffer from magnetic interference, complex computation, power consumption.

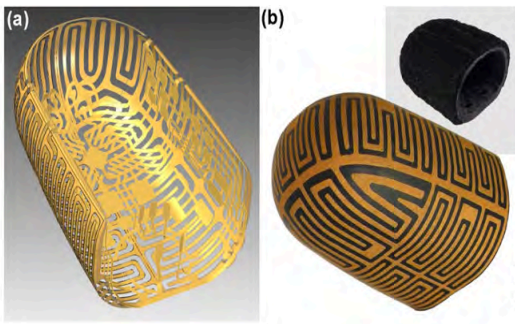

Figure 11. Flexible magnetic sensor used by Istituto Italiano di Tecnologia [18]

Piezoelectric sensors

A piezoelectric sensor is a transducer that is able to generate a charge/voltage proportional to an applied pressure/force and vice versa. Piezoelectric sensors are also used for trackpads and touchscreens like the capacitive sensors but they have bigger repercussion in medical instrumentation like force-sensing surgical instruments presents in DaVinci Surgical System. [19]

Advantages: high bandwidth.

Disadvantages: temperature sensitive.

Figure 12. EndoWrist™ instrument of the da Vinci Surgical System equipped with a piezoresistive sensor [19]

Recent trends

Late studies are focusing on soft materials for developing of tactile sensors but, why? All these previous sensors have been built on fairly rigid and solid materials while using them for anthropomorphic research but, where does the human sense of touching start and where does it propagates? In the skin and the tissues. Both are elastic and it seems reasonable to say that an elastic material could improve the properties of tactile sensors. Rubbers, powders, fluids and gels are elastic materials that act like transducers whose impedance changes when a pressure/force is applied.

Their major disadvantage is their non-linear behavior and that they are influenced by hysteresis.

Although some commercial sensors are already available, very little research is being performed on them.

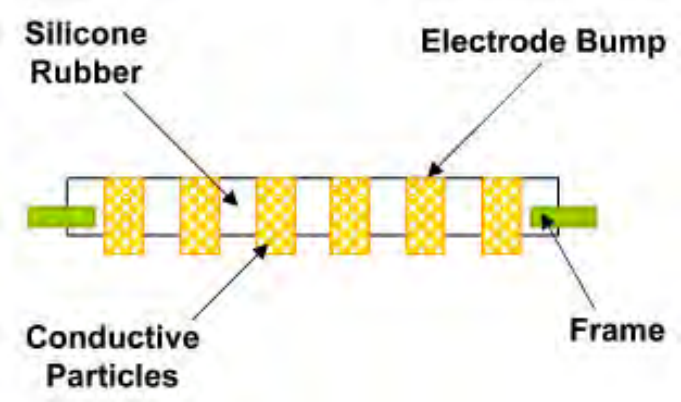

Figure 13. High performance pressure conductive rubber [20]

3. FORCE SENSING RESISTORS (FSRs). INASUTOMA SFR TYPE SENSOR

"Force Sensing Resistors (FSRs) are a polymer thick film (PTF) device which exhibits a decrease in resistance with an increase in the force applied to the active surface. Its force sensitivity is optimized for use in human touch control of electronic devices." [21]

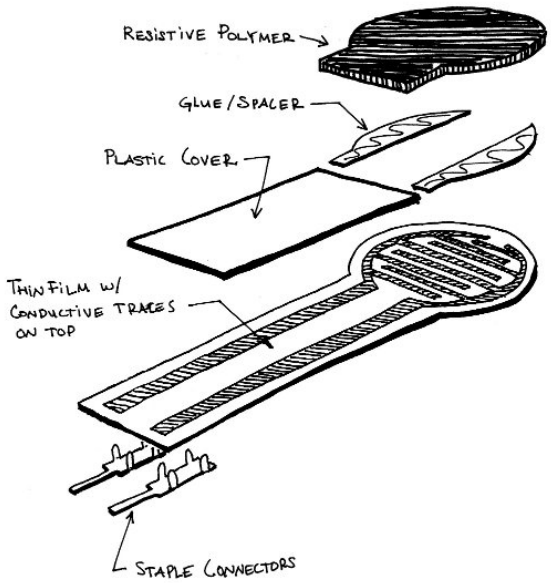

Figure 14. Scheme of a Force Sensing Resistor

There are several terms that the reader must familiarized with before further reading:

- **Active Area**: the area of an FSR device that responds to normal force with a decrease in resistance.
- **Actuator**: the object that contacts the sensor surface and applies forces to FSRs.
- **Applied force:** the force applied by the actuator on the active area of the sensor.
- **(Resistance) Drift:** the change in resistance with time under a constant load.
- **Hysteresis:** the difference between instantaneous force measurements at a given force for an increasing load versus a decreasing load.

- **Tail:** the region where the lead out or busing system terminates. Generally, the tail ends in a connector.

There are several manufacturers of such sensors in the market (E.g. Interlink, Sensitronics, ...) with very similar architecture and working principles, being their principle advantages, low cost per-unit, human touch applications calibration, little space required for installation and high variety in shapes and sizes. Despite of these advantages, its reliability depends on a prior proper calibration method and a digital handling with the force values.

In this project we will be working with a Japanese FSR called イナストマ – SFRタイプ, which means *Inasutoma SFR type*, from INABAGOMU, Inc. From now on it will be referred as *Inasutoma* sensor.

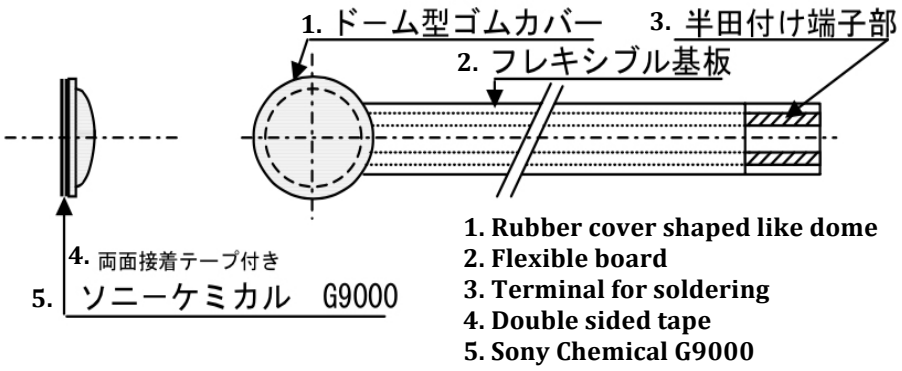

Figure 15. Inasutoma sensor physical outline [22]

This sensor has the following rating and mechanical specifications, shown in Figure 16 and Figure 17 respectively:

（１）	使用温度範囲	−5～50℃	**(1) Temperature range**
（２）	使用湿度範囲	30～85%RH	**(2) Humidity range**
（３）	保存温度範囲	−40～70℃	**(3) Storage temperature range**
（４）	保存湿度範囲	10～95%RH	**(4) Storage humidity range**
（５）	最大許容負荷	5kgf	**(5) Maximum permissible load**
（６）	最大許容電圧	30V	**(6) Maximum permissible volt**
（７）	最大許容電流	20mA	**(7) Maximum permissible current**

Figure 16. Inasutoma sensor rating specificatons [22]

（１）最大荷重 … 5.0ｋｇｆ	**(1) Maximum load**
（２）推奨荷重 … 1.0ｋｇｆ	**(2) Recommended load**
（３）リード線引っ張り強度…2.0ｋｇｆ	**(3) Resistance for the pulling lead**

Figure 17.Inasutoma sensor mechanical specifications [22]

Besides the original data sheet in Japanese, very little information could be found about this sensor, including its behavior. The data sheet provides two different calibration curves. Both of them analyze the change in resistance with load for different conditions. Calibration curve in Figure 18 aims to show the change in the behavior depending on the temperature. Calibration curve in Figure 19 aims to show the change in the behavior for several repetitions or trials.

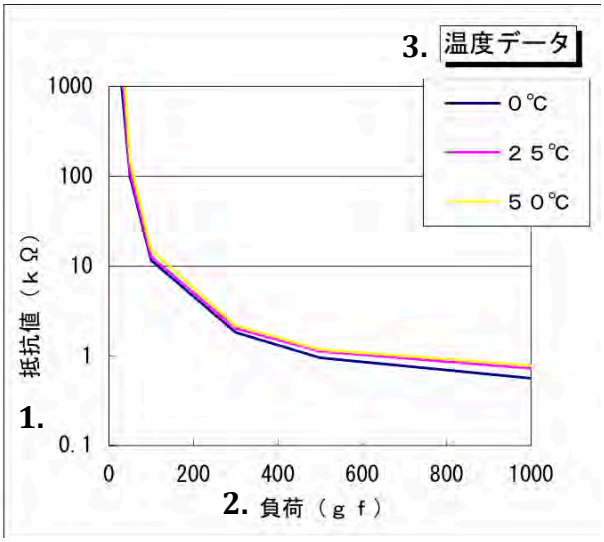

1. Resistance (kΩ)
2. Load (gF)
3. Temperature data

Figure 18. Calibration curve for different temperatures [22]

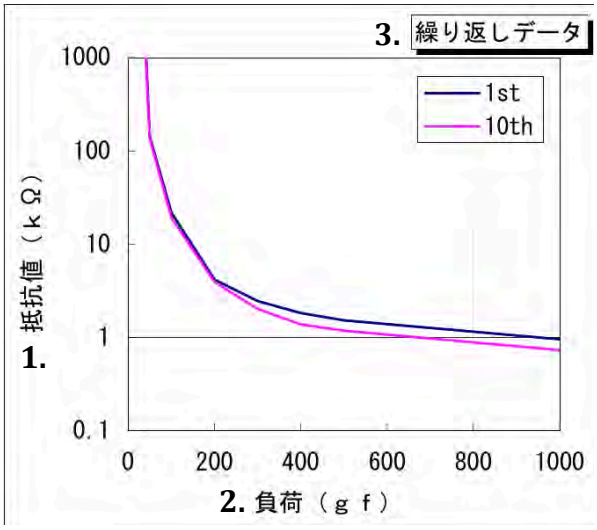

1. Resistance (kΩ)
2. Load (gF)
3. Repetition data

Figure 19. Calibration curve for different trials [22]

The manufacturer does not give any information about how these curves were obtained. Initial trials with the sensors showed that not only these results were quite difficult to reproduce but also that the sensor presents a temporal relation which is not mentioned in the datasheet nor showed in a calibration curve with temporal data.

Due to the lack of information and the behavior seen in these initial trials, it was decided that the sensor had to be calibrated and its behavior mathematically described for its proper implementation.

3.1 Calibration system

As stated before the sensor to be calibrated is the *Inasutoma* sensor, which has a sensing area of 8mm diameter. The most important part in this sensor is the rubber dome, which helps to evenly distribute the force applied to the sensor over its entire surface, allowing to measure pressure and avoiding the sensor to become saturated from punctual applied loads.

Data gathering system

The *Inasutoma* sensor was connected to an electronic circuit for high resolution and low value range measurements. The circuit consists on a voltage divider where the *Inasutoma* sensor is tied to a measuring resistor, referred in Figure 20 as FSR and RM respectively.

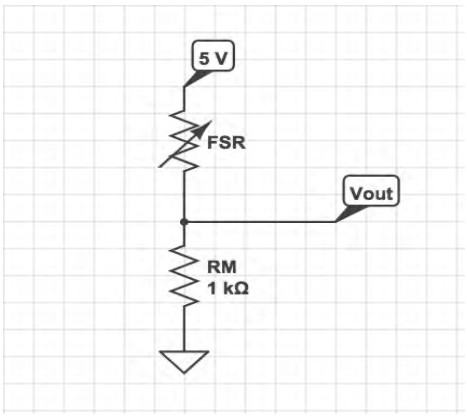

Figure 20. Measurement circuit

The value of the measuring resistor is chosen to maximize the level of sensitivity in the work range (0-1000 g F) and to limit the current through the sensor. [21]

An original and specific calibration system was built for the purposes of this project. It was designed with online Tinkercad software and later 3D printed. The assembly of the calibration system specifically developed to apply a controlled force to the *Inasutoma* sensor can be seen in Figure 21.

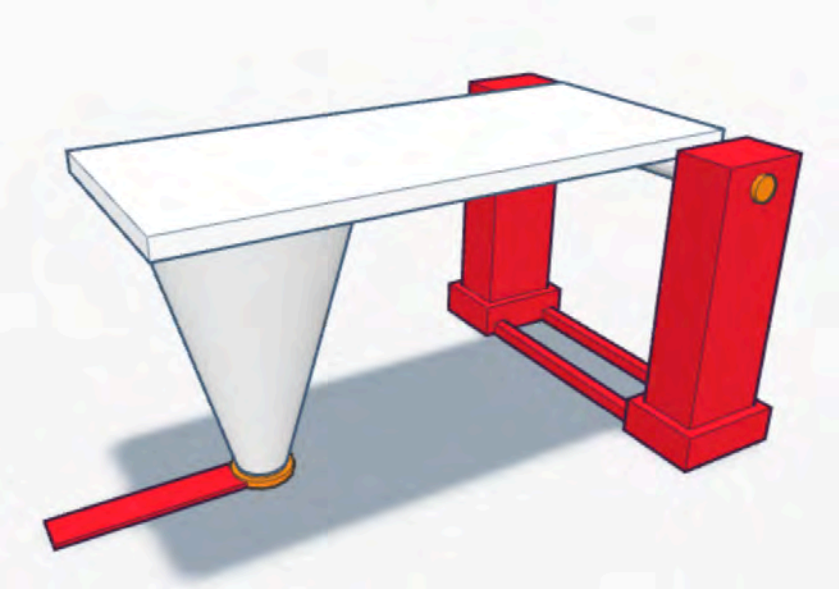

Figure 21. 3D Sketch of the calibration system

By placing weights on the flat surface, a compression force is generated and completely transmitted through the frustum. The frustum has a small surface area of 8mm just as the sensing area of the sensor. In the final implementation a scale was added to the design in order to ensure that the weight was correctly placed on the flat surface and therefore that there was no force lost due to the geometry (Figure 22).

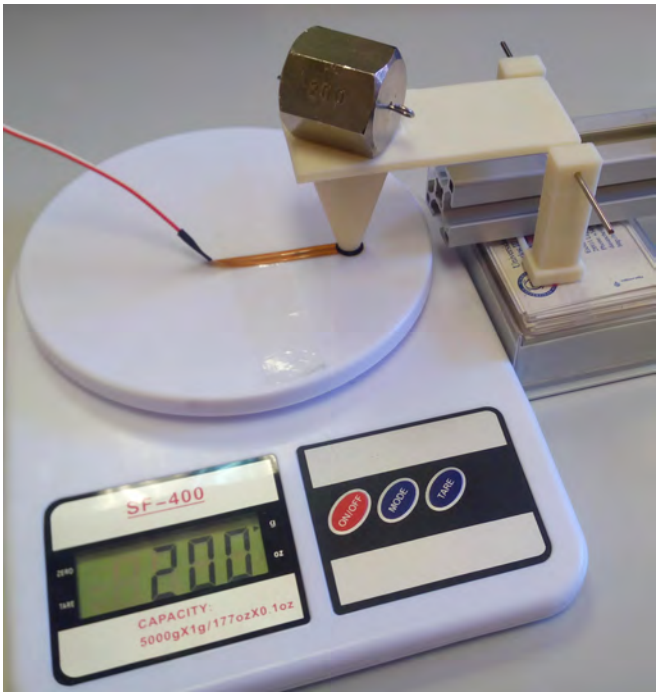

Figure 22. Real calibration system

A STM32F4 microprocessor from STMicroelectronics was programmed with MATLAB and Simulink software for data acquisition. The program reads the signal from the circuit through the microprocessor and plots in real time a (digital) voltage vs. time graph, while storing the data in vectors for post-processing with MATLAB. The program is taking ten measurements each 0.1 seconds or, in other words, it presents a sampling rate of 100 samples per second. These values are stored in a vector with dimension of Nx11. The program also implements a filter to reduce ambient noise that could be introduced during the measurement.

Methodology

Several measurements were taken covering the range 0 – 1000 grams force or 0 – 10 Newtons. The whole range was covered with 200g weights up to 1000g (200, 400, 600, 800 and 1000g). They were placed on top of each other one by one, and later removed one by one to see the hysteresis behavior of the sensor. A smaller range from 0 to 200 grams was covered as well with 40g weights up to 200g (40, 80, 120, 160, and 200g), also by placing them on top of

each other and removing them one by one. This smaller range was covered because the original calibration curve provided by the manufacturer seems to have more measurements in this range and also the sensor's sensitivity seemed to be bigger at low weights than at high weights.

Moreover measurements directly placing 200g, 400g, 600g, 800g, and 1000g weights were performed to see the difference between the behavior of the sensor with and without previous weight.

Positioning the weights

Calibrated weights were placed over the flat surface to obtain a relation between the applied force and the output voltage of the circuit.

The calibrated weights were manually handled. Because their positioning was delicate some noise was introduced in the measurement. This noise was reduced with filters integrated in the Simulink algorithm and during the post-processing of the data.

During the positioning of the weights, the actual weight measured by the scale was written down to control force-voltage relation and for future use in post-processing of the data.

Post-processing with Matlab

In order to reduce the possible noise introduced by manual handling, a mean filter was run through the vector. This mean filter calculates the mean of the 10 measurements for each 0.1s. The output is a Nx2 vector where the data in the first column remains the same, the time, while the data in the second column is the calculated mean. This noise reduction could be considered as a pre-processing step to improve the results for later processing, which in this project includes finding the relation between the applied force and the output voltage.

3.2 Results and interpretation

Figure 23 and Figure 24 show the *Inasotuma* sensor real response for weights from 0 to 1000g for Trials 1-5 and Trials 6-10 respectively. All the original measurements are collected in Annex I.

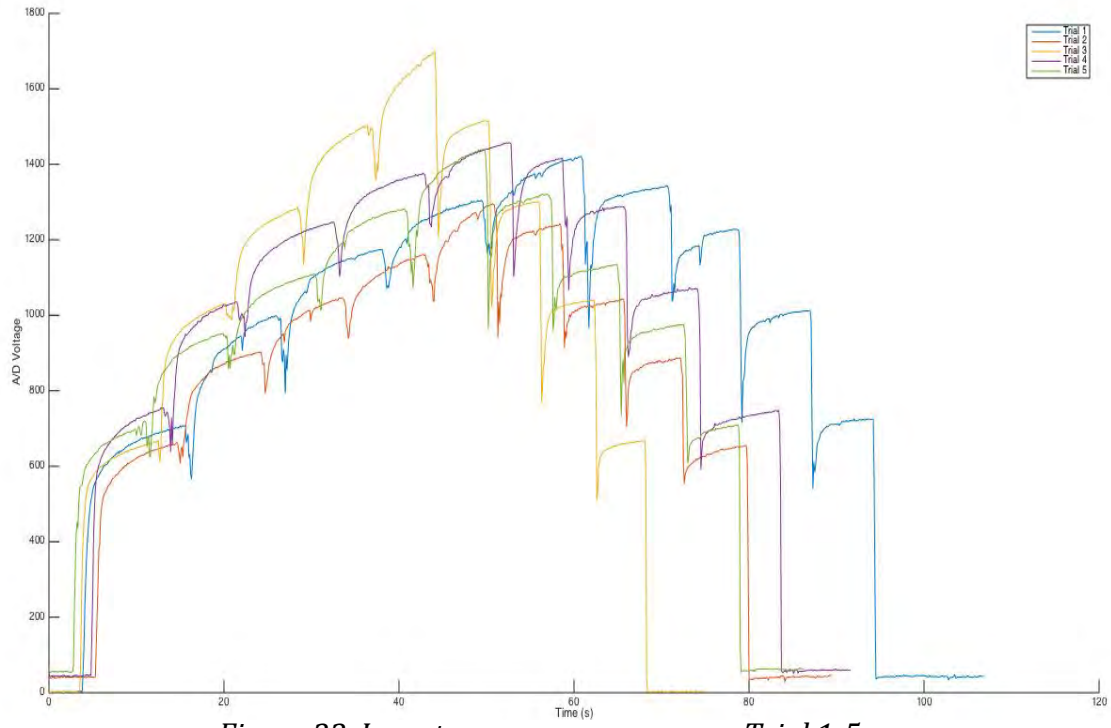

Figure 23. Inasutoma sensor response - Trial 1-5

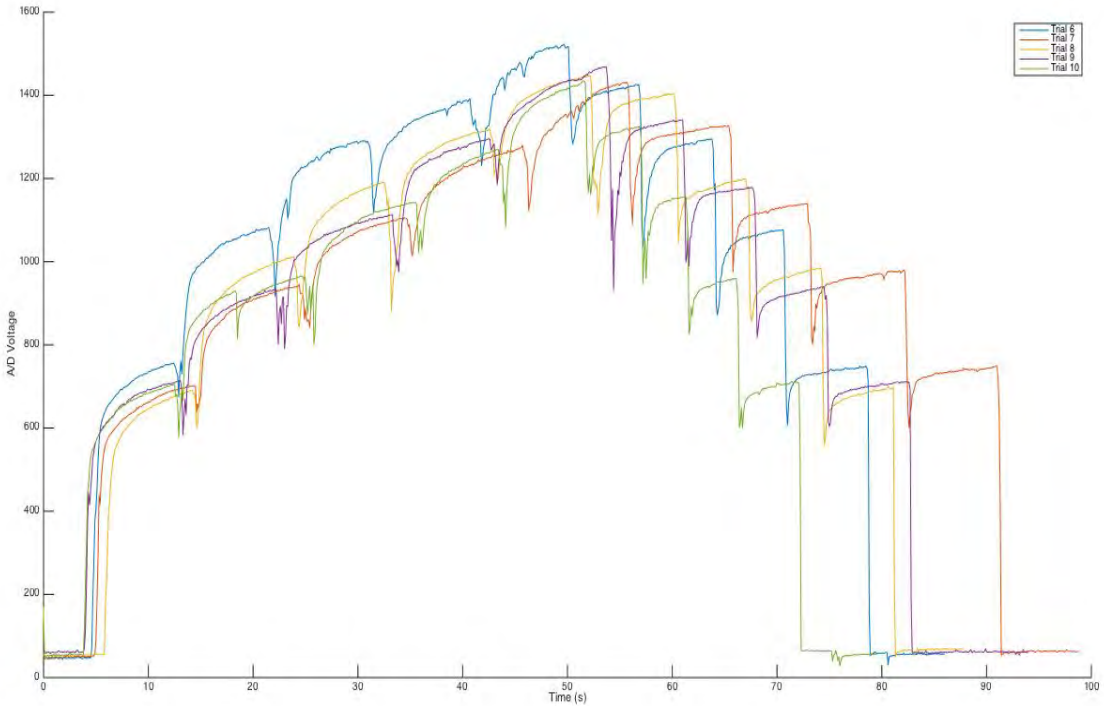

Figure 24. Inasutoma sensor response - Trial 6-10

For further clarifications graph of Trial 3 shown in Figure 25 will be explained. In order not to manipulate the results, a random number generated by MATLAB chose the trial to be explained.

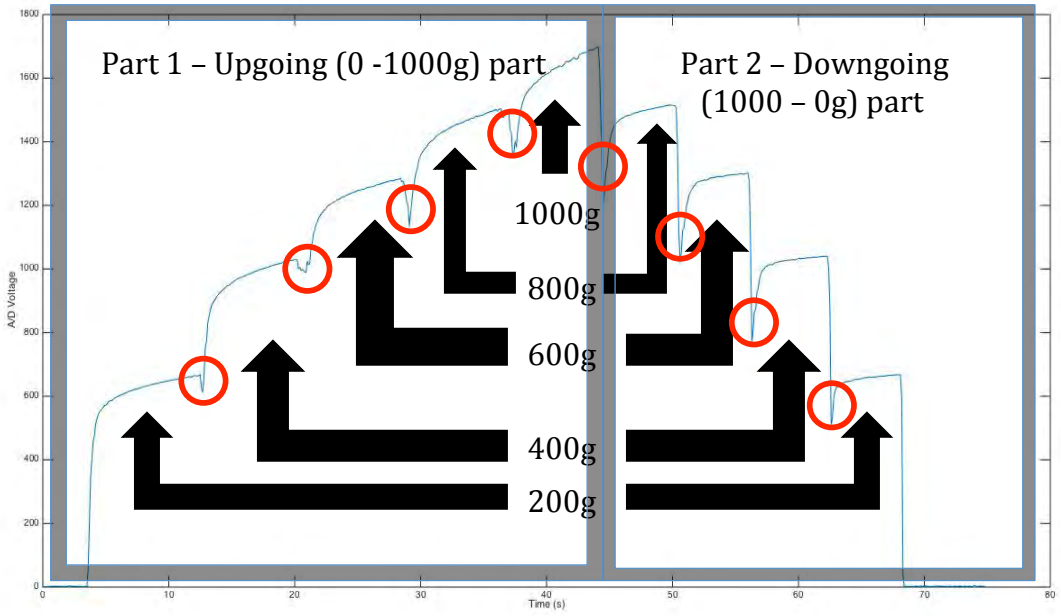

Figure 25. Trial 3 explanatory graph

For every graph there are two different parts that for simplification purposes have been called Part 1 and Part 2. Part 1 corresponds to measurements perform in the 0 – 1000g range by increasing the weight/force applied from 0 to 1000 g, while Part 2 corresponds to measurements also performed in the 0 – 1000g range but in this case by decreasing the weight from 1000 to 0 g. Part 1 will be used to define the mathematical model describing the behavior of the sensor for each weight and to find a mathematical model that defines the response of the behavior for any other weight. Part 2 will be used to see and understand the Hysteresis behavior of the sensor.

Two considerations must be taken into account:

- The sensor does not reach a saturation value, but a saturation rate; this means that a final constant value is not reached. Instead, a final growth rate is in fact reached and from that point on the values will always grow and can be neglected for this project. Manipulation of objects

with a robotic hand is a short-length task and that is why the long-term behavior of the sensor is not considered.

The proposed mathematical model in next section 3.2 does not hold true for infinite times but it does for short times applications like the ones interesting for this project.

- The peaks appearing between two consecutive weights, marked with red circles in Figure 25, are not due to the behavior of the sensor but to the manual handling of the weights during the calibration. They must not be taken into account.

  Therefore the value from where the measurement starts in a new weight has to match the last chosen value in the previous weight (Figure 26). E.g. Final value for 200g measurements is 600 so the first value for 400g measurements is not the value obtained at the next measurement point, which would correspond to a peak, but at the time where it is 600 again.

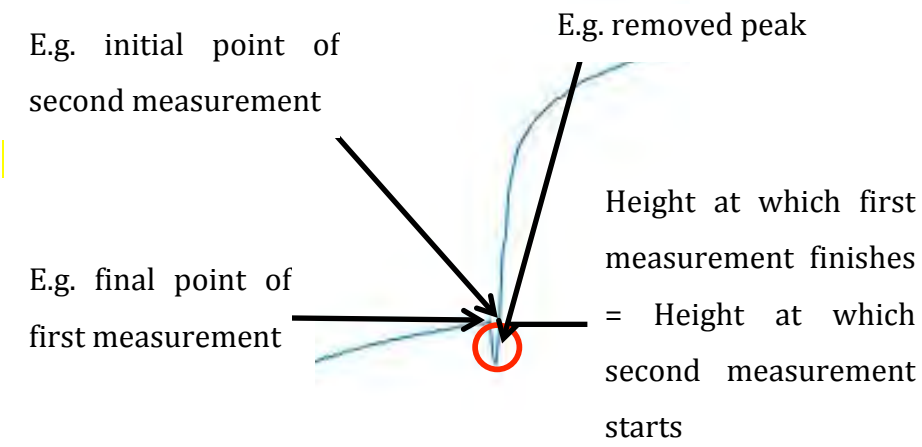

Figure 26. Explanation of the removal of the peaks

Based on these results, different behavior possibilities were considered and discharged. The calibration method designed for this project graphically showed that the *Inasutoma* sensor has a step response that changes for each weight or force applied comparable to that of a first order system (Figure 27).

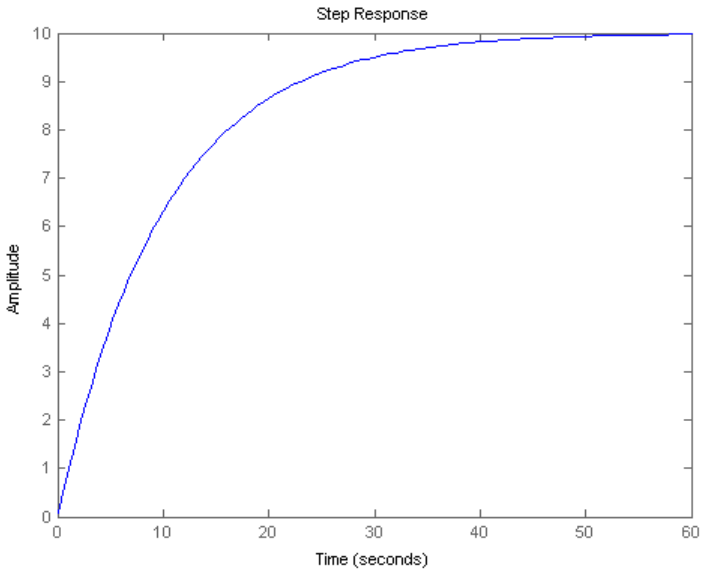

Figure 27. Example of first order system step response graph

First order systems are characterized by two different parameters: the gain k and the time constant τ. The gain k is determined by the magnitude of the output when a known input is applied, while the time constant τ is determined by how fast the system reaches the magnitude of the output.

A different response can be observed for each weight. Theses responses behave very similar to first order systems, defined by their own gains and time constants, according to the formula in Equation 1:

$$\boldsymbol{A/D\ Voltage} = \boldsymbol{k} * (\mathbf{1} - \boldsymbol{e}\text{^}(-\boldsymbol{t}/\boldsymbol{\tau})) \qquad (\mathbf{1})$$

In order to find k and τ every trial had to be divided in five parts according to each weight (200, 400, 600, 800 and 1000g). The division of the data for each graph was a complicated process due to properties of the sensor and manual handling of the calibration system, which introduced errors that had to be removed before further analysis.

By plotting all parts for the same trial in one plot (Figure 28), a pattern for k and τ can be inferred: as the weight/force applied is increased, k must decrease and τ must increase. Further analysis, which can be found in next section 3.3, confirmed this hunch.

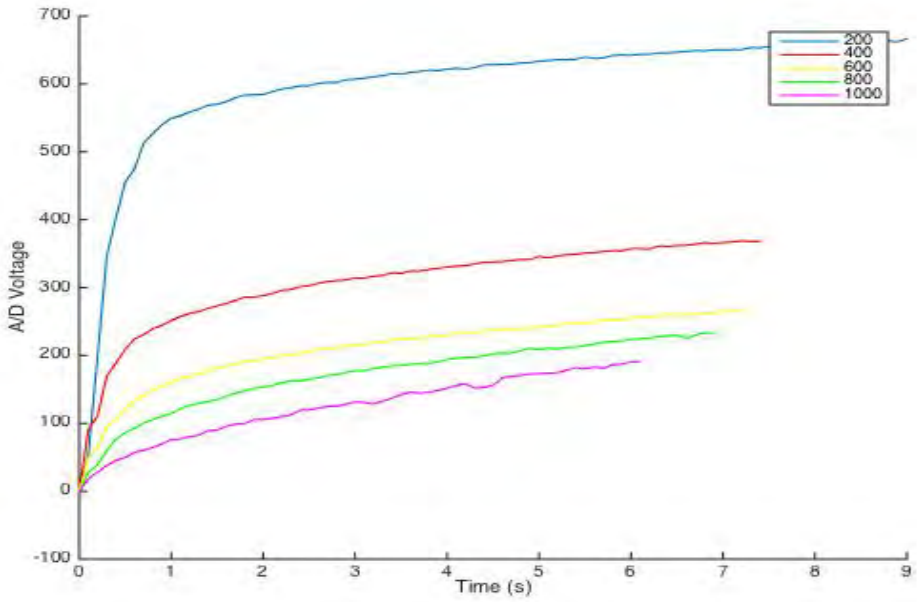

Figure 28. Trial 3 – Separated parts for 200, 400, 600, 800 and 1000g corresponding to Part 1

The same study was performed with Part 2 of each graph, shown in Figure 29. In this figure it can be observed that the values for each weight are slightly different. It was known beforehand that these sensors presented Hysteresis behavior and it was confirmed with this study.

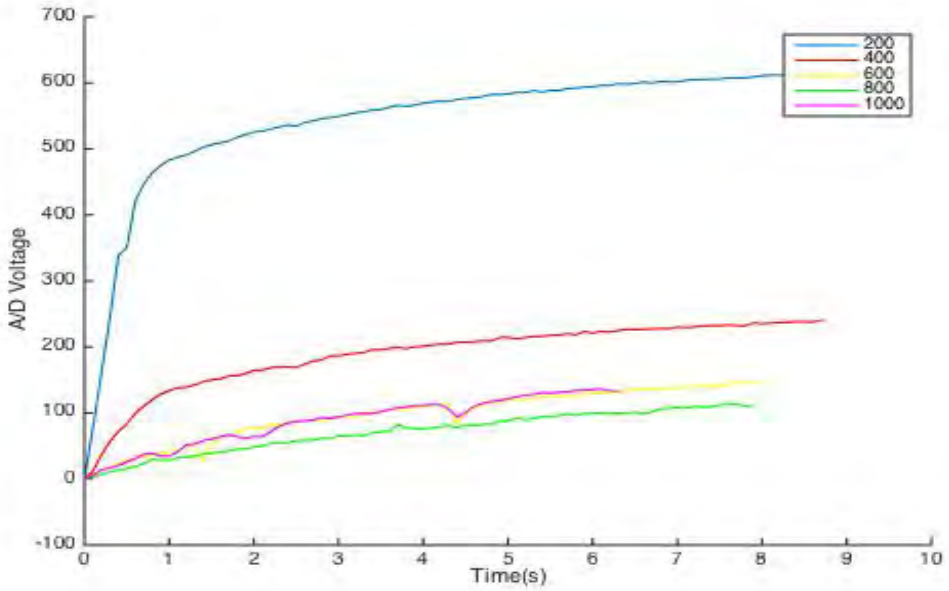

Figure 29. Trial 3 – Separated parts for 200, 400, 600, 800 and 1000g corresponding to Part 2

This procedure was also repeated for five trials in the range 0-200g, increasing 40g each time. Again by plotting all parts of the same trial in one plot, the same pattern for k and τ was observed: as the weight/force applied is increased, k must decrease and τ must increase. Also the original measurements for this range could be found in Annex I.

3.3 Mathematical models

Once the behavior was observed, a mathematical model was adjusted. Several steps are required for the adjustment of the model. The first one is to manually find the values of k and τ for each weight and each trial that model a first order system as close as possible as the real curve. Both values of k and τ were manually calculated and later introduced in a MATLAB script for modeling of the first order systems in order to compare the model with the real values obtained. The second step is to statistically adjust these values to find those that reduce the Mean Square Error.

k can be calculated straight forward from the measurements with the formula in Equation 2:

$$\boldsymbol{k = \frac{V_{final} - V_{initial}}{Weight}} \qquad (\mathbf{2})$$

where V_{final} is the A/D voltage value in the last measurement, $V_{initial}$ is the voltage in the first measurement, and *Weight* is the actual weight sensed by the scale and previously wrote down during the recording of the measurement.

Calculating τ is a rougher and more manual process than calculating k. Originally τ corresponds to a 63.7% of the time it takes to reach the final value. It is known that the *Inasutoma* sensor does not behave as a first order system for long times and therefore the final value recorded does not correspond to the interesting behavior of the sensor in this project. Accordingly the value of τ had to be adjusted to obtain a curve as close as possible to that seen in the real measurement. This was achieved by multiplying τ by a variable parameter c smaller than 1. This parameter actually reduces the total measured time so it matches the point where the sensor stops behaving as a first order system. The final formula to calculate τ is presented in Equation 3:

$$\tau = c \cdot (0.637 \cdot t_{total}) \qquad (3)$$

where t_{total} is the time elapsed from the first measurement to the last one.

As illustrative example comparison between the real response of the sensor and the modeled response of the sensor are shown in Figure 30 and Figure 31. They correspond to the response of the sensor in Trial 4 and Trial 9 with a 1000g weight, respectively.

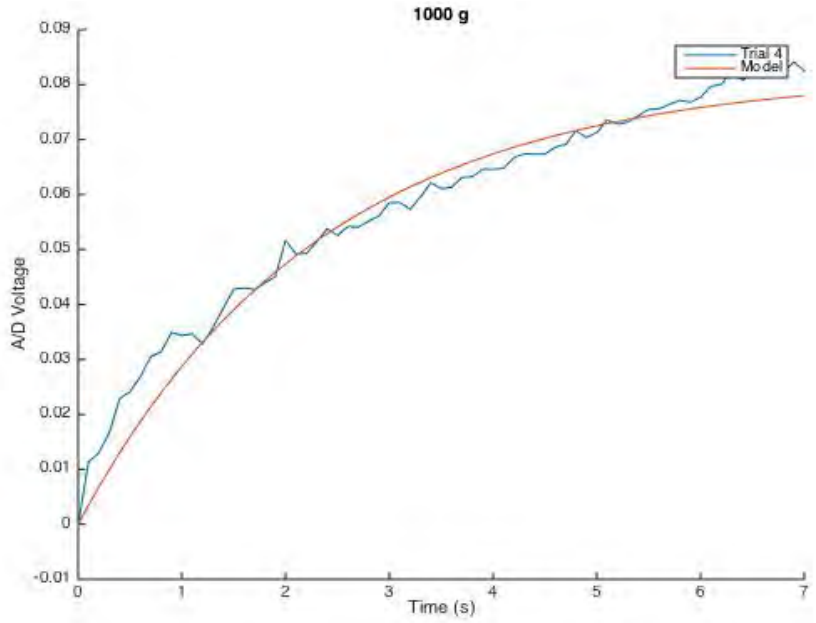

Figure 30. Trial 4 - Modeled response vs. Real response

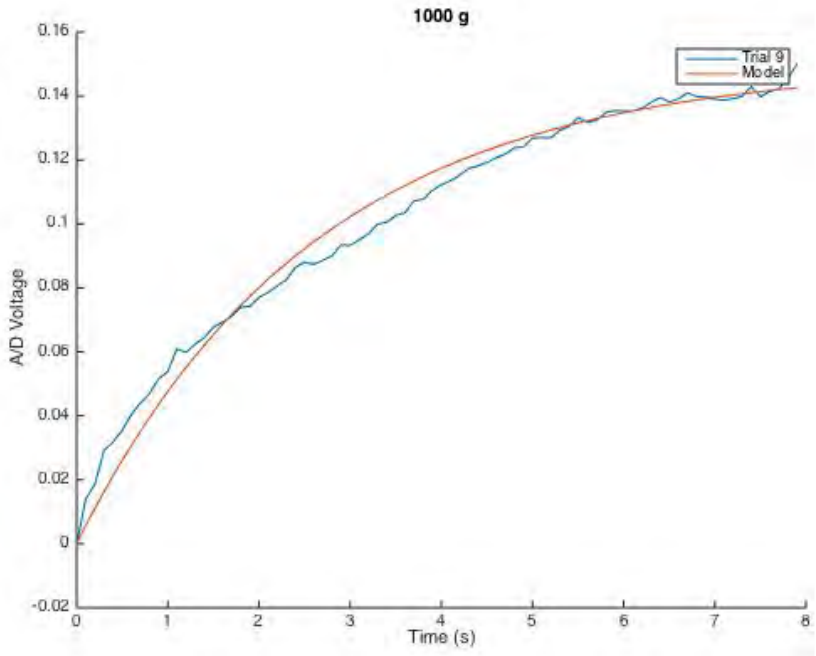

Figure 31. Trial 9 - Modeled response vs. Real response

Furthermore the mean value of k and τ for each weight for each trial (all ten from 0 to 1000g and all five from 0 to 200g) was obtained. With these values of k and τ, a modeled response for each weight was calculated, so ten models (one for each weight) were obtained. This means that for the previous example shown in Figure 30 and Figure 31 only one model was obtained (Figure 32). Models for each weight using mean values could be found in Annex II.

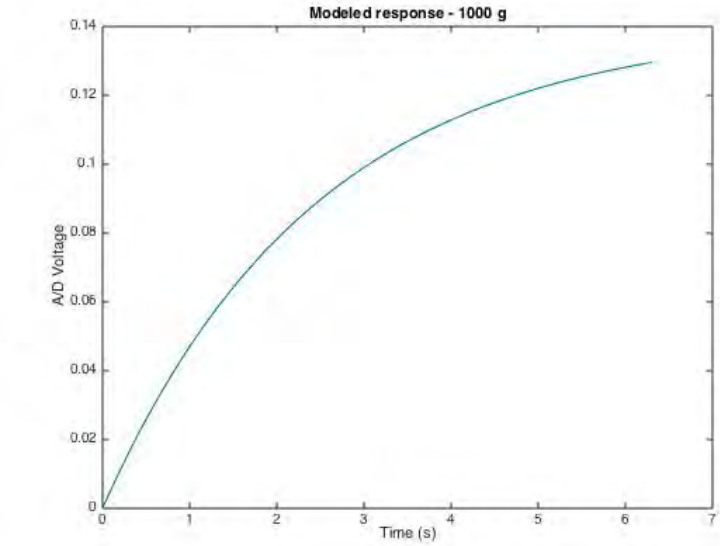

Figure 32. Modeled response for 1000g with k = 0.1403 and τ = 2.4512

After obtaining all the models based on the mean values of k and τ for the different weights, the next step is to see the error these models have and try to minimize it by statistically adjusting the values of k and τ. In this step the Mean Squared Error (MSE) is calculated and then a search is performed to find the combination of the values of k and τ that minimizes this error for each generated model.

The MSE measures the average of the squares of the errors, that is, the difference between the estimator and what is estimated. In this case the estimator is the real response of the sensor and what is estimated is the modeled response of the sensor. The formula shown in Equation 4 is used to calculate the MSE for each weight:

$$\boldsymbol{MSE} = \sqrt{\frac{\mathbf{1}}{\boldsymbol{N}}\sum_{\boldsymbol{i=1}}^{\boldsymbol{j}}(|\boldsymbol{V_{trial1}(i)} - \boldsymbol{V_{model}(i)}|^{\mathbf{2}} + |\boldsymbol{V_{trial2}(i)} - \boldsymbol{V_{model}(i)}|^{\mathbf{2}} + \cdots + |\boldsymbol{V_{trial10}(i)} - \boldsymbol{V_{model}(i)}|^{\mathbf{2}})} \quad (\mathbf{4})$$

where *j* is the minimum length of the measurement vectors. Why the minimum? Because this way it is ensured that the same number of samples are taken from each trial. *N* is the total number of samples taken into account and can be easily obtained by simply multiplying *j* by the number of trials (ten for 0 – 1000g and five for 0 – 200g).

In the previous example shown in Figure 32, the mathematical model calculated for the 1000g weight has a *MSE = 0.0852*. The MSE was obtained as well for all the weights.

These models with their respective MSEs were calculated by using the mean k and τ values of each weight, but what happens if these values are not the best fits for modeling the response? Some research must be performed in order to ensure that the model obtained is the best or if by the contrary, there happens to be another combination of k and τ that reduces the MSE for the model.

For this purpose a MATLAB code was created. It goes over all the possible combinations of k and τ in an area enclosed by the rectangle formed between the minimum and maximum values of k and τ. For example, Figure 33 shows the rectangle formed for the 1000g weight. All the areas used to find the values of k and τ that minimize the error could be found in Annex III. With these areas are also shown both the mean values of k and τ and the values of k and τ minimizing the error, as well as their respective MSEs.

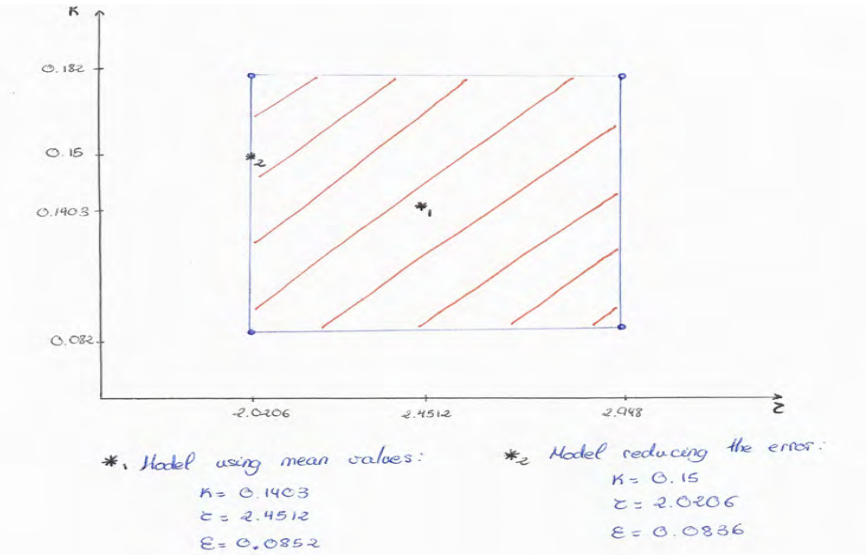

Figure 33. Area used to find the combination of k and τ that minimizes the error

The obtained values of k and τ minimizing the error will be used to generate a new model for each weight. For example, Figure 34 shows the model minimizing the error for the 1000g weight. Every final model minimizing the error for each weight could be found in Annex IV.

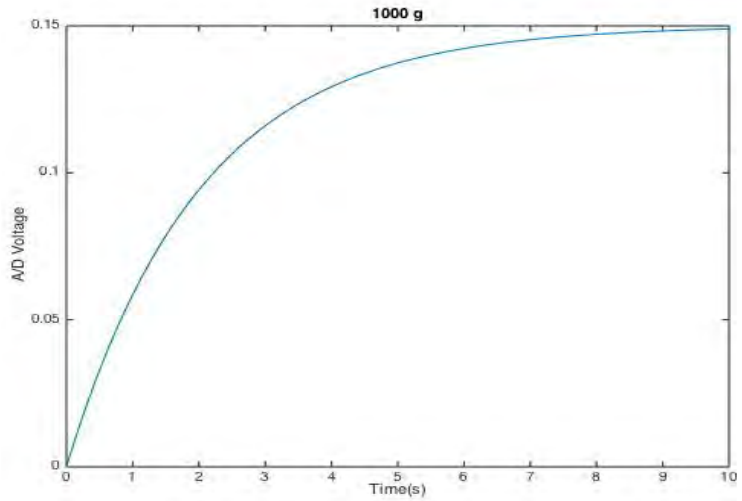

Figure 34. Modeled response for 1000g minimizing the error

Once the most accurate values of k and τ were obtained, the fashion of their behavior could be seen and adjusted in a curve as shown in Figure 35. Graphs showing the fashion followed by k and τ in both intervals 0–1000g and 0–200g could be found in Annex V.

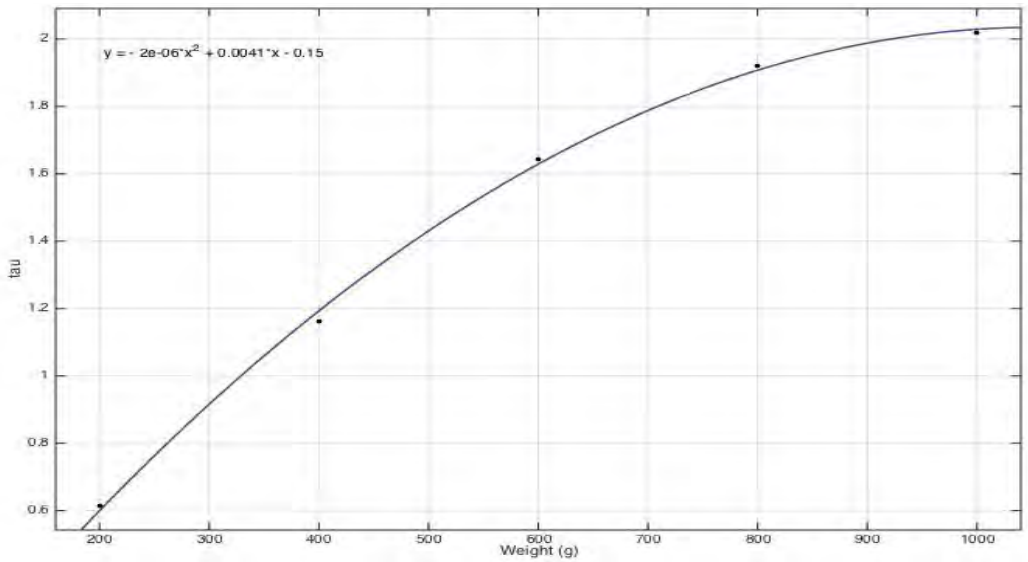

Figure 35.Fashion following by tau in the interval 0 – 1000g and the mathematical equation describing it

This way k and τ could not only be known for the trial weights but also for any desired weight. The mathematical equations describing the fashion curves are used to obtain k and τ for any weight. Once k and τ are known, a mathematical first order system describing the behavior of the sensor can be obtained.

4. INTEGRATION OF *INASUTOMA* SENSORS IN GIFU HAND III

The integration of the sensors in the Gifu Hand III was not a straightforward process. A lot of work and effort was deployed in this part in order to ensure the best performance of the sensors.

4.1 Fingertips

New fingertips had to be designed in order to mimic the anthropomorphic shape of the human hand and in order to facilitate the attachment of the sensors.

Why are the original fingertips of the Gifu Hand III, shown in Figure 36, not useful?

Figure 36. Original fingertip of the Gifu Hand III

- They are completely round. This not only implies that the fingertip is not anatomically consistent but also that the attachment of the sensor to the surface is almost impossible to be performed since it does not present any planar surface.
- They are completely curved and present no planar surface. This is also anatomically inconsistent and will be important for the response of the sensor during operation of the hand.

- Their surface is sliding. This is mostly important for sensor attachment and for grasping. The cover of the original fingertips is a very sliding plastic and therefore the sensors could not be attached by any means without risking their integrity or the integrity of the original fingertips. Moreover grasping of objects becomes a complicated process with very smooth surfaces.

With all this information, it was decided to take advantage again of the new 3D printing techniques in order to design fingertips that adapt to the needs of this project.

The two main parameters taken into account for the design were the plastic use for 3D printing and the curvature of the finger. On the one hand the plastic used for printing was Poly-Lactic Acid (PLA), which produces surfaces that are rougher than the original ones. This makes PLA suitable for the project since it will eliminate the problem of the sliding surfaces. On the other hand, the curvature of the fingertip is almost constant among individuals. It was measured and compared with different people and adjusted to the size of the Gifu Hand III.

An initial sketch that did not take into account the curvature of the fingertip was designed, as shown in Figure 37. This sketch was upgraded to include the curvature of the fingertip, as shown in Figure 38. This sketch also takes into account the future PDMS cover so that there is no hump between the fingertip and the phalanx of the finger.

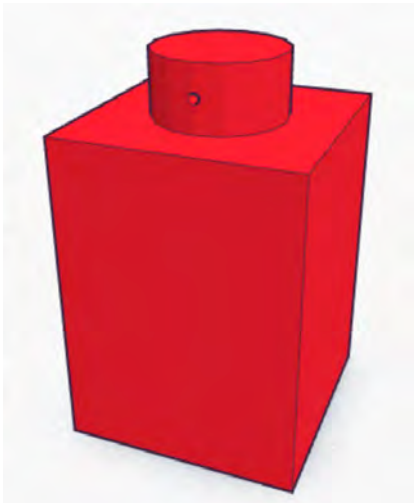

Figure 37. Initial sketch of new fingertip for Gifu Hand III

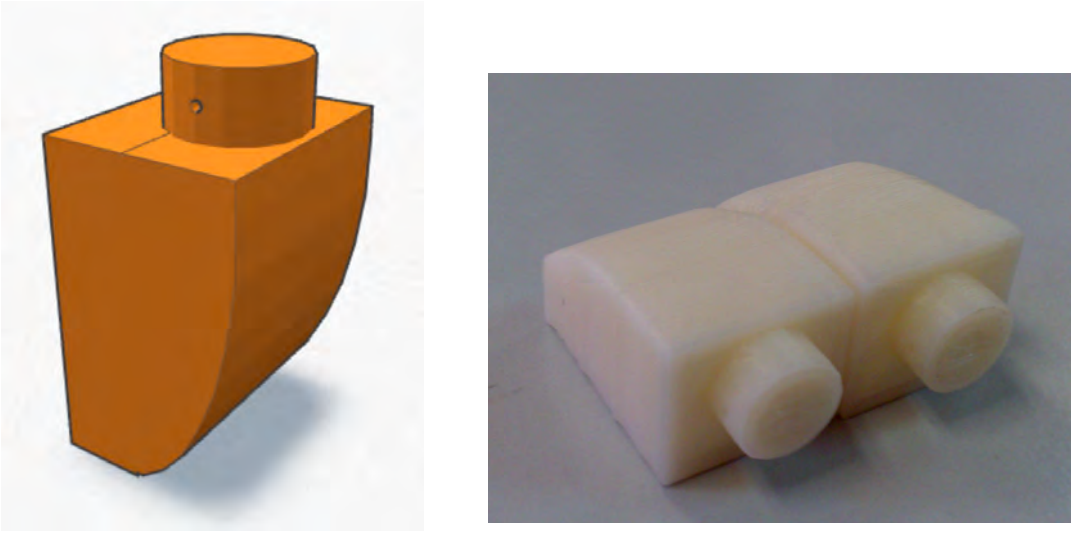

Figure 38. Final sketch (left) and real 3D-printed fingertips (right)

The most remarkable characteristics of the design are:

- Its surface is not sliding, allowing attachment of the sensors without risking their integrity.
- It is anatomically correct in the surface of interest, that means the surface where the sensors will be attached, allowing for a more real interaction of the hand with objects and therefore a correct response of the sensor.

4.2 Polydimethylsiloxane (PDMS)

Once the sensors were attached, the surface of the fingertips was covered with a rubber to improve performance. Covering the sensors with a rubber is one of the most recent advances in the field of sensors. Rubbers increase the compliance, how well it adapts to the shape of the object, as well as the grip ability of the surface.

In this project the rubber chosen was Polydimethylsiloxane (PDMS). The student suggested this polymeric rubber because he had experience working with it in the laboratory and knowledge about its properties and way of

fabrication and he could adapt it to the purposes of the project. Moreover after some research, it was found out that one of the latest publications showed tactile sensors using PDMS (Figure 39) as the dome to improve performance. [23]

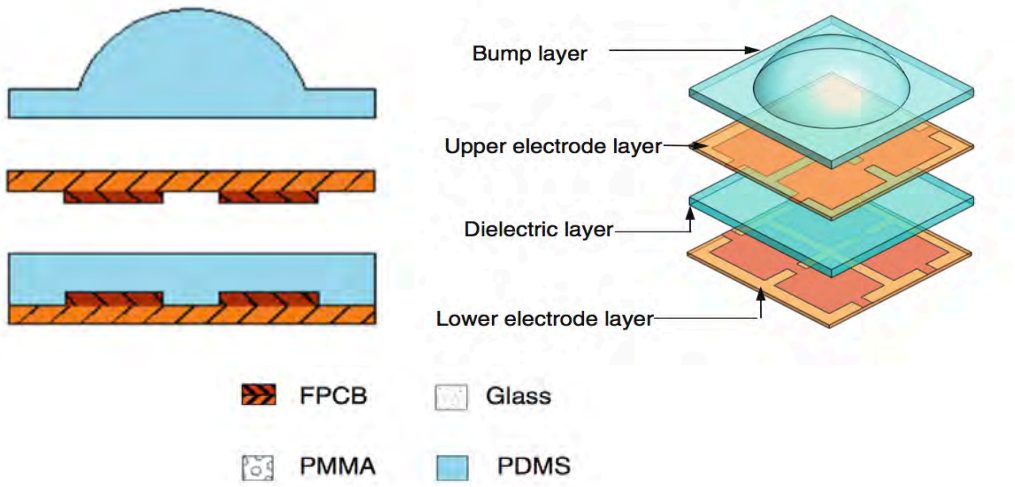

Figure 39. Tactile sensor with dome made of PDMS [23]

Properties

PMDS is a polymeric compound that belongs to the group of silicones. PDMS is quite used in biomedical applications due to its properties and it is the most used biological rubber when it comes to interaction of robotic parts with the human body, such as in prosthesis or sensors.

The most interesting properties of PDMS for this project are:

- PDMS is inexpensive. It is a very cheap material, especially when compared to the prices of robotic components.
- PDMS can be shaped during the fabrication process. Therefore it can be adapted to most surfaces and shapes like the fingertips with the sensors.
- PDMS surface roughness is similar to the skin, producing a more natural object-surface interaction.

- PDMS is a hyperelastic material, whose elasticity can be controlled during the fabrication process. This implies that PDMS exhibits great mechanical properties.
- PDMS is soft, unlikely to damage hard surfaces. This eliminates any risk of damaging the sensors or the fingertips.
- PDMS is relatively inert, making it suitable for works in hazard environments such as manufacturing of chemicals.
- PDMS is biocompatible. It does not produce immunological reactions outside (e.g. allergy) or even inside (e.g. implant rejection) the body, ensuring user safety.

Fabrication process

Fabrication of the PDMS structures to cover the fingertips with the integrated sensors is a complex process that must be carried out in the laboratory under controlled conditions. Besides the typical laboratory instrumentation (e.g. pipettes, oven, gloves, ...), three special components, shown in Figure 40, are needed to produce PDMS structures: Sylgard polymer (left), curing agent (center), and puffy paint (right).

Figure 40. Sylgard polymer, curing agent and puffy paint

The fabrication process took place as follows:

First, the sensor shape was drawn in a petri dish with puffy paint. Puffy paint becomes solid when heated, allowing for creating 3D characteristics into the PDMS structure. The petri dish was placed in the oven for this purpose. Note that in order to reduce costs each petri dish was used for 4 fingertips.

Second, the PDMS gel (Figure 41) was fabricated through a curing mechanism with Sylgard polymer and a curing agent. The amount of each determines the elasticity of the PDMS; in this case 3g of curing agent were used for each 30g of polymer. Thorough mixing of these two components is essential for good curing.

Figure 41. PDMS gel

Third, the PDMS was poured in the petri dish with the puffy paint pattern (Figure 42). Bubbles appear in the PDMS mixture. They degrade the optical qualities of the PDMS and therefore they have to be removed. This is achieved by using a vacuum chamber. Note that the optical properties of the PDMS are not of particular interest for the means of this project and therefore the remaining of some bubbles would not suppose a problem.

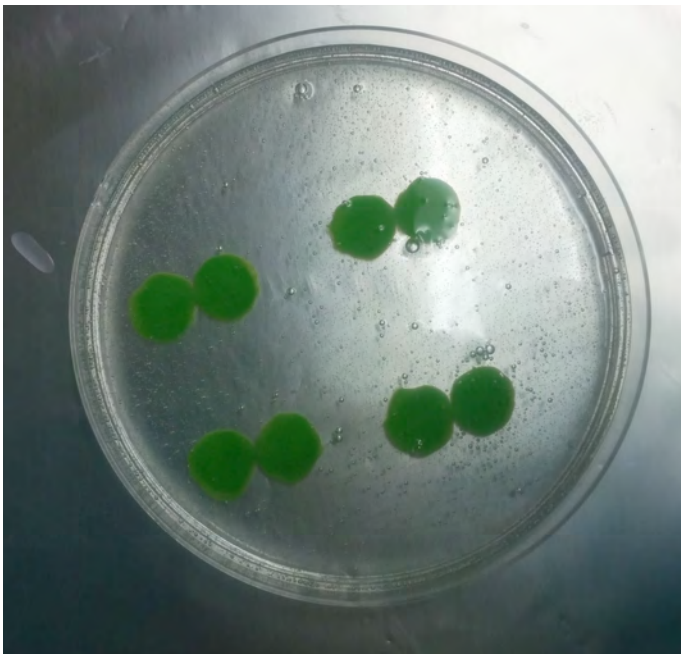

Figure 42. PDMS on petri dish before removal of the bubbles

Fourth, after removal of the bubbles, the petri dish was placed again in the oven for curing. Once cured, the PDMS becomes an elastic solid with 3D characteristics that perfectly adapt to the fingertips (Figure 43).

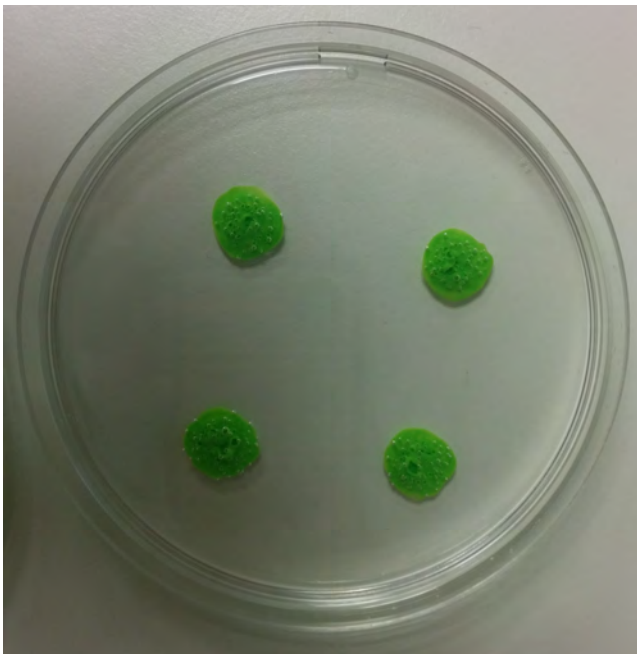

Figure 43. PDMS structure after removal of the bubbles and curing

4.3 Assembly

For the purpose of this project two different PDMS structures were created in the laboratory. The one shown in Figure 42 corresponds to a model where two sensors will be included in one fingertip, while the one shown in Figure 43 corresponds to a model where only one sensor will be included in the fingertip. Both were created following the same methodology explained in Section 4.2. These structures were designed to give 3D properties to the PDMS in such a way that the cavities introduced are later filled with the dome of the sensors, as shown in Figure 44.

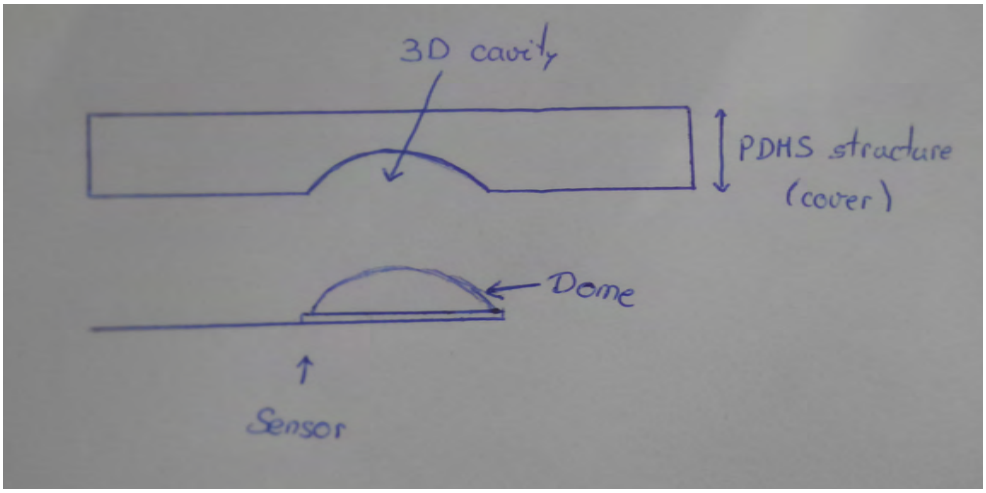

Figure 44. 3D PDMS cover sketch

The last step in the integration of the sensors in the Gifu Hand III is the assembly of the three different parts (the sensors, the new fingertips and the PDMS cover) together, and the assembly of the final structure into the robot hand.

The sensor must be attached to the surface of the fingertip. The sensor base cannot be glued to the surface because if detachment were needed, it would destroy the sensor. On the other hand the integrity of the flexible board is not compromised when glued to the surface and is easily detached by using a dissolvent. Therefore only the flexible board was glued to the surface.

The PDMS must be unmolded and cleaned in order to wash off the puffy paint. As it is biocompatible and quite resistant to chemicals, this process can be achieved by simply rinsing the surface with water. Once cleaned, it must be cut into four pieces in order to obtain four PDMS covers for four fingertips (Figure 45). Each piece was precisely measured in order to make the "hole" in the PDMS match the position of the sensor on the fingertip. This was performed with the two PDMS structures, the one designed for 2 sensors on one fingertip and the one designed for 1 sensor on one fingertip.

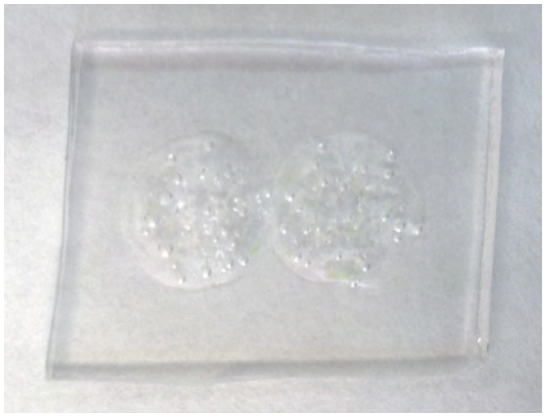

Figure 45. PDMS cover of one fingertip with 2 sensors

Then each piece must be integrated in the fingertip. Glue was spread onto the surface of the fingertip and around the sensor, and the PDMS pressed against it until total attachment. The final result for both types of fingertips, with 1 and with 2 sensors, is shown in Figure 46 and Figure 47.

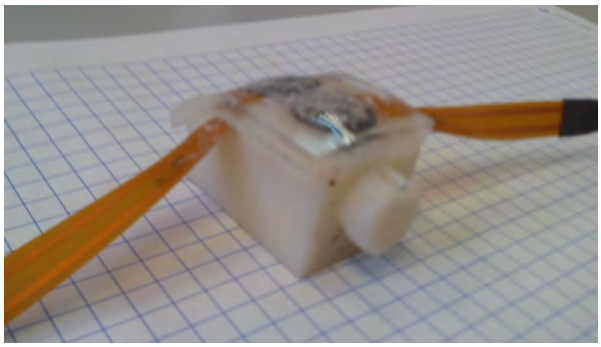

Figure 46. Integrated structure - 2 sensors

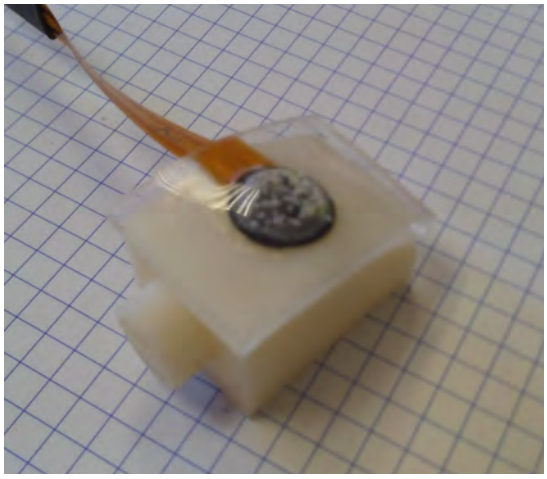

Figure 47. Integrated structure - 1 sensor

With this structure assembled, it was screwed in the hand. For this purpose the holes in the 3D-printed fingertip had to be widened so that the original screws could be re-used. Although the structure did not suffer any damage during this process, it has been decided that for further works the holes will be widened before attaching the sensors and the PDMS to the surface of the fingertip in order to reduce any chance of damage.

The final integration of the sensors in the hand is shown in Figure 48 to Figure 51.

Figure 48. Sensors integrated in Gifu Hand III

Previous figure shows Gifu Hand III with the new fingertips with the sensors assembled.

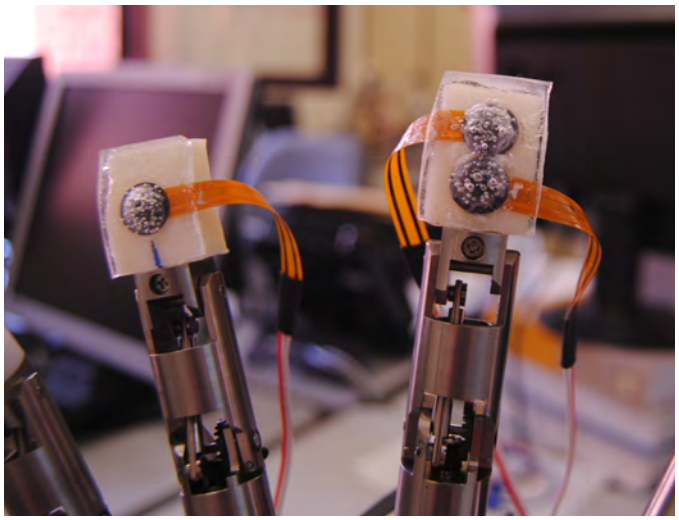

Figure 49. Sensors integrated in Gifu Hand III (Detail)

Figure 49 shows a detail of two of the fingertips, one incorporating one sensor and one incorporating two sensors.

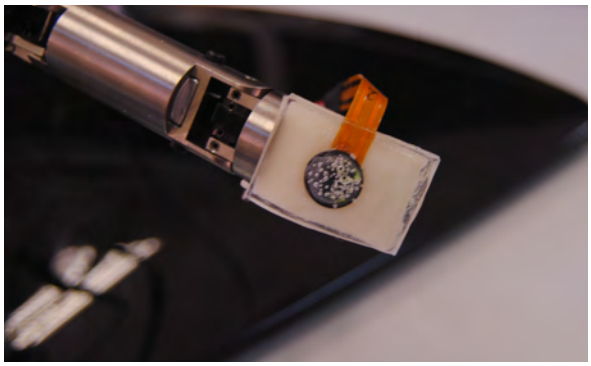

Figure 50.Sensor integrated in Gifu Hand III (Detail)

Figure 50 and Figure 51 show a detail of the fingertip assembled in the thumb. Figure 51 is a lateral view of the final structure. It is especially relevant because in this figure it can be seen that there is no hump on the surface of the PDMS and also that the PDMS surface is flush with the surface of the phalanx.

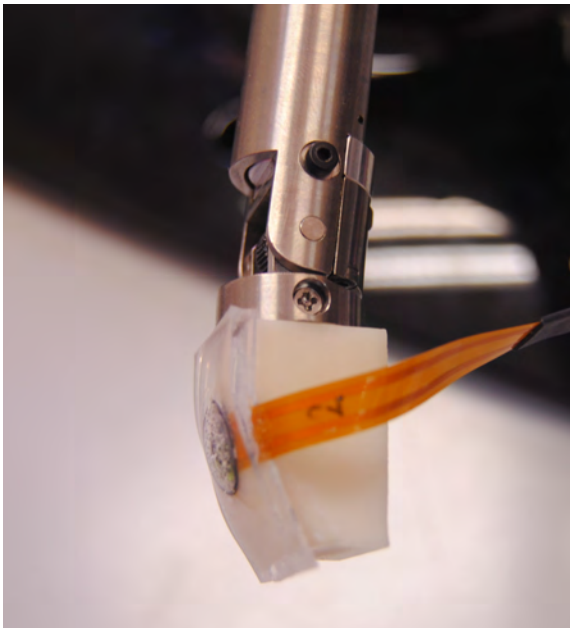

Figure 51. Sensor integrated in Gifu Hand III (Detail)

5. CONCLUSIONS AND FUTURE WORK

The present Bachelor's Thesis has been developed inside a line of research of robotic hands with tactile sensors for grasping and manipulation purposes. It has been focused on the calibration of the aforementioned sensors and their proper integration in the robotic hand Gifu Hand III.

After a review of the proposed calibration methods in the literature, an approach for the *Inasutoma* sensors was designed based on an initial behavior observation. The designed method implies a 3D printed calibration system specifically adjusted to the dimensions of this sensor.

The calibration was assessed by placing different weights on top of the calibration system. The data of the calibration was gathered for two different ranges: 0–1000g and 0–200g; this smaller second range was studied due to the higher sensitivity of the sensor for small weights. Data analysis showed that the *Inasutoma* sensors act as a first order system whose behavior could be mathematically described. With the definition of the mathematical models for each weight, a pattern to describe models for every desired weight was obtained. This way the behavior of the sensor could be known and analyze beforehand. The obtained mathematical models are not completely adjusted to the real behavior and therefore they present some error, analyzed with the Mean Squared Error. This error is in big part introduced by the hysteresis behavior of the sensors, since they do not behave in the same manner after and before being exposed to an initial deformation.

Once the behavior of the sensors was clearly defined, they were integrated in the hand. For this purpose new fingertips were designed and 3D printed to replace the original ones. Although these fingertips are anatomically correct in the region of interest, some improvement could be performed in the general design for aesthetic reasons. The sensors were attached to these new fingertips following different configurations and later covered with PDMS to improve grasping properties. This later process could be improved by curing PDMS in molds perfectly adapted to the shape of the fingertips.

Future works lines will focus on:

- Creating of new PDMS covers. This includes trials of covers with different PDMS conformation and with different thickness. The amount of polymer and curing agent used to form the PDMS gel rules the conformation the amount of PDMS gel poured in the petri dish rules the thickness.
- Analyzing the behavior of the sensor with the PDMS cover. Some trials must be performed in order to ensure that the mathematical models described for the behavior of the sensor without PDMS cover still hold true with the it.
- Trials of hand grasping and manipulation of real objects. This will check if the sensors needed repositioning within the fingertip surface or if the fingertip surface needed to be redesign for proper contact.

BUDGET

In this part the total cost of the value of the project presented along the document will be calculated, detailing each cost separately. Note that this budget is the one needed to start from scratch, without any prior resources.

Human Costs

Human costs have been divided into two categories: type of staff and project section. The first division is due to the wage gap between the thesis tutor and the engineering student while the second division details the hours spent on each section of the project.

The following structure has been used for the division of the project into sections:

- Planning. This section includes familiarization with the software, initial observation of behavior of the sensor and the general design of the project.
- Development. This section includes 3D printing of the calibration system, data gathering, data analysis, and definition of the mathematical models.
- Laboratory. This section includes the fabrication of the 3D PDMS structures.
- Assembly. This section includes 3D printing of the fingertips, the integration of the sensors with the PDMS in their surface, and the final assembly of the structure in the hand.
- Thesis. This section includes both the wording and the correction of the thesis report.

		Thesis tutor	Engineer (Student)
Planning	Familiarization (h)	0	30
	Initial observation (h)	5	15
	General design (h)	5	30
Development	Calibration system (h)	0	10
	Data gathering (h)	5	30
	Data analysis (h)	5	40
	Mathematical models (h)	5	30
Laboratory	PDMS structures (h)	0	15
Assembly	Fingertips (h)	5	15
	Integration (h)	2	10
	Final assembly (h)	0	2
Thesis	Wording (h)	0	60
	Correction (h)	10	20
Total	Total (h)	42	307
	Salario/hora (€)	50.00	30.00
	Salario total (€)	2,100.00	9,210.00
	Total (€)		**11,310.00**

Table 1. Disaggregated human costs

Material Costs

Material costs include everything associated to hardware, software and laboratory costs.

Software costs include all the licenses needed for the accomplishment of this project: Windows 8, Matlab and Simulink, and their associated toolboxes.

Although these licenses are quite expensive, they will be used in later phases of the project and therefore the cost is justified.

Software	Cost (€)
High-end laptop	900.00
Windows 8 - License	119.00
Matlab - License	2,000.00
Curve Fitting Toolbox	1,000.00
Simulink - License	3,000.00
Simulink Desktop Real-Time Toolbox	2,000.00
DSP System Toolbox	1,250.00
Communication System Toolbox	1,250.00
Tinkercad Online Software	0.00
TOTAL (€)	**11,519.00**

Table 2. Software costs

Hardware costs include a high-end laptop, the *Inasutoma* sensors (5 sensors), the microprocessor STM32, the 3D printer PRUSA II and its coil, as well as different electronic components used for the measurement circuit.

Hardware	Cost (€)
STM32 Microprocessor	15.00
PRUSA II 3D Printer	500.00
3D Printer Coil	27.00
Electronic Components	13.00
Inasutoma sensor (each) x 5	5 x 2,600.00 ¥ (5 x 18.72 €)*
TOTAL (€)	**648.60**

* Currency exchange Yen-Euro on June 16th, 2015.

Table 3. Hardware costs

Laboratory costs include the PDMS and the different lab resources used during its fabrication process.

Laboratory resources	Cost (€)
PDMS (1 kg)	139.00
Lab materials (pipettes, scale, ...)	20.00
TOTAL (€)	**159.00**

Table 4. Laboratory costs

Therefore the final material costs are as follows:

	Cost (€)
Software	11,519.00
Hardware	648.60
Laboratory resources	159.00
TOTAL (€)	**12,326.60**

Table 5. Disaggregated material costs

It is important to remark the following aspects about the material costs:

- The PRUSA II 3D Printer will not be exclusively used for this project. It is currently being used for other projects of the Systems Engineering and Automation Department. Therefore the purchase cost is the one indicated in the above table but the real cost for this project is very low.
- The same happens for the 3D Printer Coil. The amount used for this project is around a 5% of the total coil. Therefore the purchase cost is the one indicated in the above table but the real cost for this project is also very low.
- The smallest amount of PDMS that can be bought is 1kg. The real amount of PDMS that has been used for this project is 30g. This highlights one of the properties of the PDMS: it is extremely cheap.

Although the purchase cost is the one indicated in the above table, the real cost for this project is 4.17€.

Total

Adding up previous sections plus indirect costs (twenty percent – 20%) and taxes (IVA – 21%), the total cost of the project amounts to *thirty-six thousand, one hundred thirty-five euros and thirty-four cents.*

	Cost (€)
Human Costs	11,310.00
Material Costs	12,326.60
Indirect costs (20%)	4,727.32
Subtotal	29,363.92
Taxes (IVA – 21%)	5,956.42
TOTAL BUDGET (€)	**35,320.34**

Table 6. Disaggregated total costs

REFERENCES

[1] IMBd.com, Inc. *IMBd.* http://www.imdb.com/title/tt0080684/ (accessed April 24, 2015).

[2] M.R. Cutkosky, R.D. Howe. *Human Grasp Choice and Robotics Grasp Analysis.* Vol. 1. Springer-Verlag, 1990.

[3] J. Butterfass, M. Grebenstein, H. Liu, G.Hirzinger. "DLR-Hand II: Next Generation of a Dexterous Robot Hand." *International Conference on Robotics & Automation.* Seoul, Korea: IEEE, 2001. 109-114.

[4] Shadow Robot Company. "Shadow Dexterous Hand Technical Specification." 2013.

[5] Robot hand - unit for research. *Robot hand - unit for research.* http://robothand.eu/en/products/robotic_hands/robot_hand_gifu_hand_iii/ (accessed April 20, 2105).

[6] Tetsuya Mouri, Haruhisa Kawasaki, Keisuke Yoshikawa, Jun Takai, and Satoshi ito. "Antrophomorphic Robot Hand: Gifu Hand III." *International Conference on Control, Automation and Systems.* Korea: Institute of Control, Automation, and System Engineers (Korea), 2002.

[7] M.H. Lee, H.R. Nicholls. "Tactile sensing for mechatronics - a state of the art survey." *Mechatronics* (Pergamon Press) 9 (1999): 1-31.

[8] Heinz Wörn, Karsten Weiß. "The Working Principle of Resisitive Tactile Sensor Cells." *International Conference on Mechatronics & Automation.* Niagara Falls: IEEE, 2005. 471-476.

[9] A.G.S. Electronics Semicustoms. *A.G.S.* www.ags-one.com/EN/content/17/30/Resistive-Touch-Sensor.aspx (accessed April 03, 2015).

[10] I. Gaiser, S. Schulz, A. Kargov, H. Klosek, A. Bierbaum, C. Pylatiuk, R. Oberle, T. Werner, T. Asfour, G. Bretthauer, R. Dillmann. "A New Anthropomorphic Robot Hand." *International Conference on Humanoid Robots.* Deajeon, Korea: IEEE, 2008. 418-422.

[11] Institute Mihailo Pupin Robotics Laboratory. *Research Topic: SMART HANDS – Building of Intelligent Dexterous Dual-arm Manipulation of Advanced Service Robots.* www.pupin.rs/RnDProfile/research-topic10.html (accessed March 24, 2015).

[12] YWR Amarasinghe, AL Kulasekera, TGP Priyadarshana. "Quantum Tunneling Composite (QTC) Based Tactile Sensor Array For Dynamic Pressure Distribution Measurement." *Seventh International Conference on Sensing Technology (ICST).* Wellington: IEEE, 2013. 1-4.

[13] Zaman Md. Mostafa, Ehsan Mohammad Nazmul. "Quantum Tunnelling Composite, a new facilitate sensing and switching tecnhology in textile Keypad." *Textile Today*, January 2011.

[14] Giorgio Cannata, Marco Maggiali, Giorgio Metta, Giulio Sandini. "An Embedded Artificial Skin for Humanoid Robots." *International Conference on Multisensor Fusion and Integration for Intelligent Systems.* Seoul, Korea: IEEE, 2008. 434-438.

[15] Lee, Mark. "Designer's guide to rapid prototyping of capacitive sensors on any surface." *Planet Analog*, January 2007.

[16] Hanafiah Yussof, Jiro Wada, Masahiro Ohka. "Analysis Of Tactile Slippage Control Algorithm For Robotic Hand Performing Grasp-Move-Twist Motions." *International Journal on Smart Sensing and Intelligent Systems* 3, no. 3 (September 2010): 359-375.

[17] Barman's Lego creations. "Amazing LEGO Robot Hand does everything your hand can do." *Robotic Humanoid Hand.* Tech Tripper, January 3, 2013.

[18] Stefano Stassi, Valentina Cauda, Giancarlo Canavese, Candido Fabrizio Pirri. "Flexible Tactile Sensing Based on Piezoresistive Composites: A Review ." *Sensors*, March 2014: 5296-5332.

[19] University of California Irvine. *Robotics: An Approach to Minimally Invasive Surgey.* 2014. bme240.eng.uci.edu/students/10s/sgupta1/ForceTactileSensing.html (accessed April 03, 2015).

[20] aps Solutions GmbH. *Technology for Better Contacts.* www.aps-munich.com/ts-wwt-pcr-vers3.htm (accessed May 08, 2015).

[21] Interlink Electronics. "FSR Force Sensing Resistors." *FSR Integration Guide.* Camarillo, CA.

[22] INABAGOMU, Inc. "イナストマ – SFR タイプ Datasheet.

[23] King Fong Lei, Kun-Fei Lee, Ming-Yih Lee. "A flexible PDMS capacitive tactile sensor with adjustable measurement range for plantar pressure measurement." *Microsystem Technologies* (Springer), no. 20 (September 2013): 1351-1358.

ANNEX I: MEASUREMENTS

Range 0–1000g

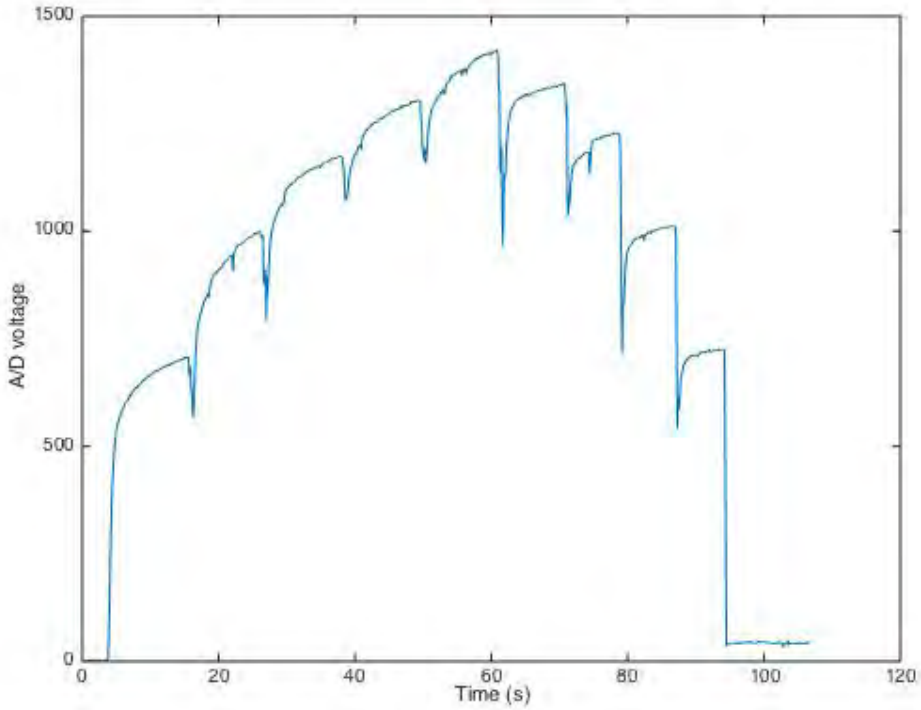

Annex I.1. Trial 1 measurement

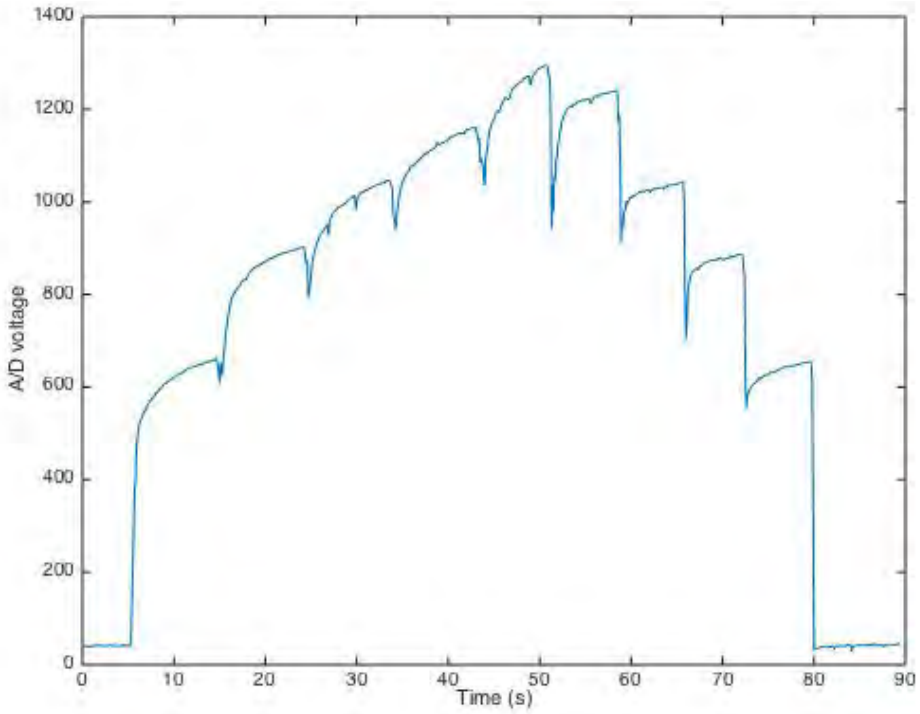

Annex I.2. Trial 2 measurement

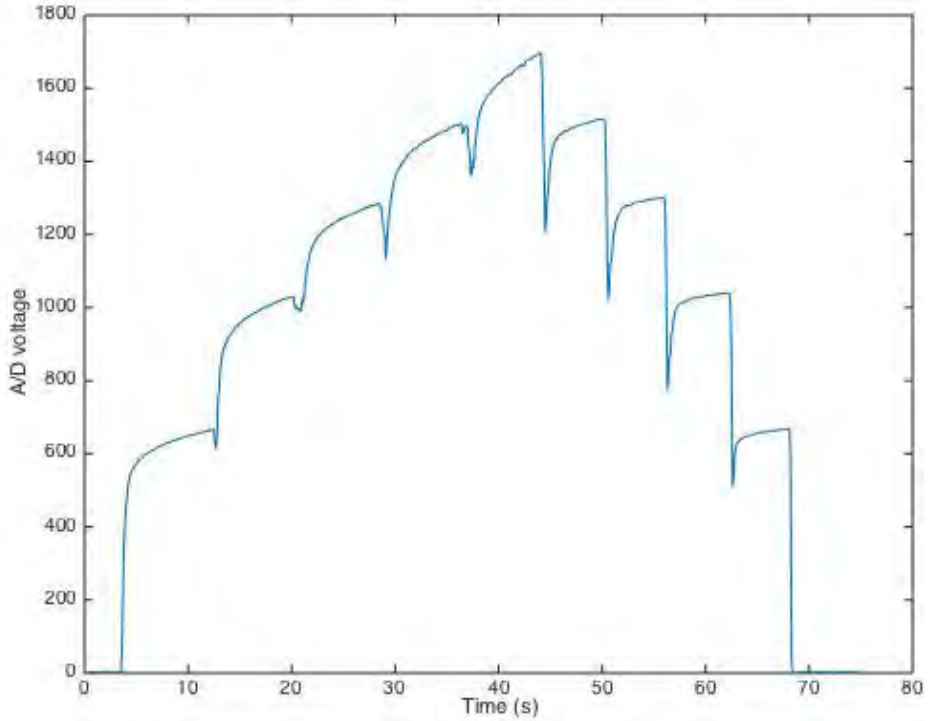

Annex I.3. Trial 3 measurement

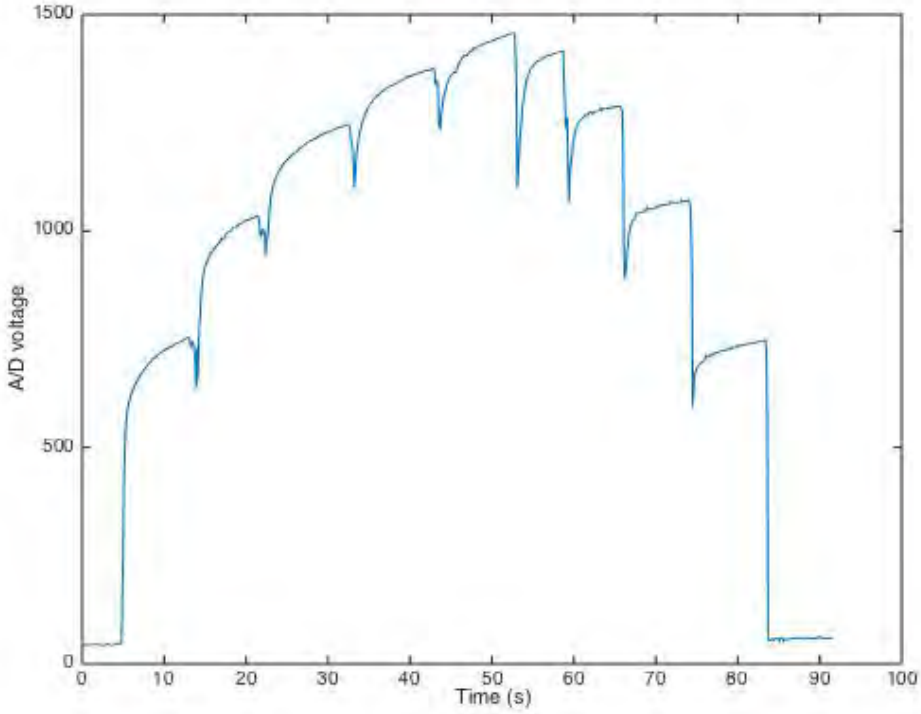

Annex I.4. Trial 4 measurement

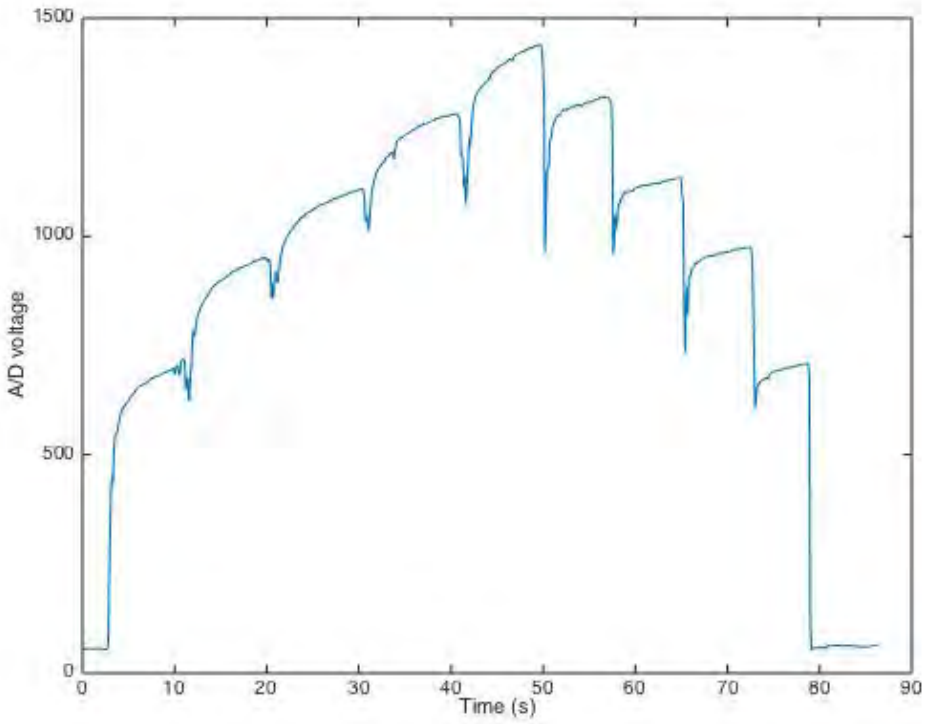

Annex I.5. Trial 5 measurement

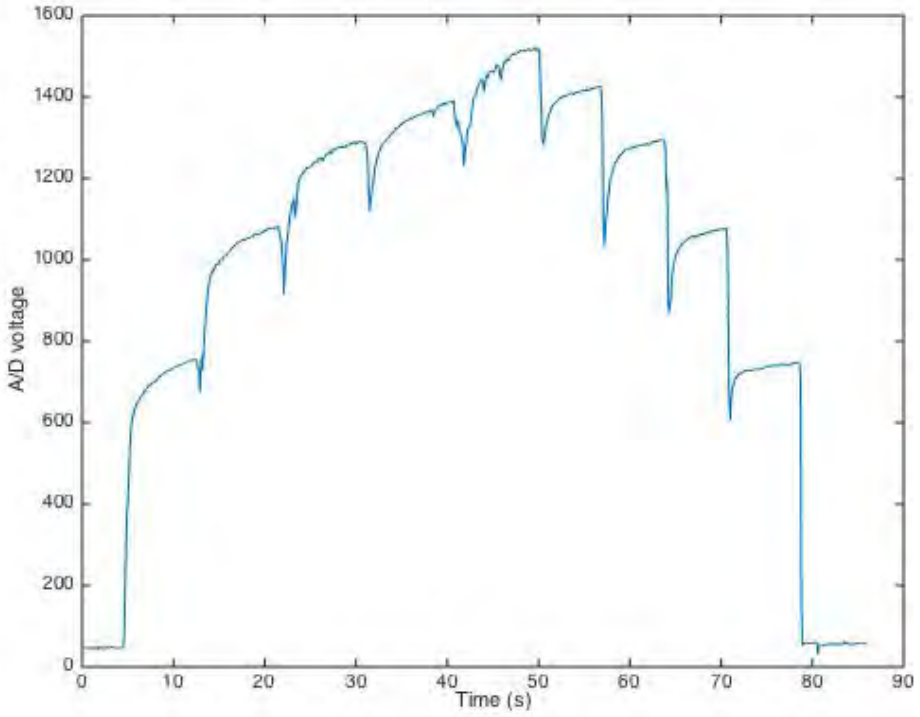

Annex I.6. Trial 6 measurement

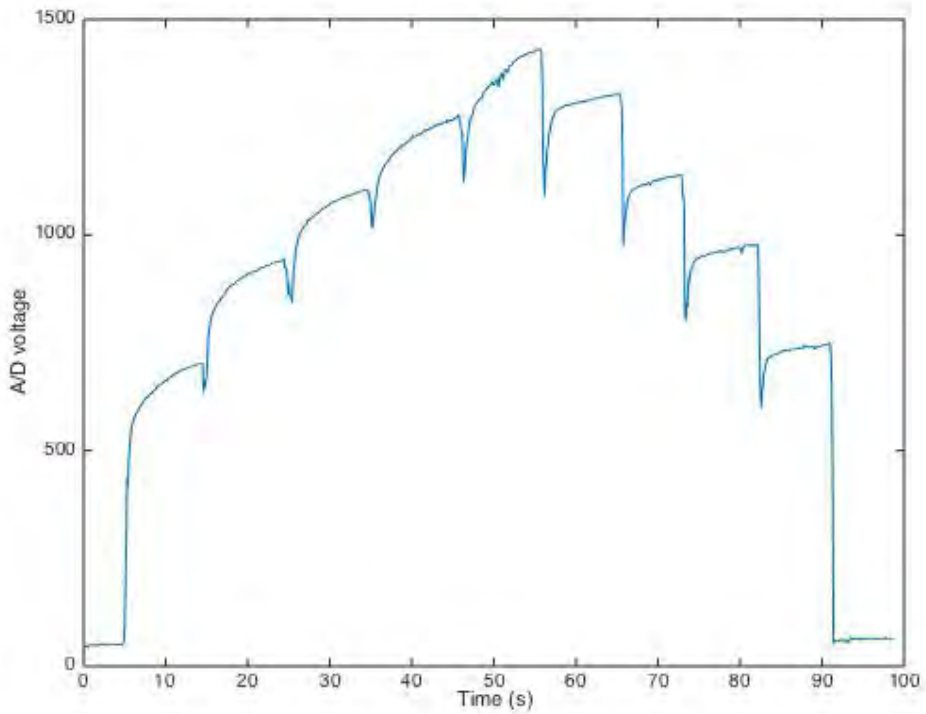

Annex I.7. Trial 7 measurement

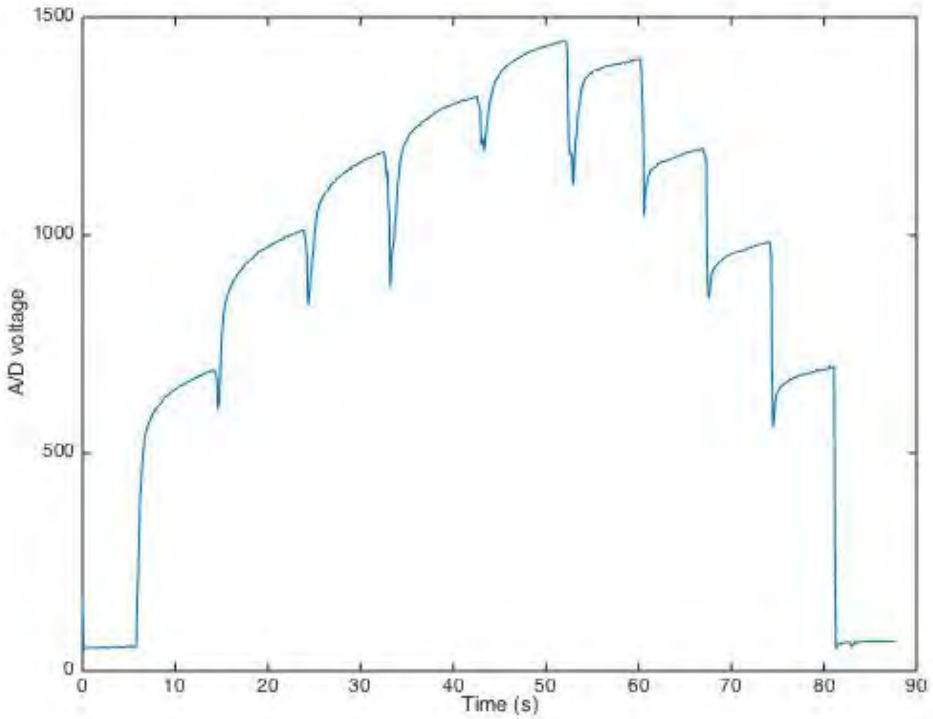

Annex I.8. Trial 8 measurement

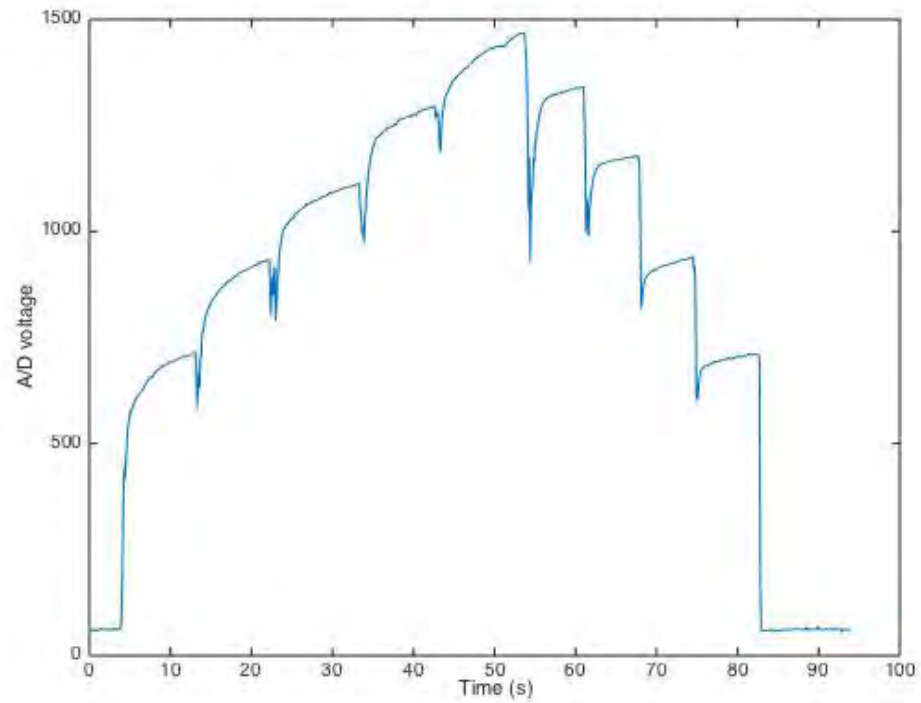

Annex I.9. Trial 9 measurement

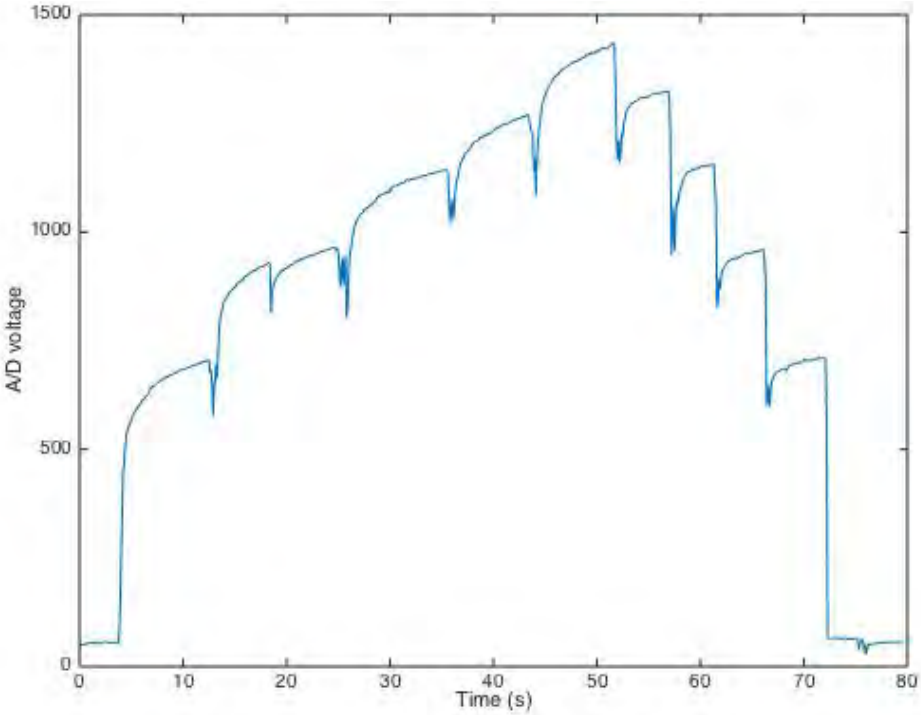

Annex I.10. Trial 10 measurement

Range 0–200g

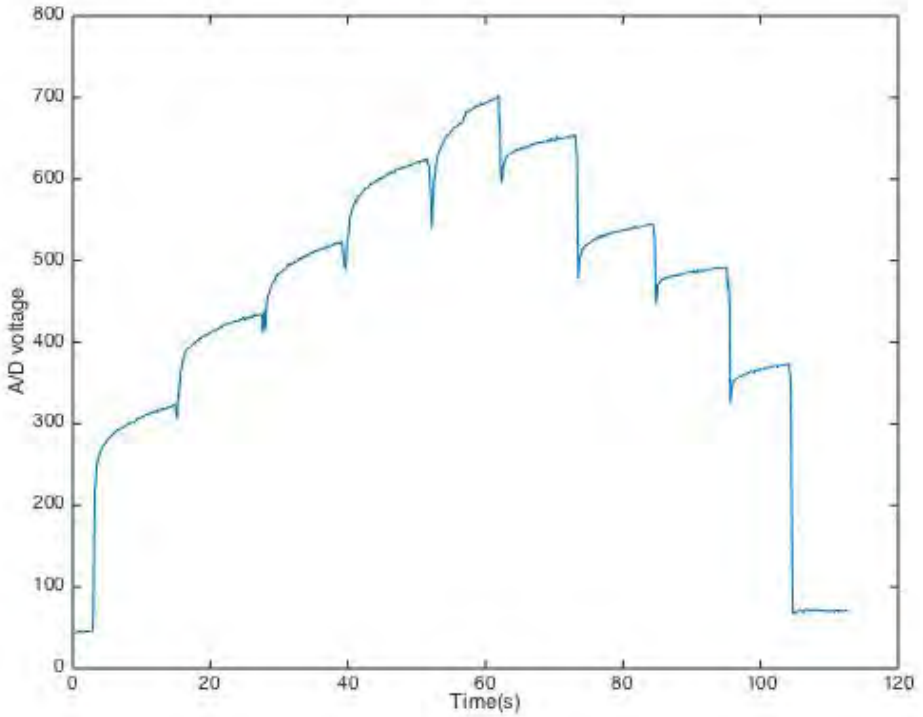

Annex I.11. Trial 1 measurement

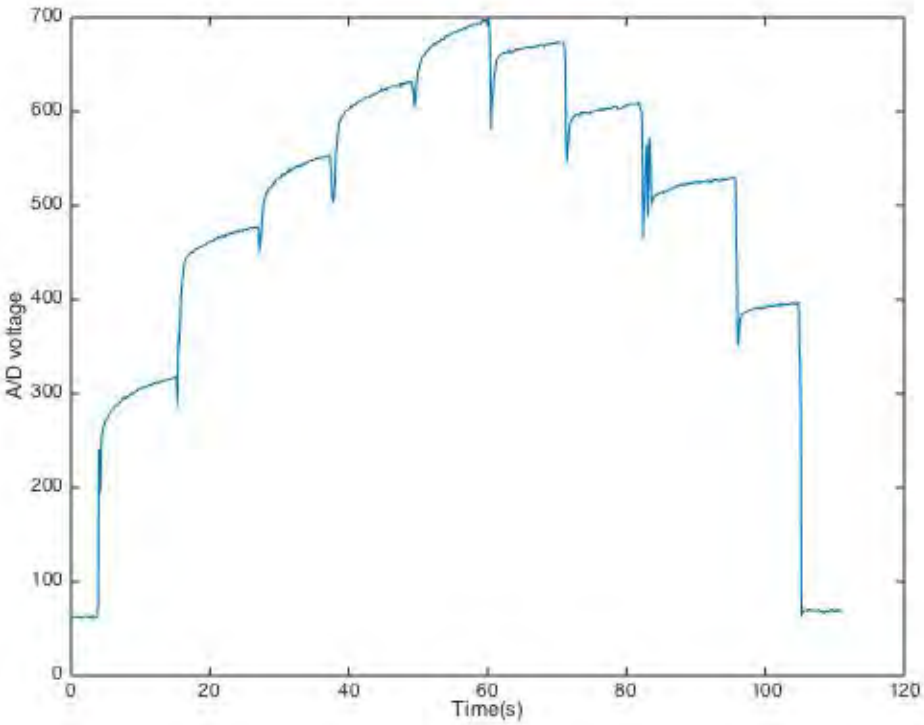

Annex I.12. Trial 2 measurement

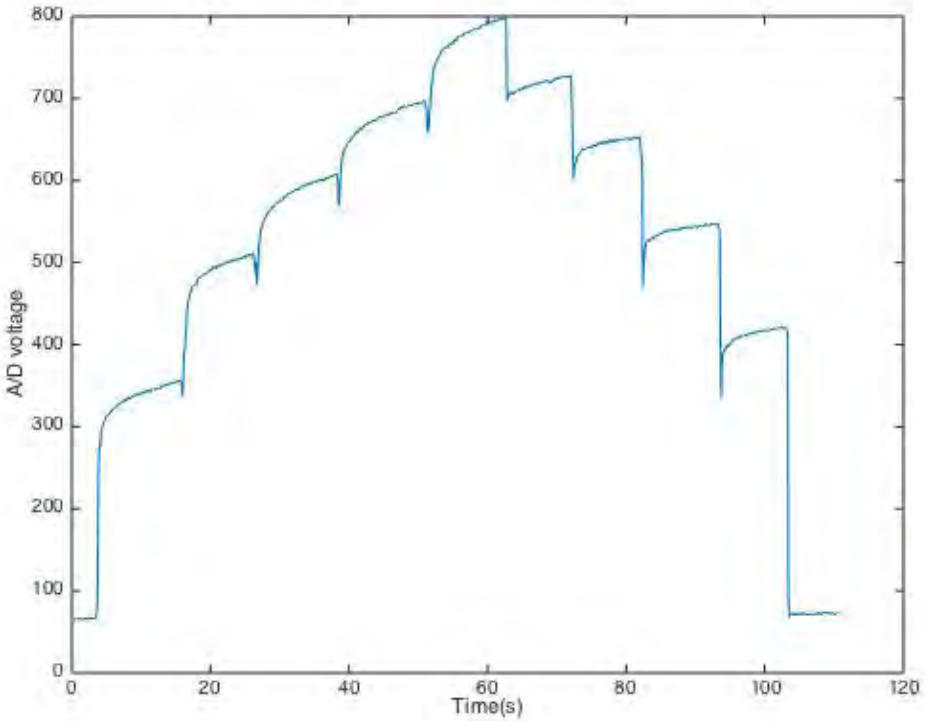

Annex I.13. Trial 3 measurement

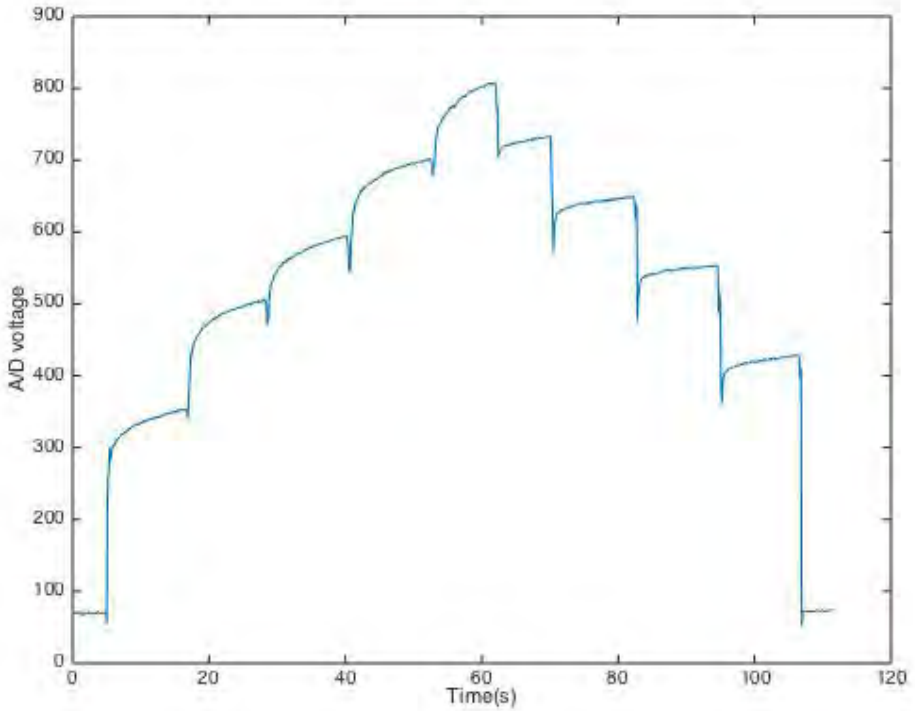

Annex I.14. Trial 4 measurement

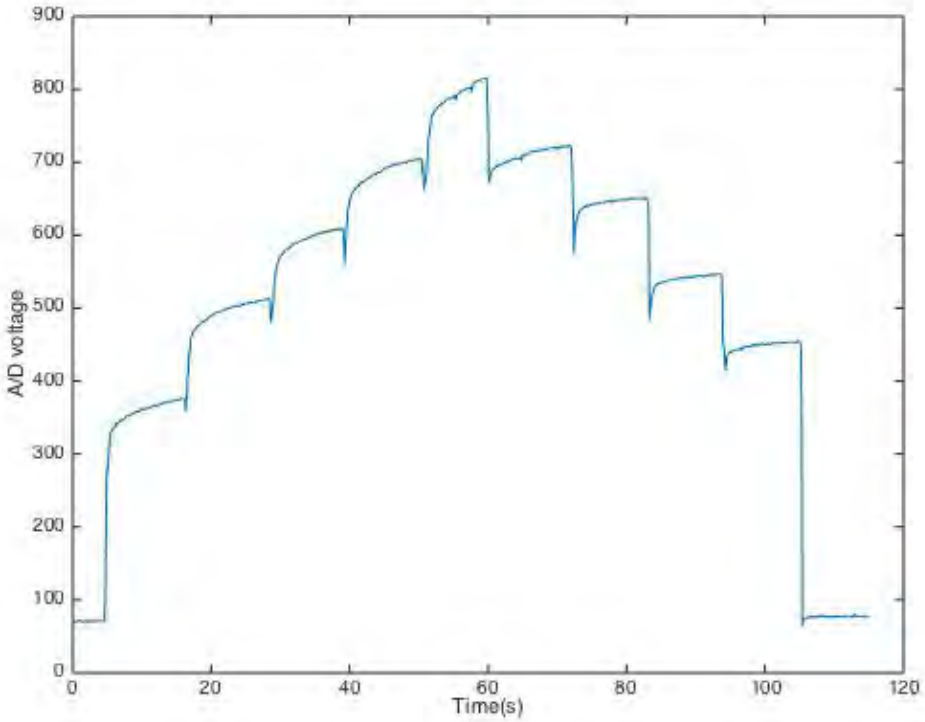

Annex I.15. Trial 5 measurement

ANNEX II: MODELS USING MEAN VALUES

Range 0–1000g

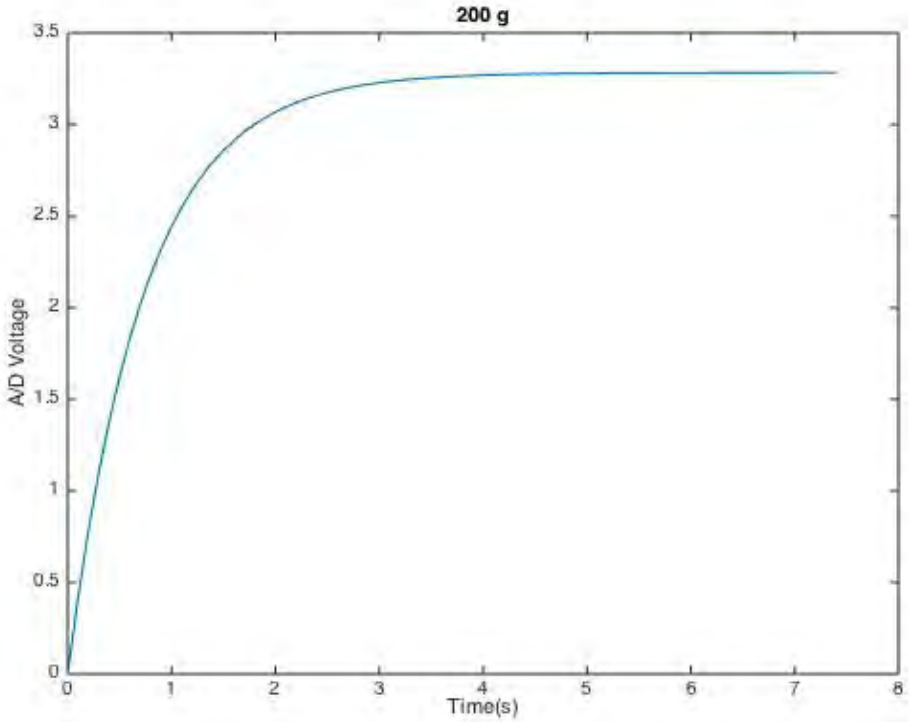

Annex II.1. Modeled response for 200g with k = 3.283 and τ = 0.7329
ECM = 0.3219

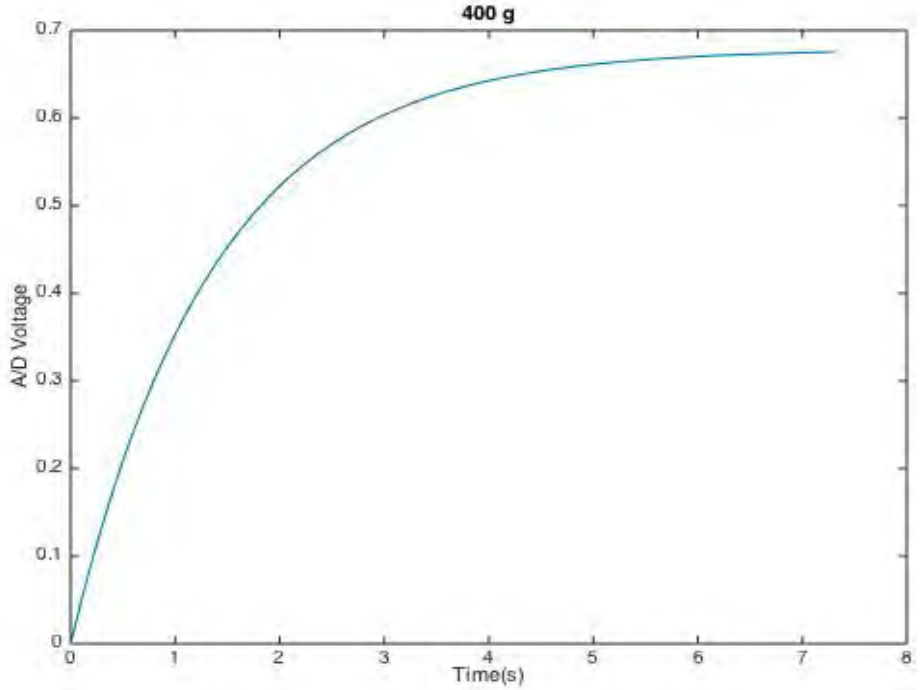

Annex II.2. Modeled response for 400g with k = 0.6785 and τ = 1.3616
ECM = 0.1751

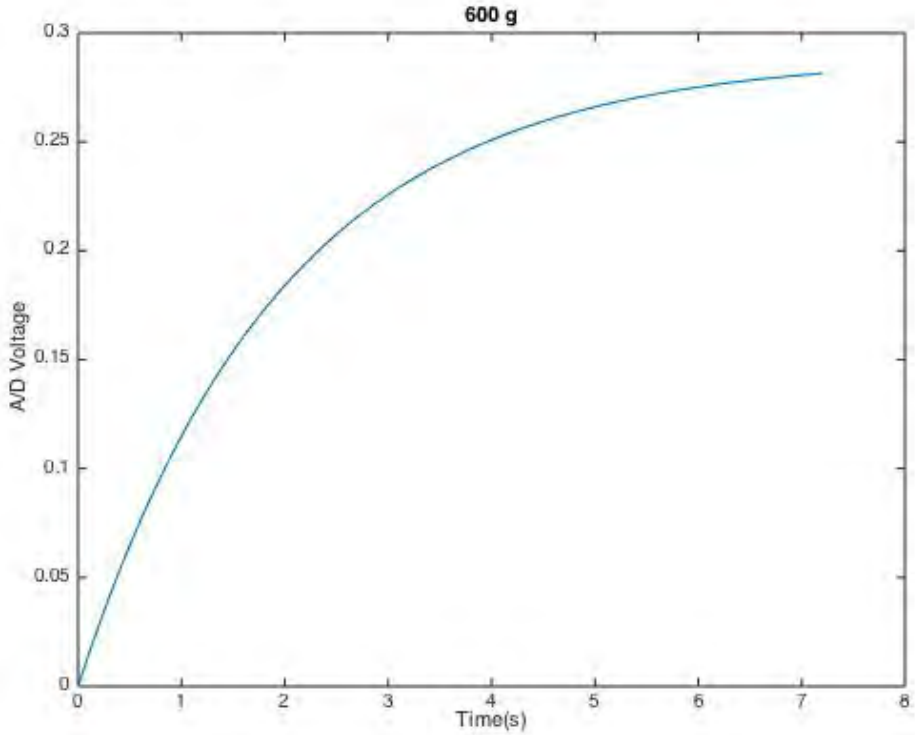

Annex II.3. Modeled response for 600g with k = 0.289 and τ = 1.9731 ECM = 0.1399

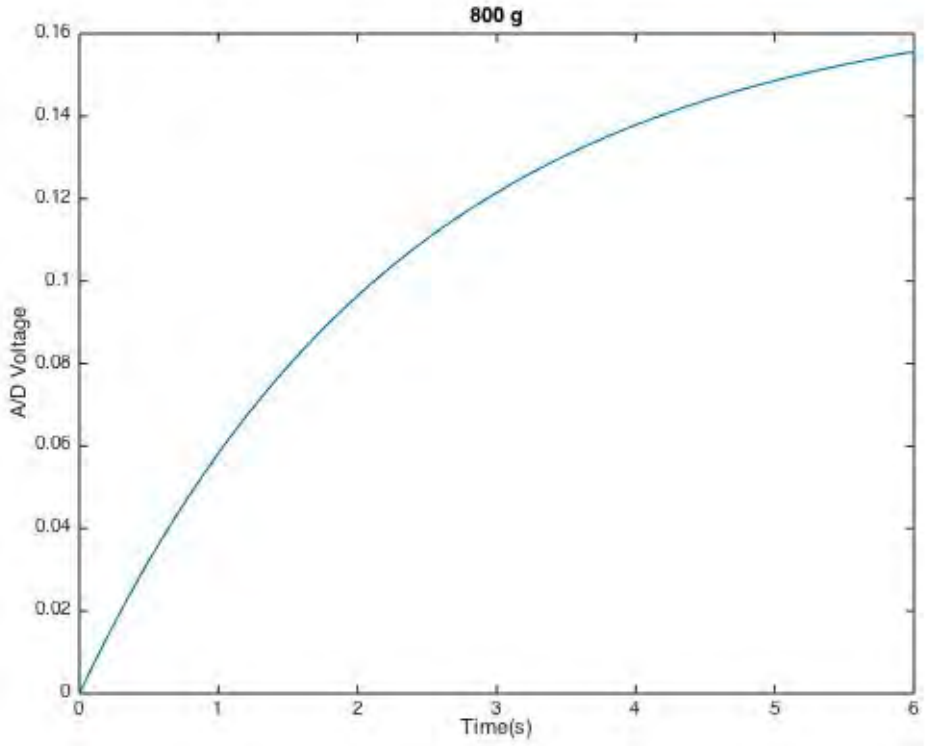

Annex II.4 Modeled response for 800g with k = 0.169 and τ = 2.3649 ECM = 0.1817

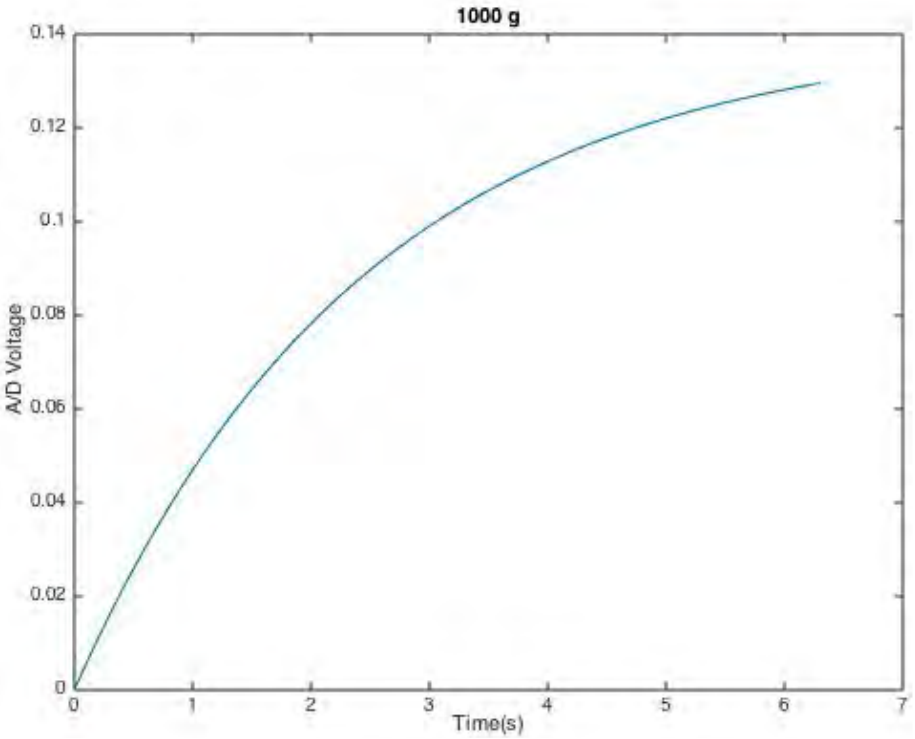

Annex III.5. Modeled response for 1000g with k = 0.1403 and τ = 2.4512 ECM = 0.085

Range 0–200g

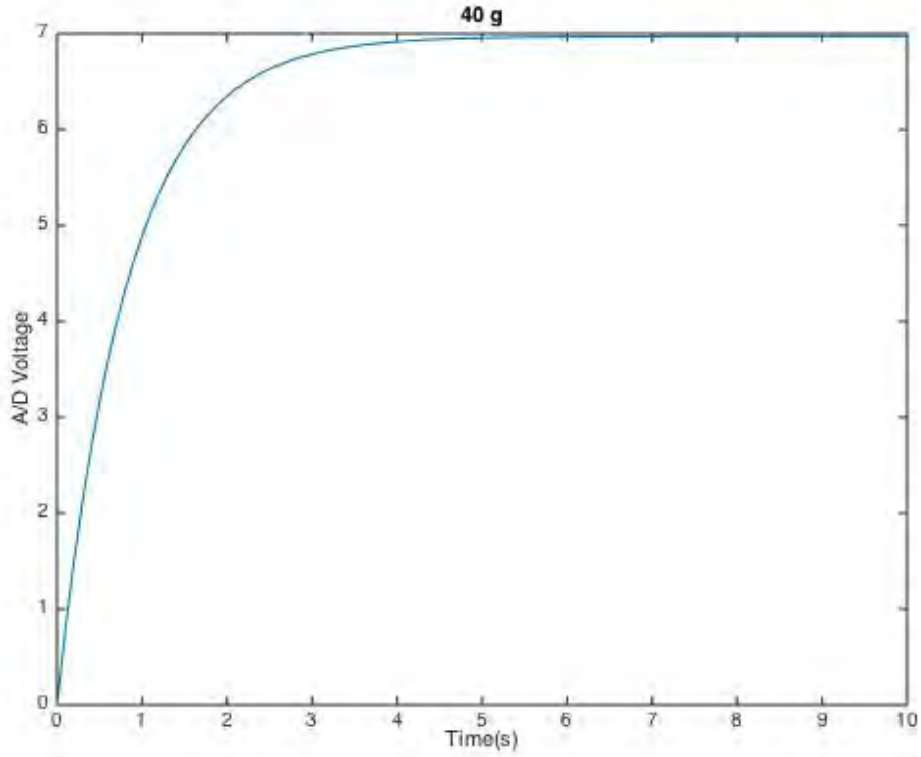

Annex II.6. Modeled response for 40g with k = 6.972 and τ = 0.8281 ECM = 0.6886

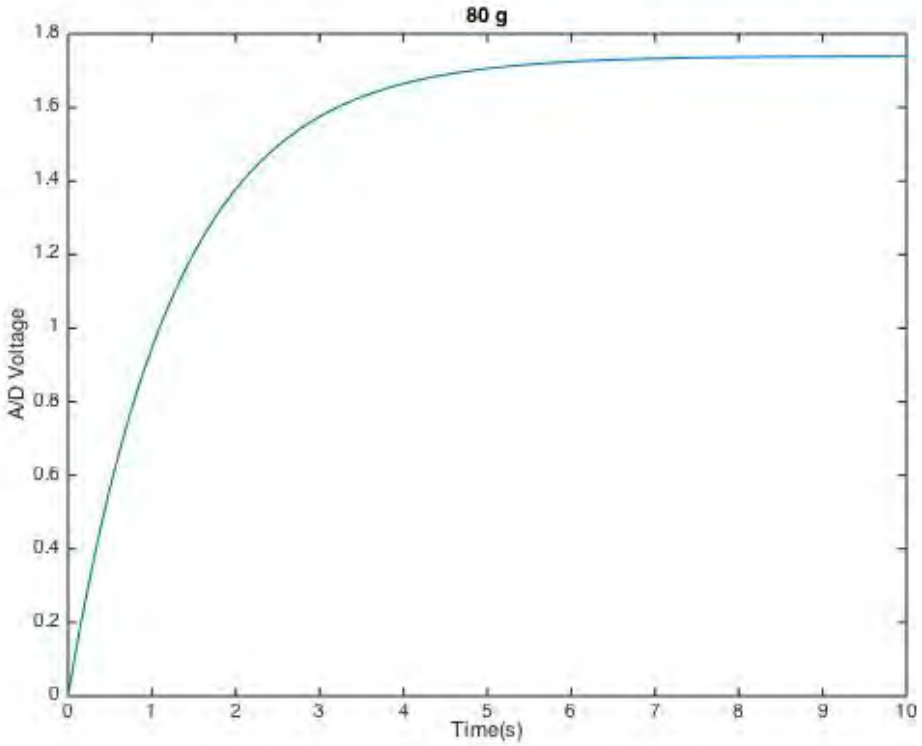

Annex II.7. Modeled response for 80g with k = 1.74 and τ = 1.274 ECM = 0.2469

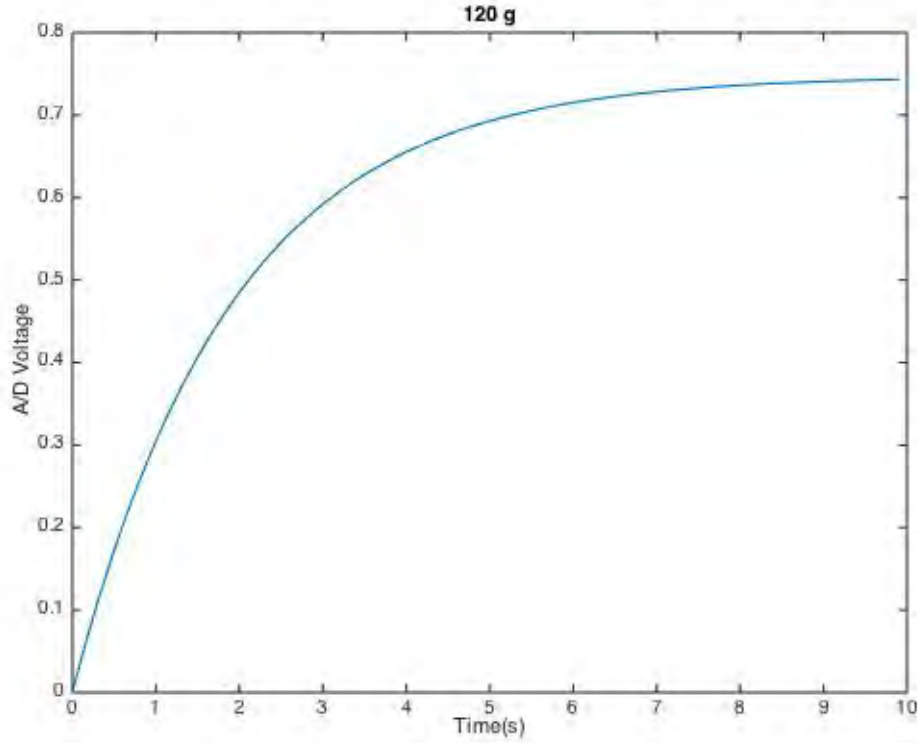

Annex II.8. Modeled response for 120g with k = 0.7475 and τ = 1.911 ECM = 0.086

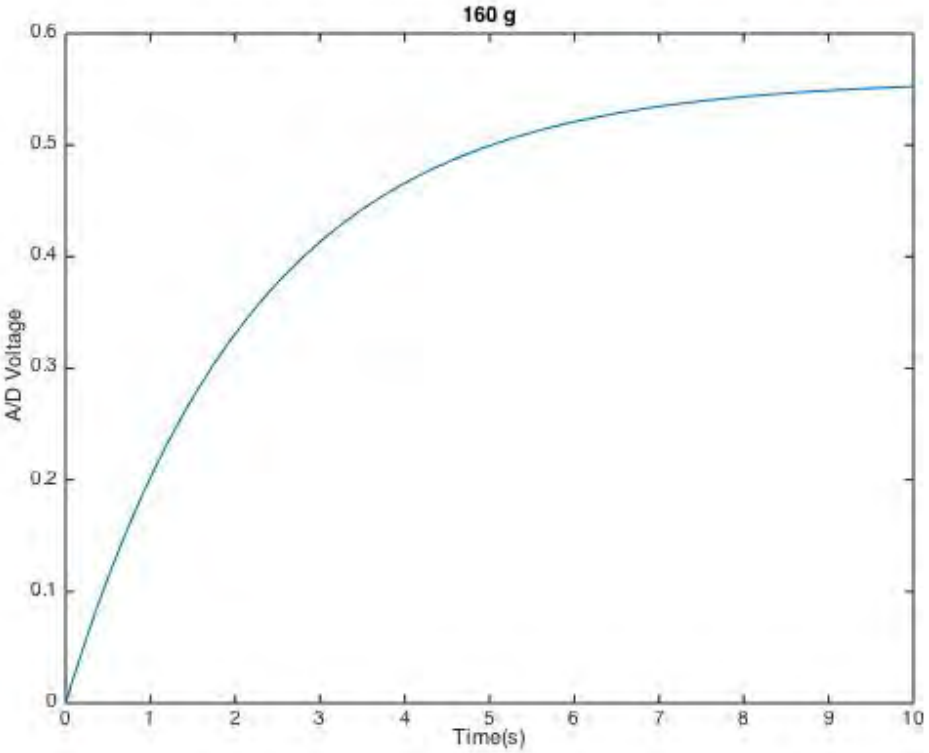

Annex II.9. Modeled response for 160g with k = 0.5588 and τ = 2.2295 ECM = 0.063

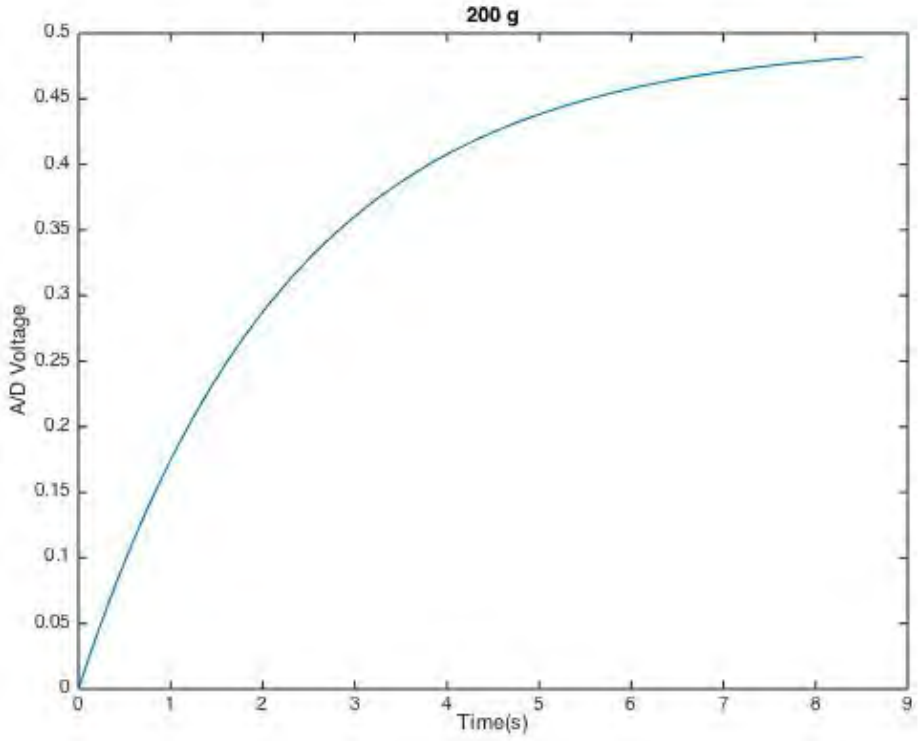

Annex II.10. Modeled response for 200g with k = 0.494 and τ = 2.2932 ECM = 0.091

ANNEX III: MEAN SQUARE ERRORS

Range 0-1000g

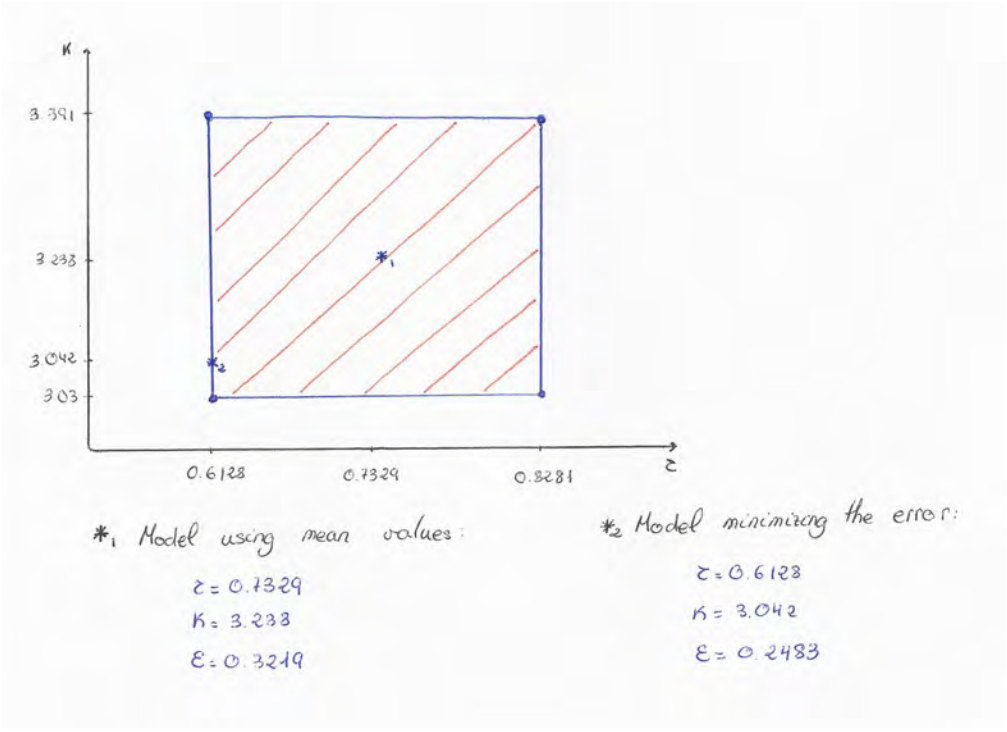

Annex III.1. 200g

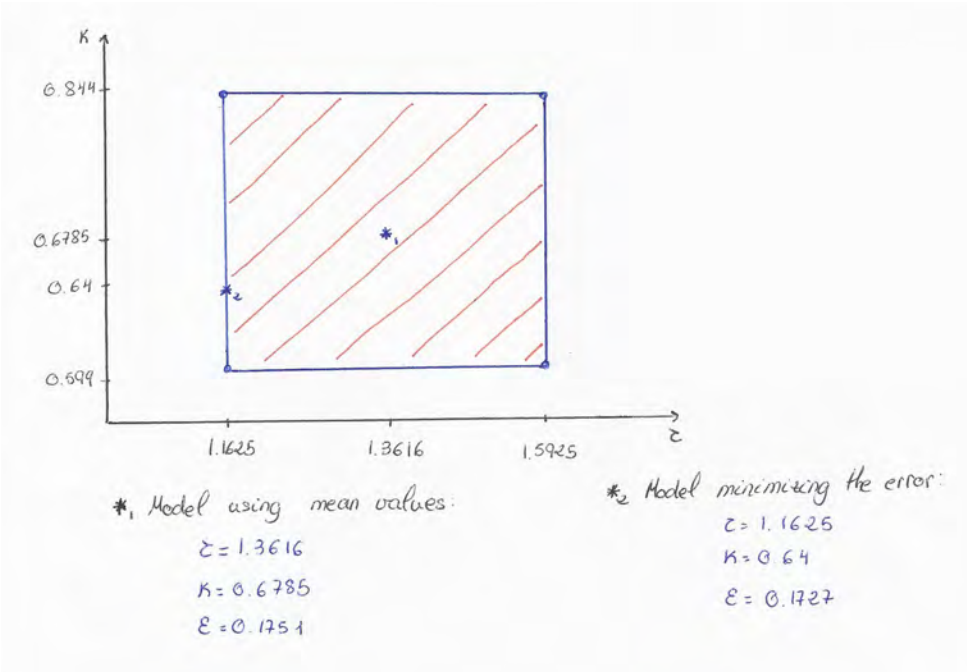

Annex III.2. 400g

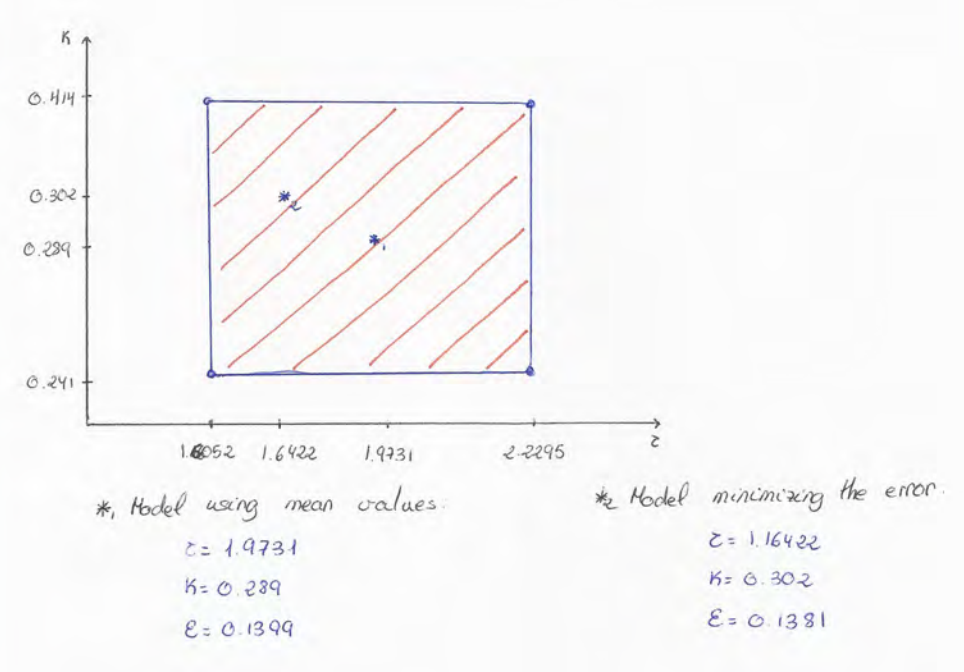

Annex III.4. 600g

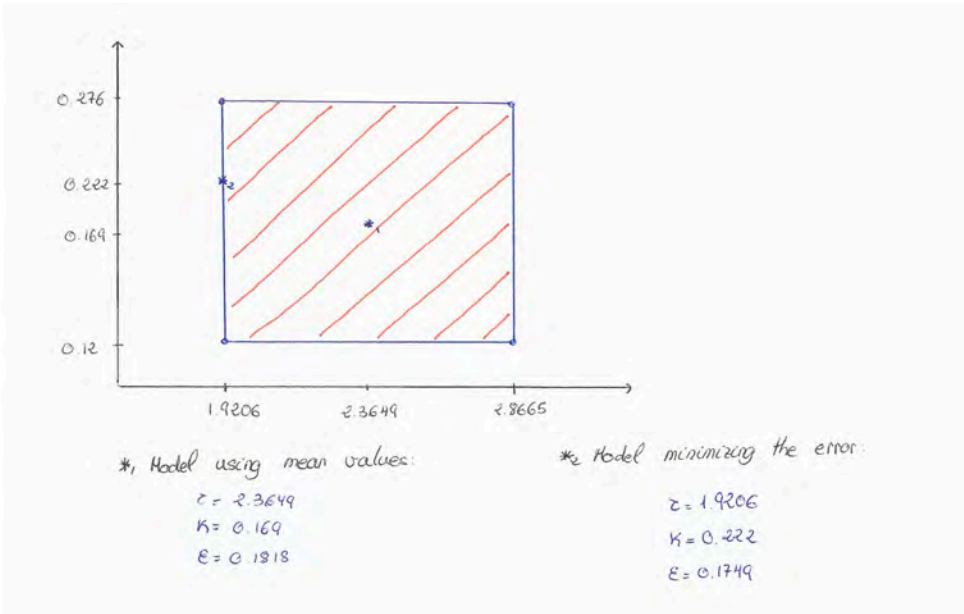

Annex III.5. 800g

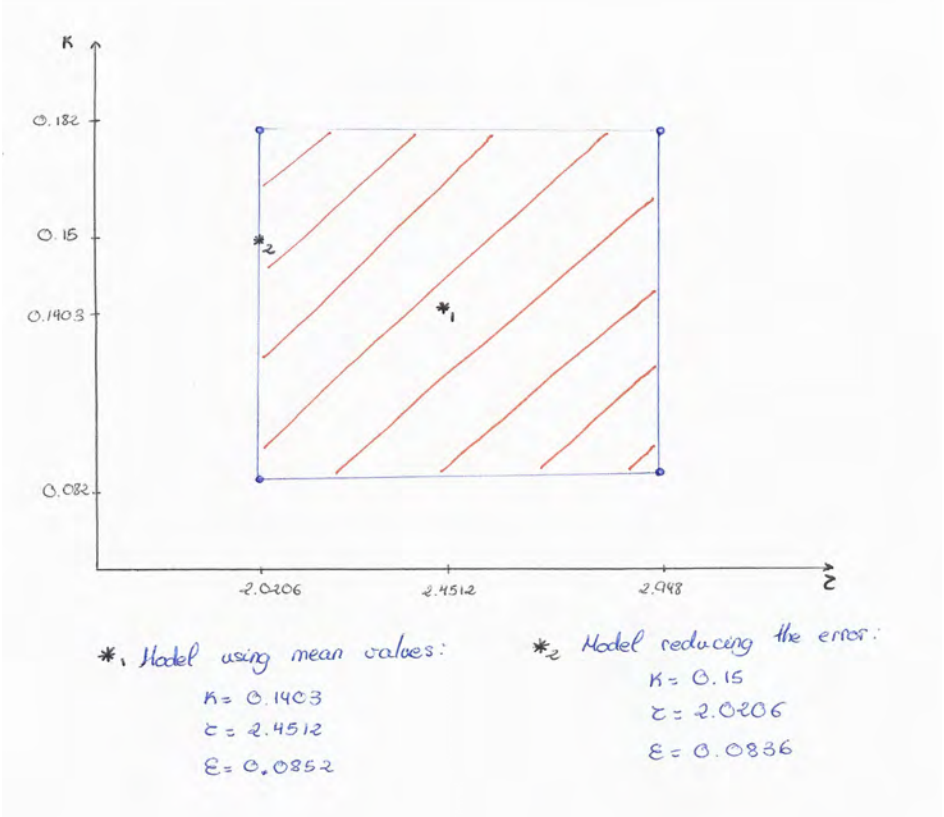

Annex III.6. 1000g

Range 0-200g

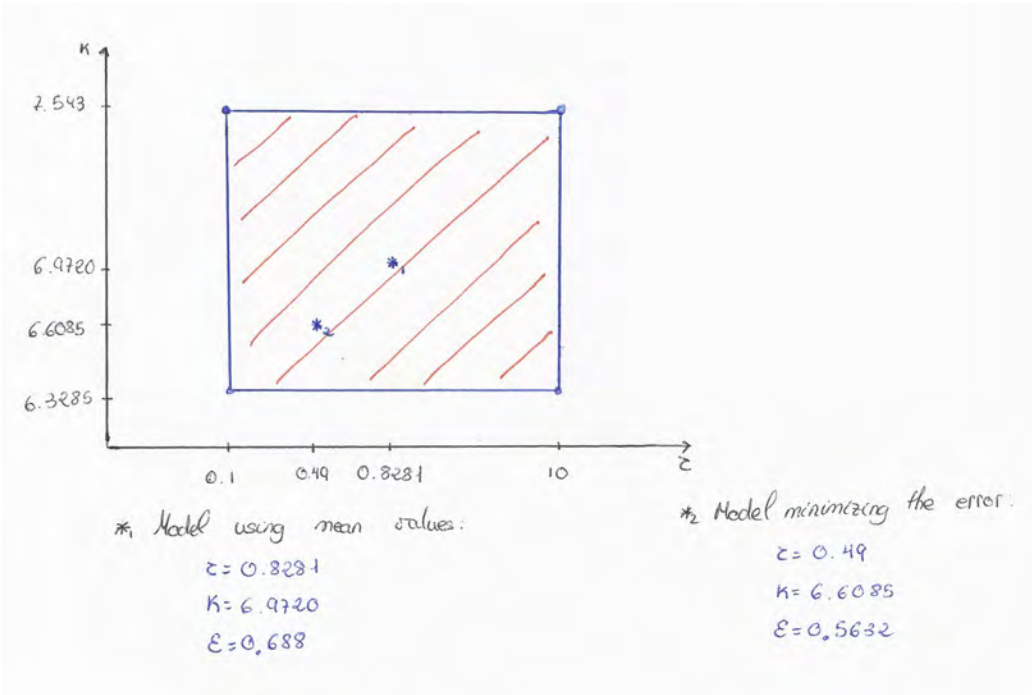

Annex III.7. 40g

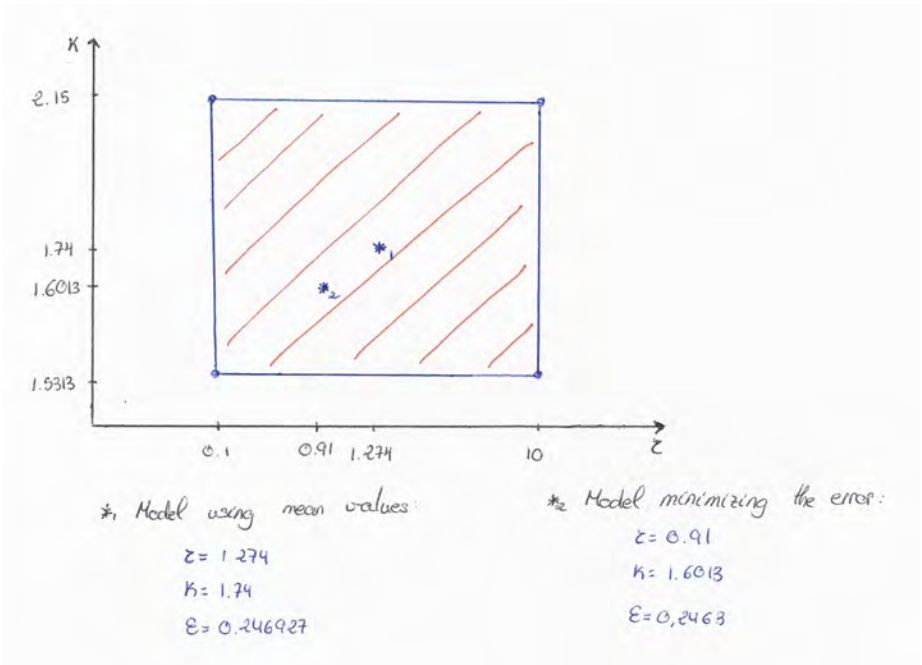

Annex III.8. 80g

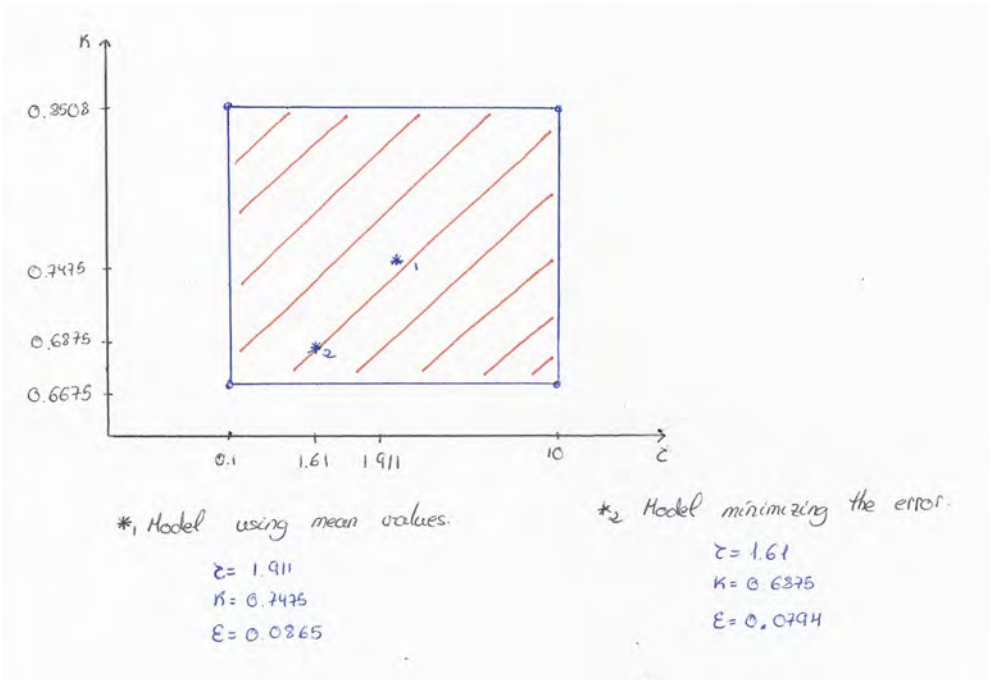

Annex III.9. 120g

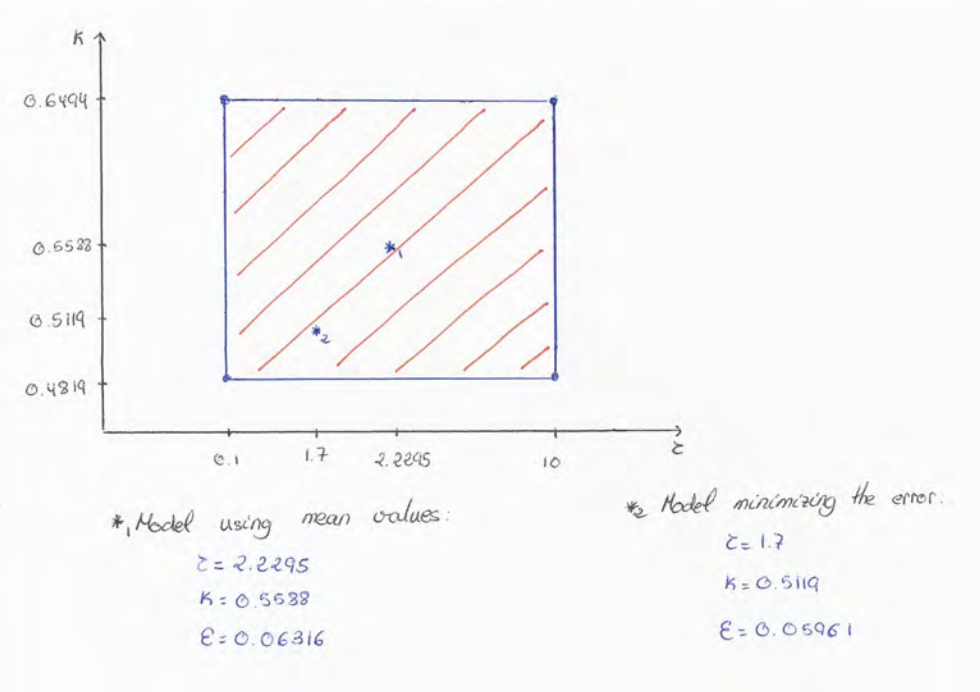

Annex III.10. 160g

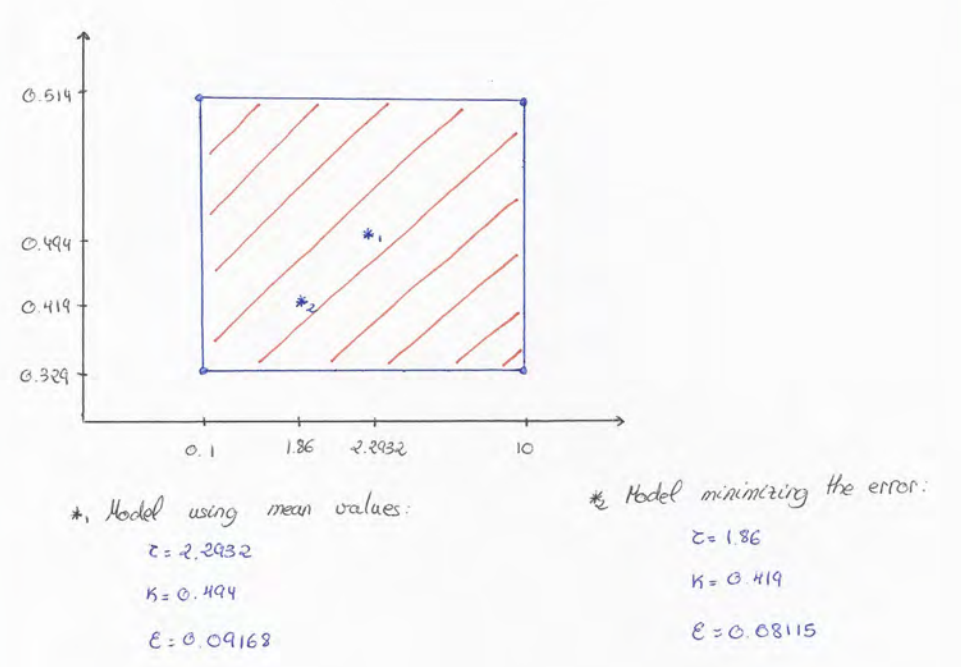

Annex III. 11. 200g

ANNEX IV: MODELS MINIMIZING THE ERROR

Range 0–1000g

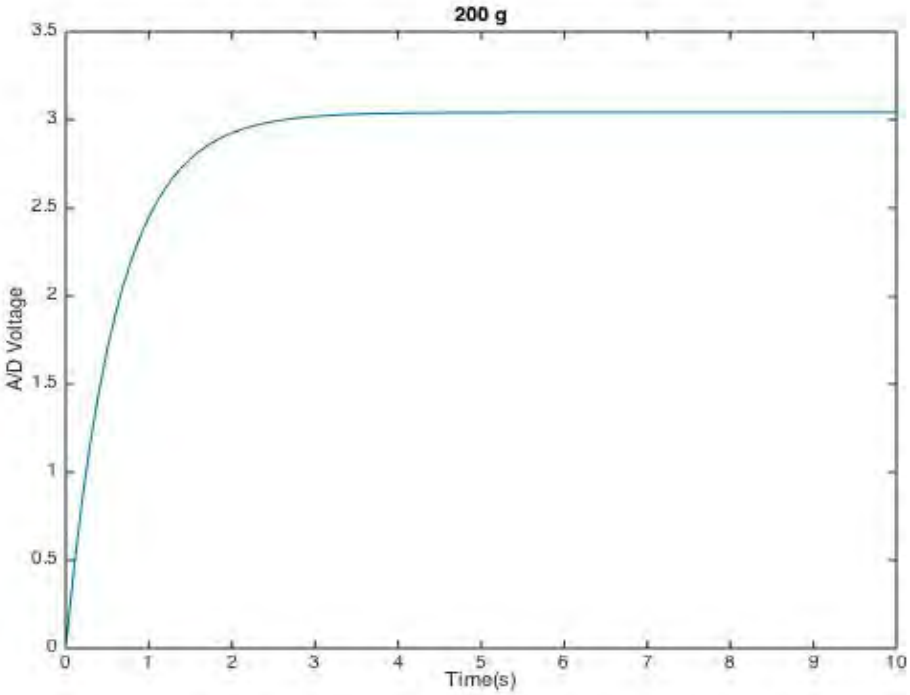

Annex IV.1. Modeled response for 200g with k = 3.042 and τ = 0.6128 ECM = 0.2483

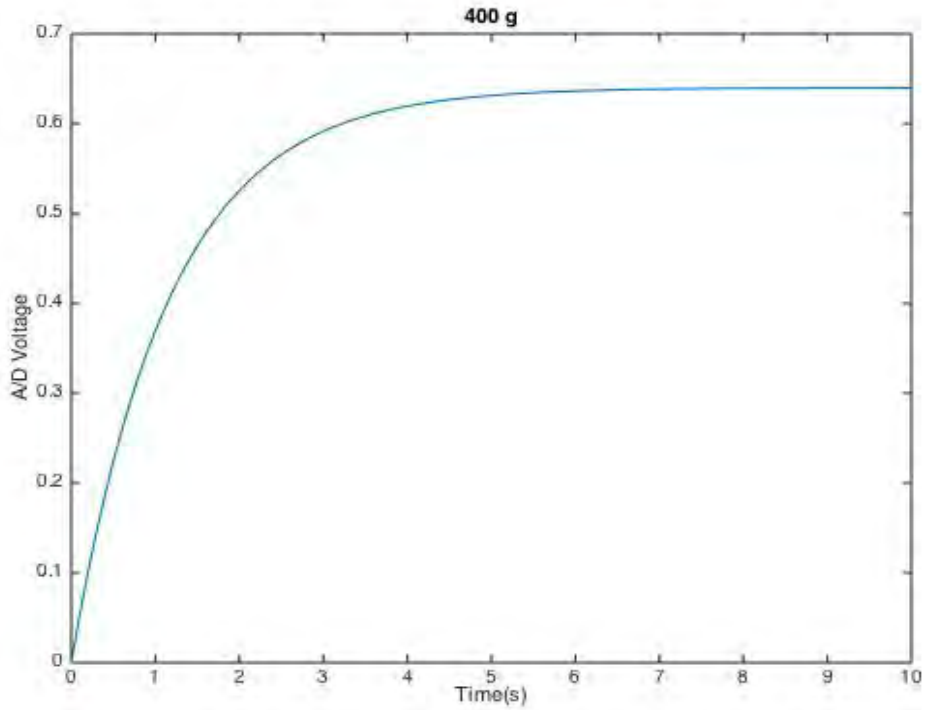

Annex IV.2. Modeled response for 400g with k = 0.64 and τ = 1.1625 ECM = 0.1727

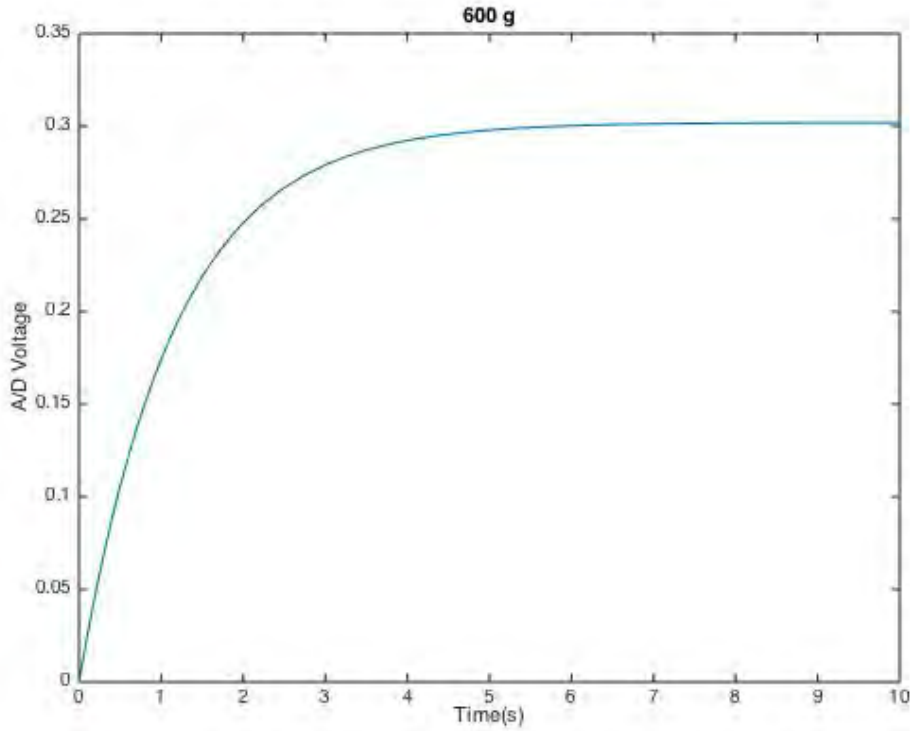

Annex IV.3. Modeled response for 600g with k = 0.302 and τ = 1.16422 ECM = 0.1381

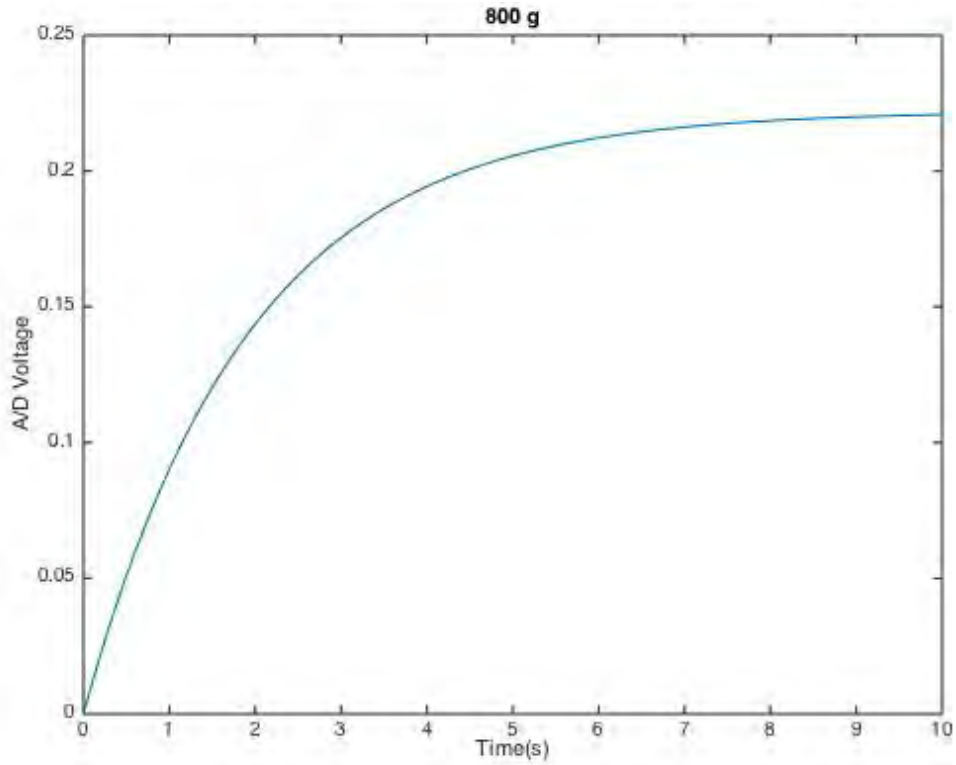

Annex IV.4. Modeled response for 800g with k = 0.222 and τ = 1.9206 ECM = 0.1818

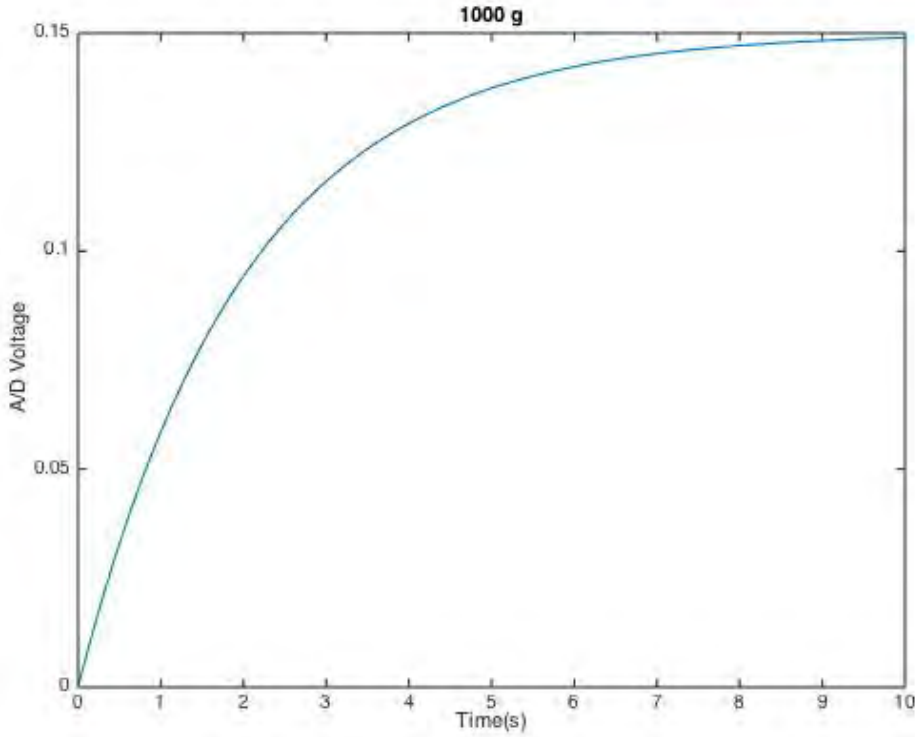

Annex IV.5. Modeled response for 1000g with k = 0.15 and τ = 2.0206 ECM = 0.0836

Range 0–200g

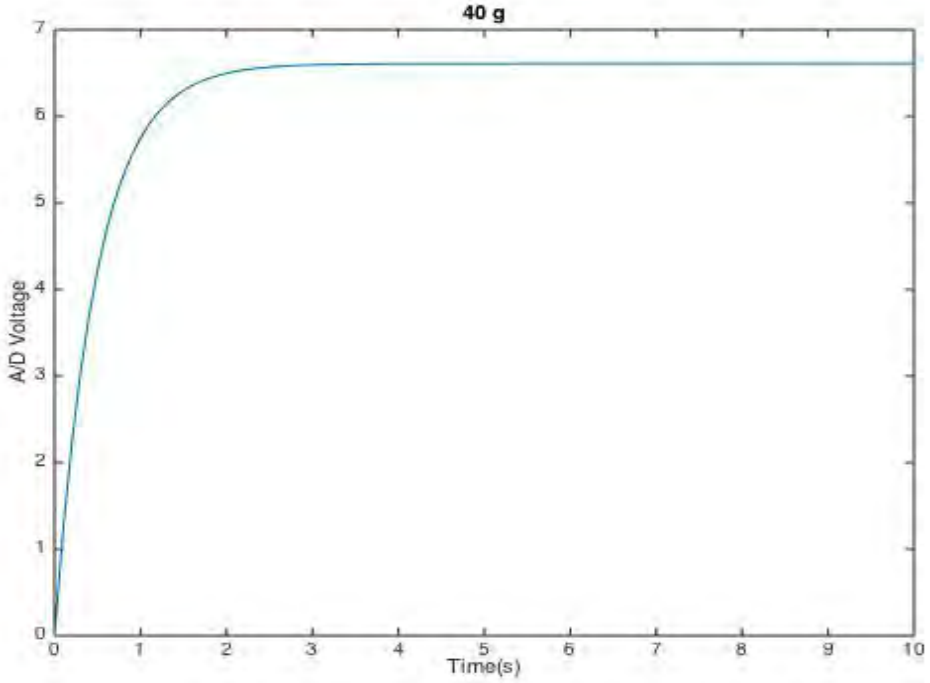

Annex IV.6. Modeled response for 40g with k = 6.6085 and τ = 0.49 ECM = 0.5632

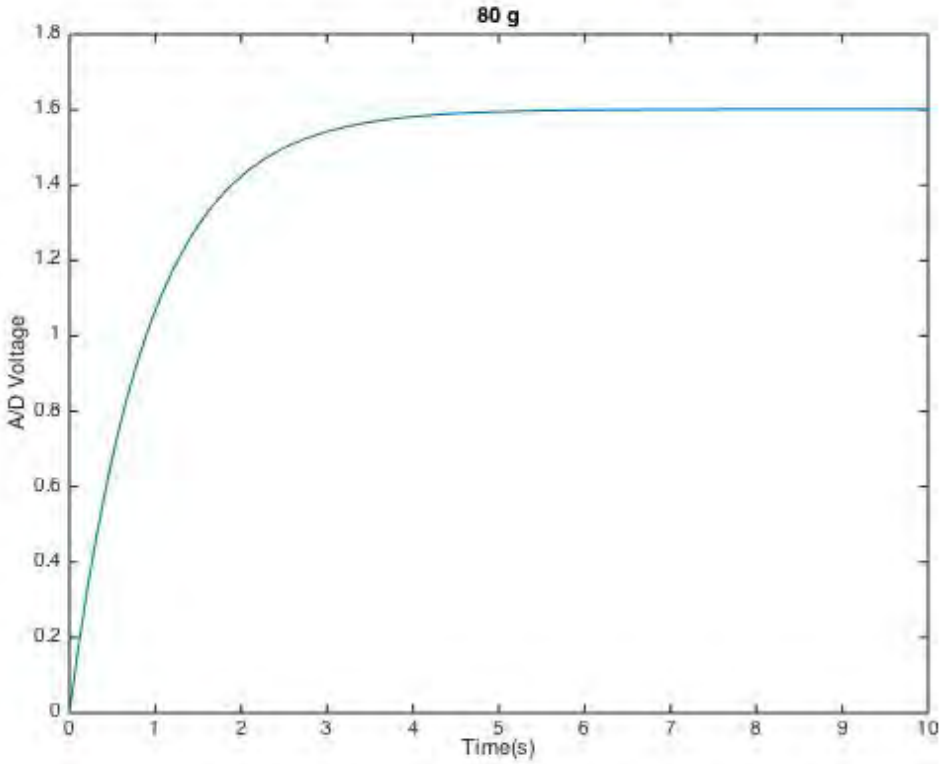

Annex IV.7. Modeled response for 80g with k = 1.6013 and τ = 0.93 ECM = 0.2413

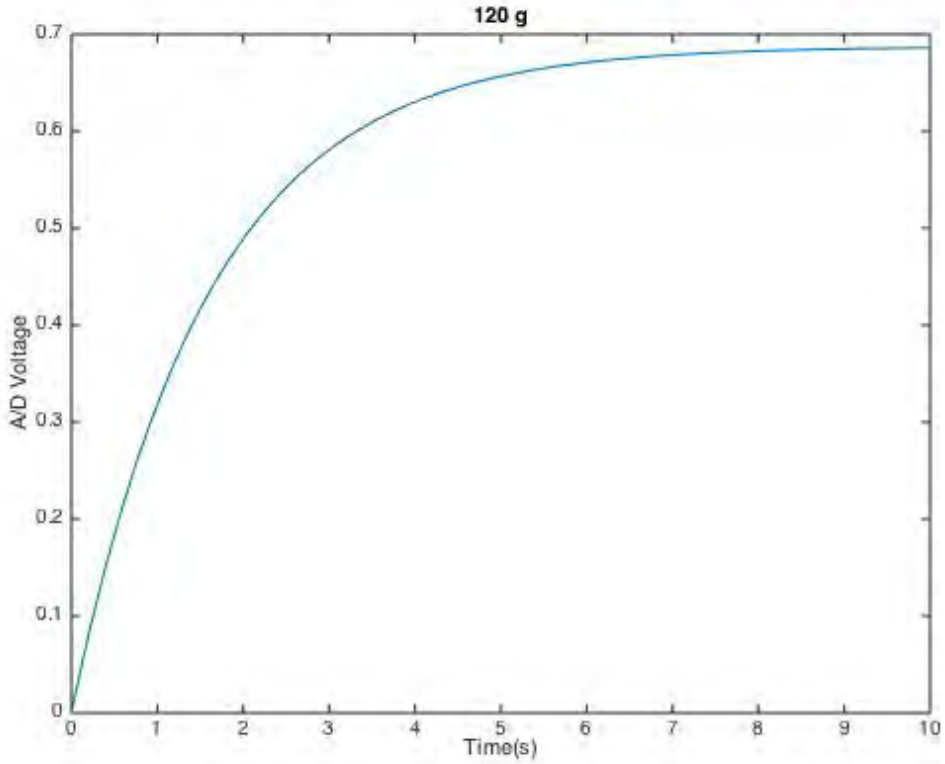

Annex IV.8. Modeled response for 120g with k = 0.6875 and τ = 1.61 ECM = 0.0794

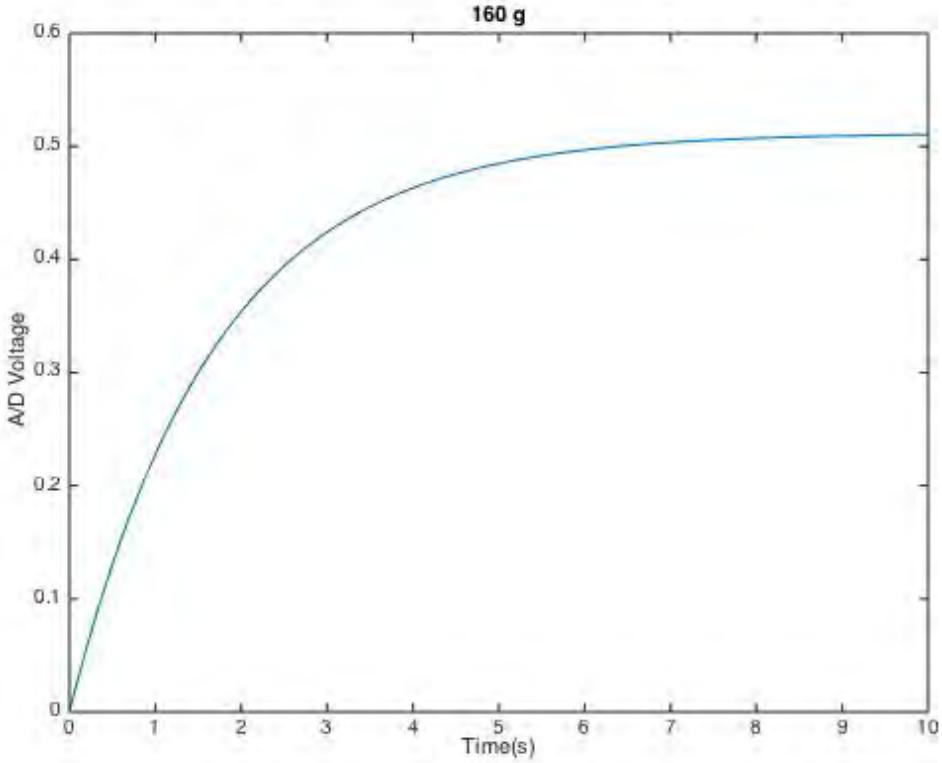

Annex IV.9. Modeled response for 160g with k = 0.5191 and τ = 1.7 ECM = 0.05961

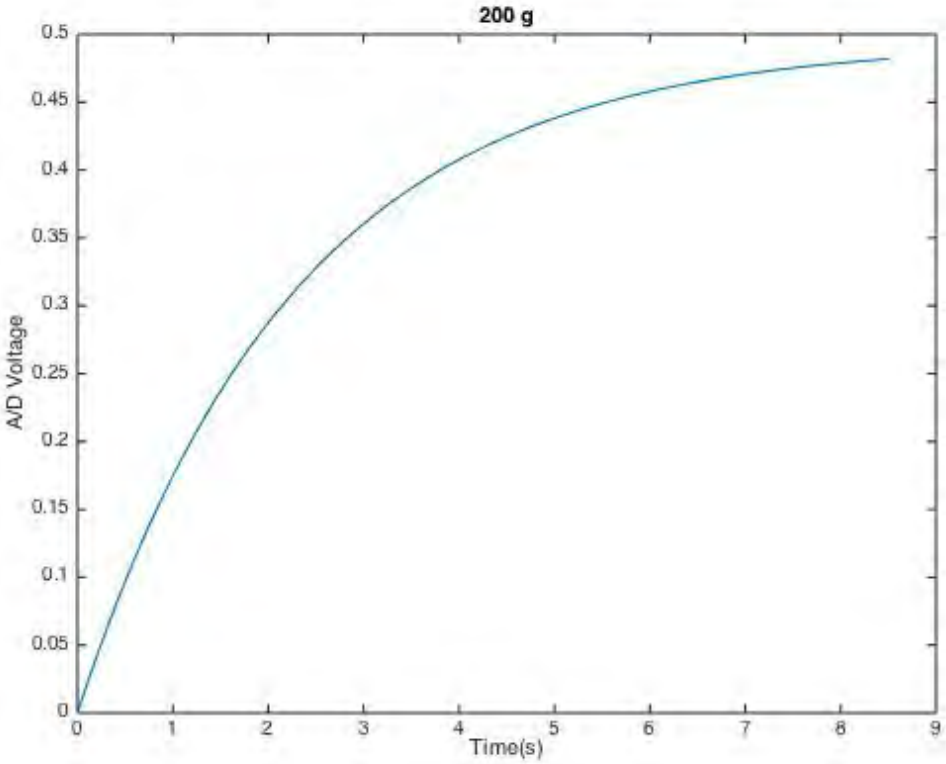

Annex IV.10. Modeled response for 200g with k = 0.419 and τ = 1.86 ECM = 0.08115

ANNEX V: K AND TAU FASHIONS

Range 0–1000g

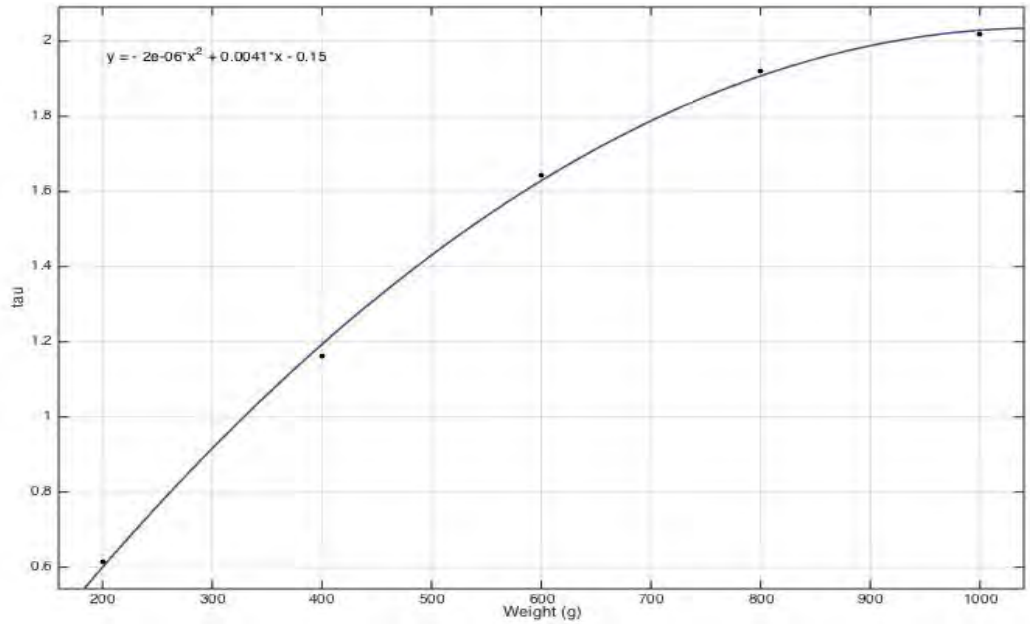

Annex V.1. Fashion followed by τ in the interval 0–1000g and the mathematical equation describing it

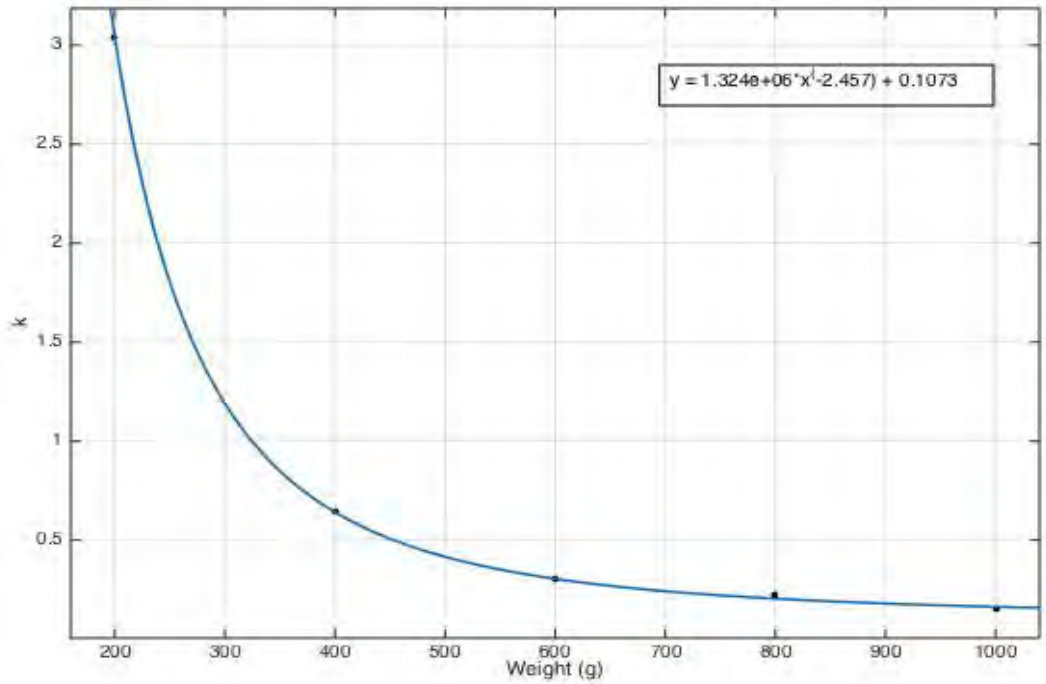

Annex V.2. Fashion followed by k in the interval 0–1000g and the mathematical equation describing it

Range 0–200g

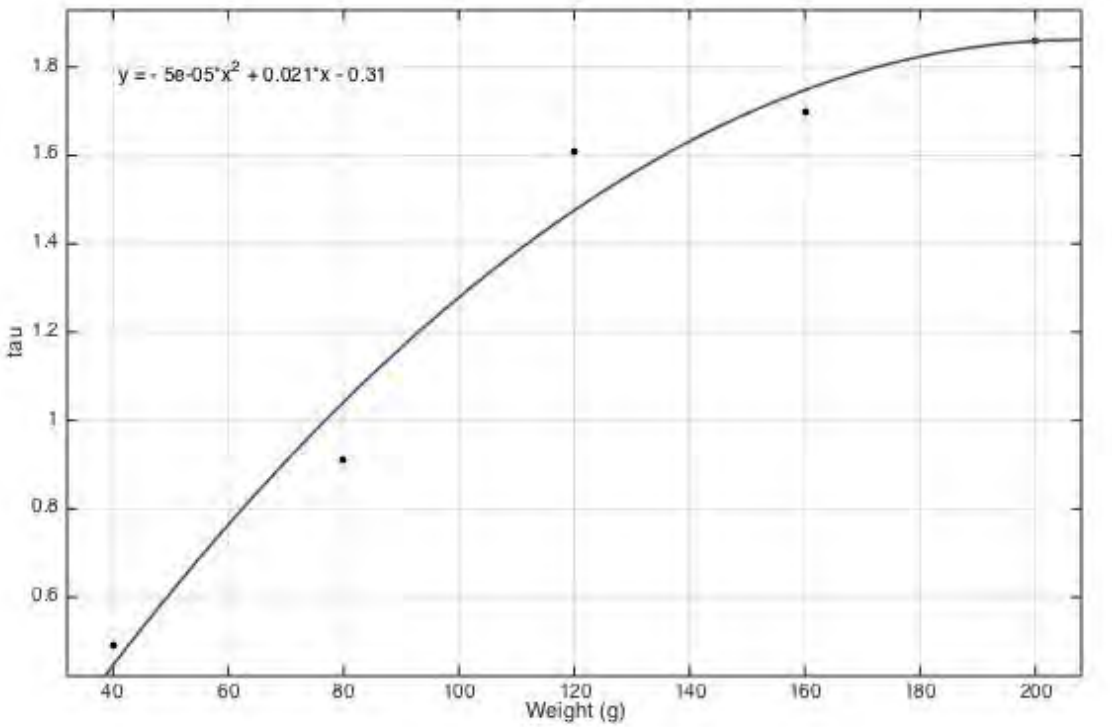

Annex V.3. Fashion followed by τ in the interval 0–200g and the mathematical equation describing it

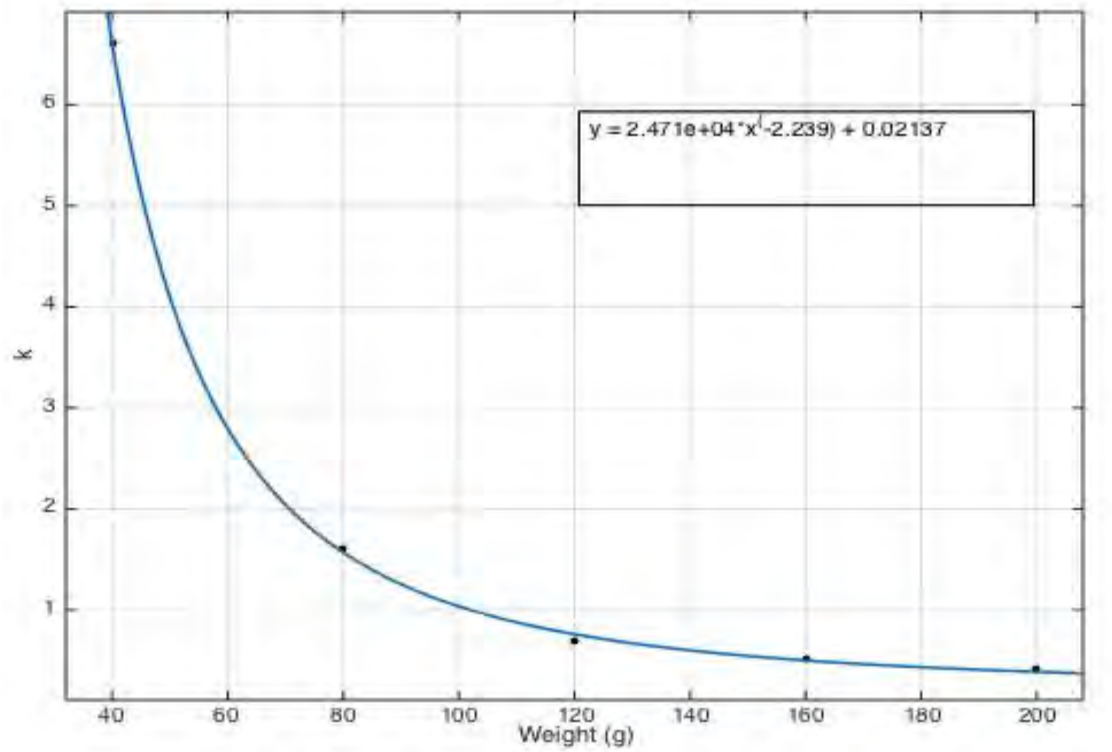

Annex V.4. Fashion followed by k in the interval 0–200g and the mathematical equation describing it

ANNEX VI: PLANES OF 3D-PRINTED STRUCTURES

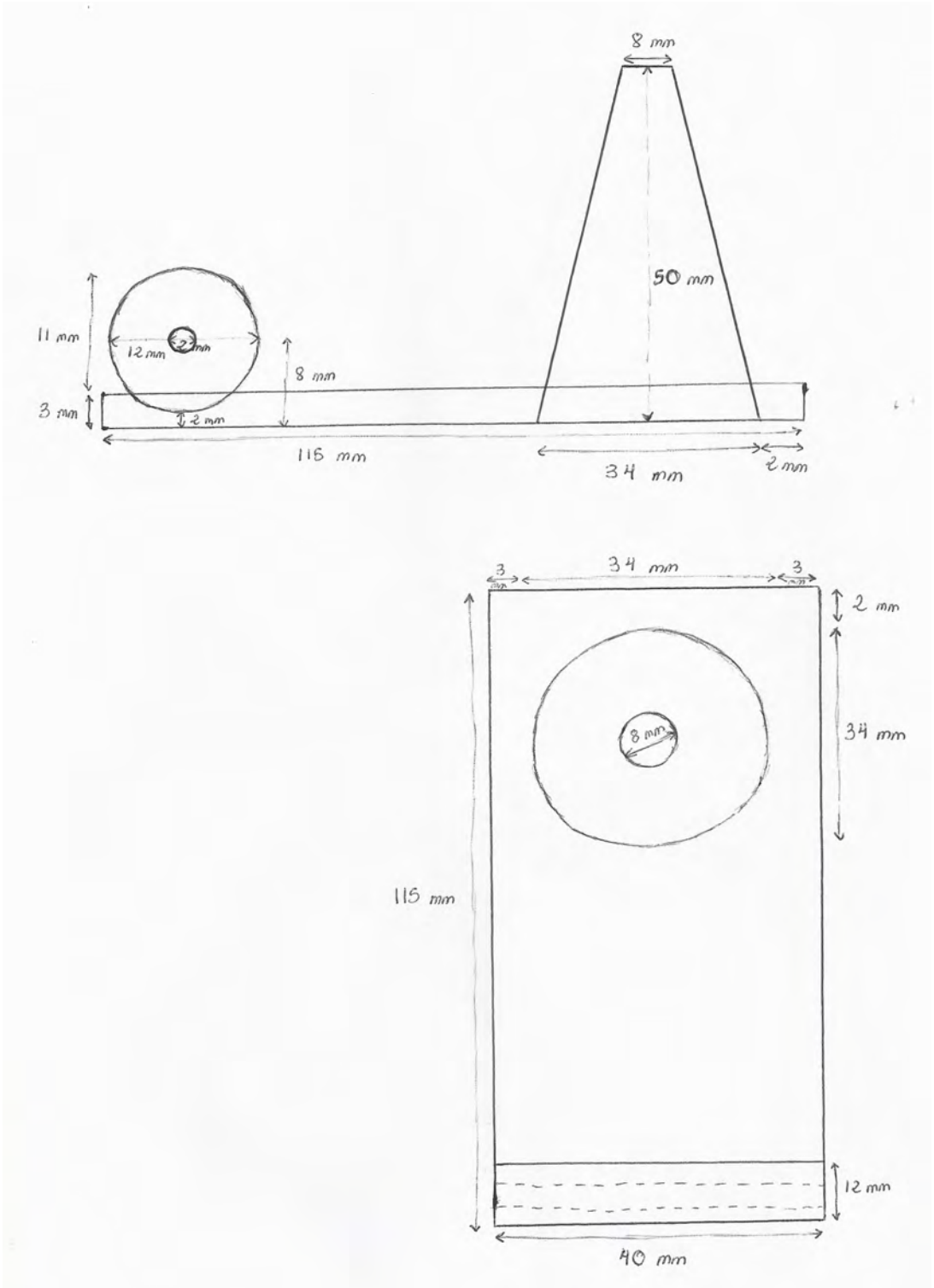

Annex VI.1. Calibration system plane

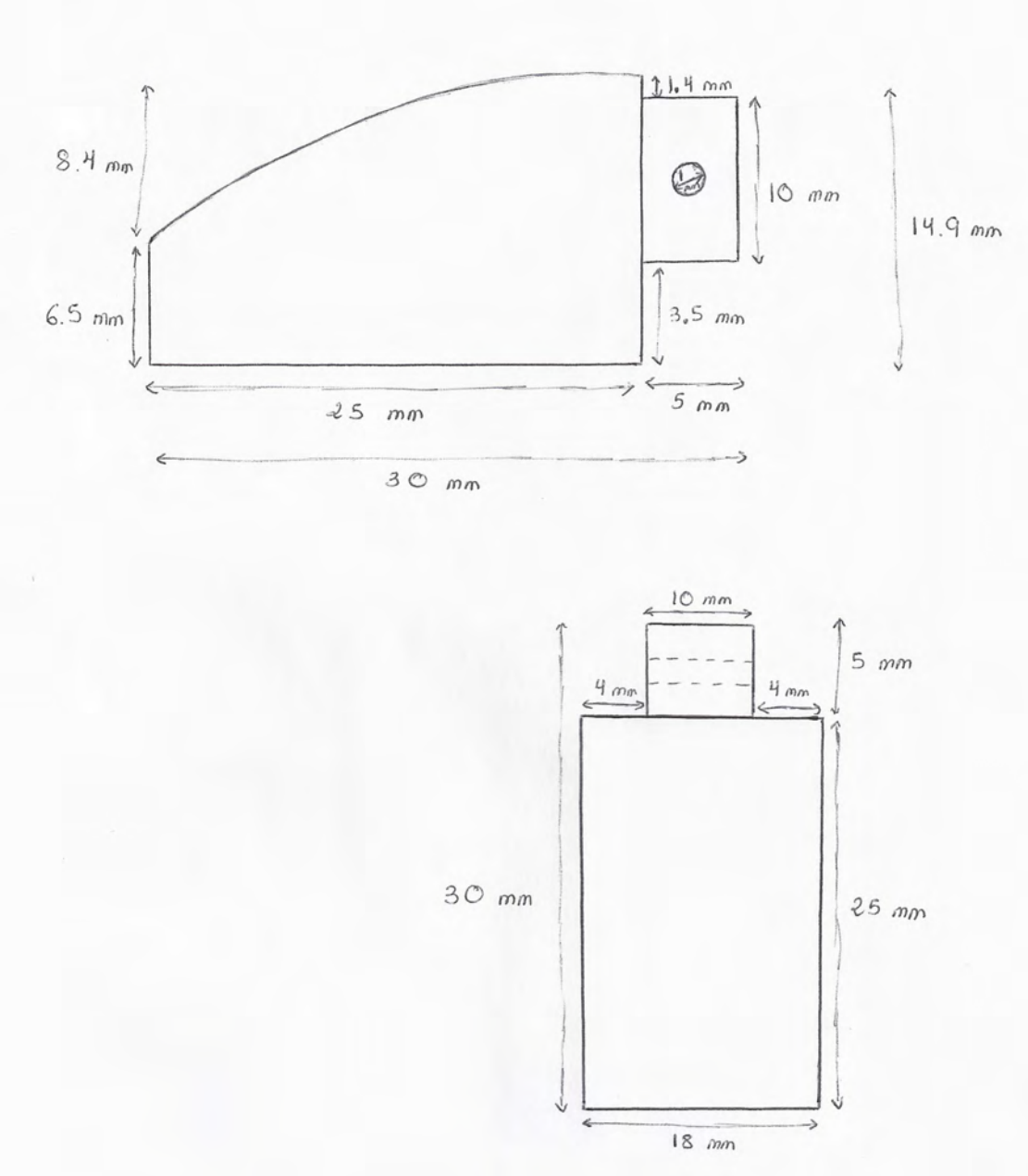

Annex VI. 2. Fingertip plane